Università di Genova

DEPARTMENT OF EXPERIMENTAL MEDICINE

PhD COURSE IN EXPERIMENTAL MEDICINE

Curriculum of Pharmacology and Toxicology (8230)

MODELS OF NEUROLOGICAL DISEASES
BASED ON FEEDBACK LOOP DYNAMICS

Candidate	**Tutor**
Serena Losacco	**Bruno Burlando**

PhD Program Coordinator
Prof. Ernesto Fedele

Academic Year 2020-2023

XXXVI Cycle

INDEX

1. INTRODUCTION

1.1. Feedback loops and multistability in living systems

Starting from the work of Von Bertalanffy [1] it has been understood that many systems of living beings behave as control systems, and that the feedback mechanisms described in physiological processes are inherent to this kind of functional organization [2]. As the importance of feedback loops increased in biological studies, concepts used in engineering were applied to explain some functional aspects of living systems [3]. The collaboration between physiologists and engineers was fundamental to analyze biological processes at the metabolic, cardiovascular, and respiratory levels [4, 5], as well as in regulatory systems involved in thermoregulation, water exchange control, endocrine regulation, and pupillary reactions [6-8]. By this new approach, living beings, and specifically the human body, were assimilated to a machine made up of processes finely regulated by specific dynamics that prevent the reaching of catastrophic levels of activity in the system [9]. Feedback loops are characterized by three main properties: homeostasis, amplification, and switching. Homeostasis is guaranteed by negative feedback loops, known to maintain physiological homeostatic processes by reporting the different cellular functions to baseline levels after perturbations [10]. By contrast, the ability of a system to generate multiple internal states in response to external inputs is the fundamental requirement of a functional switch. Hence, though the knowledge about feedback mechanisms was initially focused on negative loops providing homeostasis, the increasing discovery of positive loops led to the 'Demand theory' based on the idea that high demand cell functions are under the influence of positive regulatory elements, whereas those in low demand are under the influence of negative ones [11, 12]. Both positive and negative feedback loops admit stability, but positive feedback loops are the only one who possess the ability of generating multistability. In prokaryotes many bistable behaviors have been identified. These include lactose use by *Escherichia coli* [13], bacterial cell competence [14], sporulation [15], phenotype differentiation [16], kinase activation [17], and metabolic responses to environmental stimuli [18]. In eukaryotes, positive feedback loops are at the basis of the dynamic regulation of aminoacid [9], and pyrimidine biosynthesis [19], gene transcription [20], and the activities of protein kinases [21, 22], membrane transporters [23], cell signaling [24], gene activation [25], cell cycle transitions [26], and cell fate decision [27].

1.2. The Loopomics hypothesis and its consequences in pathophysiology

Based on the spreading knowledge about feedback loops as regulator mechanisms of living beings, a new hypothesis has been formulated, named 'Loopomics' [28]. This hypothesis could have deep implications in biomedical research, where many physiological processes remain puzzling, and consequently, many diseases remain obscure for what concerns etiology, thus hindering the possibilities of finding efficient treatments.

Living beings appear characterized by a high complexity and biodiversity. These features are serious obstacles for the advancement of knowledge in life science. Biomedical investigations need theoretical models and a new redefinition of pathophysiological processes, i.e. transitions from physiological to pathological conditions. The Loopomic hypothesis makes a generalization with the aim of proposing a more suitable approach to the study of physiological dynamics. The hypothesis starts from the assumption that any functional element of a biological system is influenced by at least one functional element upstream, and influences at least one functional element downstream, which entails that each functional element is involved in a closed chain of interactions, namely a feedback loop [28]. By considering the sign of the interaction, i.e. activatory or inhibitory, two kinds of loops can be distinguished, viz. negative loops, having an odd number of negative interactions, and positive loops, having no negative interactions or an even number of them. Negative feedback loops are known to maintain homeostasis, or to generate oscillations, depending on a short or long delay, respectively, of the response ensued by the interaction. In contrast, positive feedback loops can give rise to multistationary systems, acting as switches that give rise to changes or transitions, frequently permanent and irreversible [29].

It has been estimated that the human body consists of about $3.7 \cdot 10^{13}$ cells and that each cell carries out about 10^{10} chemical reactions per second, making up a total of about 10^{23} chemical reactions per second in the whole body [30]. Despite such a huge number of processes, our body can maintain a metabolic steady state, and this is possible only if we assume that metabolic processes are strictly cross adjusted and regulated [28, 31]. This suggests that reciprocal control is a prerequisite of life processes and that biological control mechanisms must be analyzed accurately to understand the dynamics of life processes. Systems and Control Theory has been developed mostly in the engineering field to provide general principles for the analysis of dynamic systems consisting of negative or positive feedback loops [29]. However, the advent of Systems Biology has brought back these arguments to the analysis of living beings, by focusing on the interactions among

the functional elements of these systems, rather than on the myriad of objects that make up their biodiversity [32, 33].

The shift from the analysis of life objects to the analysis of life processes is an essential step for achieving the possibility of formulating general, unifying paradigms about physiological and pathological processes. A huge amount of data highlights the essential role of loops in living beings [31], supporting the idea that loop systems characterize the activity of all the functions of a biological system. According to this hypothesis, a living being can be conceptualized essentially as an interconnected array of loops. The classical objects of biological studies, namely macromolecule arrays, cells and intracellular organelles, tissues, organs, and individual living beings, are then considered epiphenomena emerging from the activity of loops [28]. The balance between positive and negative loops enables the integrity and development of living beings, including their most distinctive feature, namely reproduction. Hence, living beings need the spatiotemporal continuity of their constituents, but also the ability of carrying out changes, which are made possible by positive loops acting as multistable systems undergoing transitions between different equilibrium points [34].

As said above, several life processes have been modeled as positive feedback loops, including gene expression [35], cell cycle [36-38], cell division [39], cell migration [40], cell differentiation [41], and axon growth [42, 43]. Moreover, diseases can also be thought as changes occurring within the body, and therefore, at the basis of each disease there must be at least one multistable positive feedback loop that generates a transition toward an equilibrium point representing a pathological condition [44]. Accordingly, many diseases have been modeled as bistable switches, including cancer [45, 46], prion infections [47], immunological disorders [48], dermatitis [49], neurological problems [50], neurodegenerative diseases [51-53], and microbial infections [48].

Up till now, the modeling of pathogenic processes as loop systems has been applied on a case-by-case basis, without any attempt to build a general theory. However, the possibility of defining a general paradigm can be envisaged. First, diseases can be seen as changes occurring inside the body. Even genetic diseases can have an incubation period before producing detectable symptoms, thus showing that a certain threshold or turning point must be reached, which can be seen as a crucial change or transition. Second, despite various drawbacks and difficulties, diseases are classifiable (see e.g. https://www.who.int/standards/classifications/classification-of-diseases), showing that they constitute an ordered system. Consequently, biological changes giving rise to specific diseases must follow predictable pathways. Third, diseases are recurrent over time, continuing to appear

identical through generations, thus proving that pathophysiological transitions are the result of clonable metabolic pathways that have been fixed by natural selection. Stability is an essential prerequisite for the possibility that a biological element be selected. Hence, given that the starting point of a pathophysiological process can be considered a stable functional condition, and that also its ending point displays the same property, it is possible to conclude that the process giving rise to a pathological condition must depend on the activity of a multistable system.

Systems admitting different stable equilibrium points generate predictable changes, and so, the modeling of their dynamics appears to be the correct approach in order to study pathophysiological processes. Diseases could then be considered as the result of predictable dynamical transitions in multistationary loop systems, and this idea provides a possible unifying model that could be extremely powerful for the understanding of pathophysiological processes leading to the identification of critical therapeutic targets [28]. The reason for the suitability of loop systems in the analysis of therapeutic targets resides in the possibility of identifying bifurcation parameters, i.e. the factors that modulate the strengths of interactions and ultimately the system dynamics. Changes in the activity or amount of biological elements acting as bifurcation parameters can induce the system to transient from a monostable to a bistable (or multistable) condition, thus posing the basis for jumping from one to another equilibrium point upon the insurgence of specific external stimuli [54]. Hence, bifurcation parameters are the key elements that govern the dynamics of the system, and therefore, they are the ideal targets of pharmacological and non-pharmacological strategies. The targeting of the biological components that act as bifurcation parameters of the loop system is expected to allow the control of biological processes leading to diseases. Ideally, this would make it possible to prevent, reduce, or revert the disease development. The identification of bifurcation parameters is possible through the mathematical analysis of the loop system, while the physical correspondents of these elements can be single functional agents or pathways.

1.3. Loopomic model of a pathophysiological process

The dynamical interaction between the functional agents involved in a pathophysiological process can be described mathematically by a system of differential equations yielding the rate of change of the functional agents involved. As a schematic example, a positive feedback loop can be represented by two functional agents, indicated by X and Y (Figure 1). Each functional agent evolves along time with time constant τ, and undergoes spontaneous inactivation. The elements considered

in the system may represent enzymes, signal molecules, cellular activities, or the number of cells. The schematic form of the system of differential equations is the following:

$$\tau_X \dot{X} + \theta_X X = f(Y) \qquad (1)$$

$$\tau_Y \dot{Y} + \theta_Y Y = f(X) \qquad (2)$$

Where $\dot{X}$ and $\dot{Y}$ are the time derivative of X and Y, respectively, θ is a coefficient representing the weight of the spontaneous inactivation element and τ is the time constant measuring the delay between the input received by the variable and the output produced by it. Different functions could appear in the differential equations. The most used function to model the input/output relationships between biological entities is the Hill function [46, 55]:

$$f(x) = \frac{\alpha x^h}{1 + \beta x^h} \qquad (3).$$
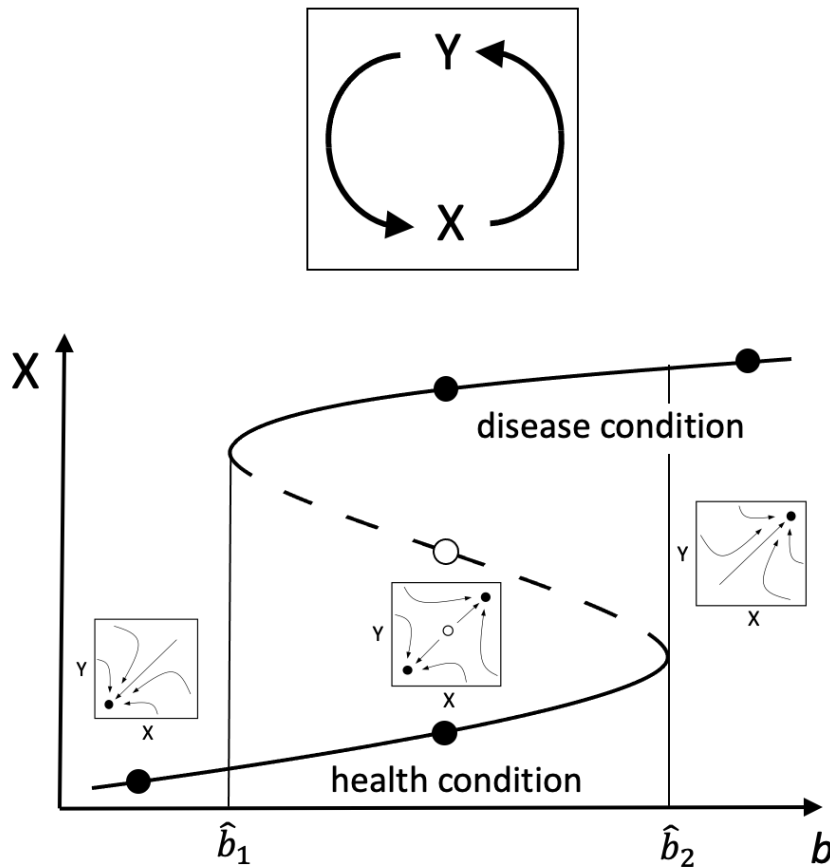
Figure 1. Top: Diagram of a loop system consisting of two mutually interacting agents represented by variables X and Y. Bottom: Bifurcation diagram showing the equilibrium values of X for different values of the bifurcation parameter *b*. A corresponding plot can be derived for Y. Continuous lines in the main plot represent stable equilibrium points while the dashed line represents unstable equilibrium points. Transition from monostability (one stable equilibrium point) to bistability (two stable equilibrium points and an

intermediate unstable equilibrium point) occurs at bifurcation points $\hat{b}_1$ and $\hat{b}_2$. Increasing values of b make the system jump from physiological to pathological steady state at $\hat{b}_2$. In addition, the system displays hysteresis, since after transition from physiological to pathological condition at $\hat{b}_2$, the reverse transition requires that b decreases down to $\hat{b}_1$. The insets of the bottom plots show phase portraits with the trajectories of the system and the basins of attraction of stable equilibrium points (full dots). Empty dot: unstable equilibrium point.

1.4. Application of the loopomic approach to disease management

According to the loopomic hypothesis, each disease should have a pathophysiological starting point that could be analyzed through the following steps:

- localization of the body region of disease onset;

- identification of the essential biological factors involved in the disease insurgence;

- detection of the positive loop responsible for the pathophysiological transition;

- development of a mathematical model of the loop, in order to find out the bifurcation parameter(s) of the system;

- *in vitro*/*in vivo* validation of the loopomic model of the disease and of the role of bifurcation factors.

Once the above steps have been successfully completed, the way is open to the development of precisely targeted therapeutic tools, followed by clinical trials. By following this procedure, the field of drug discovery would become completely renovated in its analytical approach. Current methods are based on large latin-square arrangements, involving the intersection of series of possible therapeutic molecules with series of hypothetical targets. The loopomic analysis of diseases would be more keenly oriented since the starting phases, leading to the identification of distinct biomolecular targets for the development of drug prototypes.

Possible drawbacks of this method could reside in the vast number of biological interactions possibly involved in a certain pathogenic process. However, theorems of the Systems and Control Theory hold that it is possible to simplify metabolic pathways by aggregating various elements within input/output monotone subsystems, thus allowing to combine different chain elements into a single element [56]. In addition, it has been shown that, if monotonicity is satisfied, conditions for bistability can be mathematically assessed in feedback loop systems of arbitrary order, thus allowing the analysis of systems having a complex topology, i.e. with numerous branches and different loops combined together [57]. Besides helping to solve pathological conditions, the loopomic approach could also be relevant in preventive healthcare. The understanding of the dynamics of multistable

systems could allow to predict the critical state in proximity to a bifurcation point, thus manipulating the biological factors involved in the loop dynamics to drive the system back to its physiological stable equilibrium [58, 59].

2. AIMS OF THE STUDY

The aim of this PhD has been the formulation of theoretical models of pathogenesis for diseases of the Central Nervous System (CNS) having unclear etiology and lacking a resolutive cure. The development of these models has been inspired by the Loopomics theory, i.e. by trying to detect feedback loop systems with multistable dynamics able to drive a transition from a physiological to a pathological condition.

The activity has been divided into two steps:

- formulation of theoretical models of pathophysiological processes;
- development of *in vitro* models of brain networks allowing to characterize the essential elements of their electrophysiological activity.

The first step has allowed to realize pathogenesis models based on brain networks arranged to form loop systems. This part of the activity has been developed as follows:

- identification of brain or endocrine systems forming positive feedback loops, putatively involved in the pathophysiological processes leading to the insurgence of the disease;
- development of mathematical models of these loop system allowing to study their dynamics under different conditions;
- identification of bifurcation parameters and of their corresponding biological elements;
- validation of the model by using real data;
- identification of possible treatments targeting the critical elements of the system.

The dynamics of brain networks are represented by the activities of neuron populations expressed as mean firing rates. This is a schematic representation of the activity of neural networks in the absence of more refined data. However, a detailed description of neural network activity could allow to develop models allowing a higher degree of prediction of the system behavior. To this aim, we have developed a second step of research activity as follows:

- development of *in vitro* neural networks using cell cultures of primary neurons;
- development of experimental systems for the electrophysiological recording of the network activity by using Micro-Electrode Arrays (MEA);
- development of multi-network assemblies on MEA by subdividing the cultured neurons different interconnected clusters using removable plastic masks;
- analysis of multi-channel recordings for the identification of functional features representing the essential elements of spontaneous neural network activity.

The use of multiple, interconnected neuron clusters has allowed to record the electrophysiological pattern of each neural network as consisting of two components:

- the spontaneous activity of a neuron cluster (single neural network);
- the modulation of such activity by the inputs deriving from the other neuron clusters.

Hence, this experimental system represents a suitable model for the *in vivo* characterization of brain neural networks.

3. PATHOGENESIS MODEL OF FIBROMYALGIA AND FIRST ASSESSMENT WITH QUESTIONNAIRE DATA

3.1. FM pathogenesis model: Background

Fibromyalgia (FM) is an idiopathic syndrome characterized by chronic, widespread pain and tender points [60, 61]. Non-pain symptoms are also present, including sleep problems, fatigue, and a series of comorbidities. FM has been now fully recognized as a central problem and classified among the group of syndromes collectively named "central sensitivity syndromes" (CSS) [62, 63]. It also belongs to a group of idiopathic pain disorders named Chronic Widespread Pain, whose classification and diagnosis are challenging [64]. FM prevalence is about 2-5% in the adult population worldwide. Women are more affected than men with a reportedly variable male to female ratio overall rating around 1:3 [65]. The marked female-biased sex ratio and perimenopause prevalence suggest a possible gonadal involvement that should be better investigated [66]. The mean age of onset is between 30 and 50 years of age [67].

FM diagnosis is especially difficult because of the lack of biomarkers, and the presence of secondary symptoms overlapping with other disorders. Several comorbidities of FM have also female prevalence, such as depression [68], migraine [69], and central vestibular disorders [70]. The occurrence of vestibular symptoms in FM patients, such as vertigo and dizziness [71-74], suggests that FM is a multi-sensory syndrome, or a dysfunction in sensory integration [75]. The American College of Rheumatology (ACR) and the American Pain Society have repeatedly updated diagnostic criteria in the past years [76, 77], by re-setting threshold values for a series of parameters (number and position of tender points, symptom duration, widespread pain index, symptom severity scale). Basically, FM diagnosis is usually given to individuals experiencing chronic widespread musculoskeletal pain that could not be associated to specific damage or inflammatory status [61, 78].

The management of FM patients is very difficult not only for the problematic diagnosis, but also for the lack of effective treatments [79]. The complex of clinical problems that characterize FM are doubtless linked to the disappointing absence of knowledge about the etiology of the disorder. Many hypotheses have been postulated on the pathophysiological processes at the basis of FM, but none of these has led to substantial clinical improvements [80].

The most important new paradigm about pathogenesis has been the revision of the initial site of FM onset, from peripheral musculoskeletal tissue to the central nervous system. Thanks to innovation in pain management, new genetic tests, experimental pain testing, and functional

neuroimaging, FM is now considered as a central disorder characterized by pain processing alteration [81]. Pain processing abnormalities result in chronic widespread pain generated from non-painful or mildly painful stimuli. Hyperalgesia, i.e. hypersensitivity in pain processing, and allodynia, i.e. pain processing of physiologically non-painful stimuli, are the main features of the central sensitization process [82]. These alterations are currently unsolved by canonical treatments, and therefore, FM patients are left without effective therapies resulting in poor wellbeing [83]. Therapeutic options are focused on improving symptoms, such as pain, quality of sleep, and physical functions [84].

The lack of decisive treatments emphasizes the need for advancements in knowledge about the insurgence and development of the condition [85, 86]. The hypotheses that have been advanced over the years about FM pathogenesis fail to provide a comprehensive explanation of the complex of features that characterize the disorder. The ones more closely related with the hypothesis of a central problem concern imbalances of neurotransmitters such as norepinephrine, serotonin, glutamate, and substance P, or an abnormal functioning of the hypothalamic-pituitary adrenal axis [80]. Conversely, the idea of our work was to develop a hypothesis able to unify epidemiological, neuroimaging, and neurophysiological features of FM, thus providing a unifying paradigm. To do this, we underwent an analysis based on the principles of Systems and Control Theory [29], considering different data about FM [87], and the interplay among endocrine axes and neurotransmission [82, 88, 89]. To this aim, we focused on fundamental FM aspects, summarized as follows:

- the consolidated idea of FM as a central disorder [90], suggesting that the dysregulation of some spinal and/or supraspinal network involving pain processing must be involved;
- the significant female prevalence affecting FM patients, with a worldwide average female:male ratio of 3:1 and local prevalence of about 10:1 [90, 91], suggesting that the hypothalamus-pituitary-gonadal endocrine axis (HPG) must have a relevant role;
- the evidence that FM is a stress-related disorder [92], suggesting that the HPA axis could be involved in the mechanism of pathogenesis.

In support of this latter hypothesis, hypothalamus–pituitary–adrenocortical (HPA) dysfunction has been observed in FM patients [93, 94], while there is also strong evidence that physical and psychological stressful events, including early life traumatic experience, are FM predisposing factors [95, 96].

3.2. FM pathogenesis model: Methods

3.2.1. Feedback loop model of FM pathogenesis

3.2.1.1. Literature search for brain and endocrine loops involved in FM pathogenesis

We did an online literature search on the Pubmed database (https://pubmed.ncbi.nlm.nih.gov/), concerning pain processing, loop-arranged brain networks putatively involved in FM pathogenesis, and endocrine feedback loops putatively involved in the modulation of the above brain networks. Different search activities were performed considering a series of key words including "pain processing" and the names of the brain regions involved in the pain matrix network. In addition, we used the combination of "pain" and "fibromyalgia" terms with other terms such as "GABA", "glutamate", "glucocorticoids", "gonadal hormones", "androgens", "estrogens", "HPA axis", and "HPG axis". The search was conducted from the database inception to the end of 2020 for brain networks, and to the end of 2022 for endocrine feedback loops.

3.2.1.2 Development of a mathematical model based on Systems and Control Theory

3.2.1.2.1 Thalamocortical loop system involved in pain processing

Based on the above literature search, a feedback loop thalamocortical brain network was identified as being possibly responsible of FM pain. The dynamics of this network are described by a mathematical model representing functional interactions among the specific agents involved in the system:

- somatosensory cortex (SC);

- thalamic reticular nucleus (TRN);

- thalamic ventroposterolateral nucleus (VPL) (Figure 2).

Differential equations were used to model both inhibitory and excitatory interactions, to represent the evolution of the activities of the different regions. These interactions were described by using specific Hill-type functions, which are commonly used to describe the input-output relationships among different neural population and intracellular signaling networks [46, 97]. Hill functions can model both increasing activation functions, denoted by *f(x)*, and decreasing inhibition functions, denoted by *g(x)*:

$$f(x) = \frac{\alpha x^h}{\beta^h + x^h} \qquad (4)$$

$$g(x) = \frac{\gamma}{\delta^h + x^h} \qquad (5)$$

where h is the Hill coefficient, while α, β, γ, and δ, are positive real parameters.

In our model, each functional agent x evolves along time with time constant τ, undergoing a spontaneous decreasing of its activity. So, the time derivative of x, denoted by $\dot{x}$, measures the time evolution of the activity of the element. A system of differential equations was therefore built to describe the dynamics of the specific agents involved. First, the glutamatergic excitatory connection exerted by VPL on SC was modeled by an increasing Hill Function [55, 98, 99],

$$\tau \dot{S} + \theta S = m_1 \frac{bV^h}{e^h + bV^h} \qquad (6)$$

where S and V represent the mean firing rates of SC and VPL, respectively, the parameter e is the input firing rate obtaining half-maximal output firing rate, h is the Hill coefficient, the parameter m_1 is the maximal output firing rate of SC, θ is a coefficient measuring the weight of the spontaneous inactivation element, and b is a coefficient measuring the strength of glutamatergic transmission and varying in the interval [0,1].

Second, the combination of the excitatory glutamatergic outputs arising from VPL and SC and acting on TRN were described by the following equation:

$$\tau \dot{T} + \theta T = m_2 \frac{(bV + bS)^h}{e^h + (bV + bS)^h} \qquad (7)$$

where T is the mean firing rate of the GABAergic fibers of TRN, and m_2 is their maximal firing rate. Other parameters as above.

Third, the combination of the opposite activities exerted by SC (excitatory, glutamatergic) and TRN (inhibitory, GABAergic) on VPL, was represented by using an increasing Hill function of variable S whose parameters m and e were expressed as Hill functions of variable T. Literature data reported the effects of GABAergic fibers on input-output responses to excitatory fibers with a reduction of the maximal output firing rate, or a decreased neural sensitivity to excitatory inputs resulting in a rightward shift of the input-output firing rate curve, or as a combination of these effects [55, 99]. We considered both effects in our model equation, in which increasing T values correspond to a reduction of the maximal output firing rate m, according to a decreasing Hill function, while they also correspond to an increased value of the parameter e, modeled by an increasing Hill function, starting from basal value e_0. Moreover, the strength of the GABAergic interaction was also modeled, by multiplying the variable T by the coefficient a varying in the interval [0,1]. The resulting differential equation is the following:

$$\tau \dot{V} + \theta V = \frac{g(aT) \cdot S^h}{S^h + f(aT)^h} \qquad (8)$$

where:
$$g(aT) = \frac{m_1}{1 + \left(\frac{aT}{e}\right)^h} \; ; \qquad\qquad f(aT) = e_0 + m_2 \frac{(aT)^h}{e^h + (aT)^h}.$$

The computational analysis of the model dynamics was conducted by using MATLAB (version R2021, MathWorks, Natick, MS, USA). The values of the parameters used in the differential equations were set according to literature reports, as reported in Table 1.

Table 1. Nominal values of parameters used in equations (6), (7), and (8).

Symbol	Name	Value	Reference
τ	Time constant	0.5 (sec)	[100, 101]
m_1	Excitatory fibers: max output firing rate	100 (Hz)	[99, 102, 103]
m_2	Inhibitory fibers: maximal output firing rate	80 (Hz)	[55, 104]
e	Input corresponding to half-maximal output	20 (Hz)	[102, 105, 106]
h	Hill coefficient	2.5	[102, 105, 106]
a	GABAergic strength	[0,1]	
b	glutamatergic strength	[0,1]	
θ	self-limiting factor	[0,1]	

3.2.1.2.2. Endocrine loop system involving the HPG and HPA axes

Based on the hypothesis that the HPG and HPA axes are involved in FM pathogenesis, we extended our literature search to the possible interactions between these two axes. We then identified an endocrine loop able to interact with brain networks due to the production of neurosteroids that modulate central neurotransmission. Evidence argues for the possibility that the HPG and HPA axes could become entangled to form a single system due to a reciprocal negative control on each other [108]. For this reason, a single simplified loop consisting of two elements was considered, in which each element represents one of the axes. On the mathematical side, each axis was considered as an aggregate of monotone subsystems and then embodied in a condensed element within the mathematical model of the dynamical system, still allowing the analysis of its behavior thanks to the presence of signed interactions [56]. In this model, two inhibitory arcs depart from each node. One represents the self-inhibition of the axis, i.e. its negative feedback loop. The other is the inhibition exerted by each axis on the other element.

The system dynamics were described mathematically by using two differential equations. These equations represent the time variations of percent endocrine axis activity ranging in the interval (0,100] (e.g. referring to the plasma concentration of cortisol for HPA, and of progesterone for HPG). The mathematical model describes the self-inhibition resulting from the negative feedback of each axis (self-limiting factor), and the reciprocal inhibition between the two axes (positive loop, double inhibitory), this latter emerging for wide variations of hormone plasma levels. The variation of axis activity was described by using two decreasing functions representing the inhibition of the other axis (mutual inhibition) and self-inhibition, respectively. Evidence argues for decreasing Hill functions being the best fit for endocrine effects (see below), and consequently, we used these functions for modeling these specific interactions.

The system of differential equations was defined as follows:

$$\tau \cdot \dot{H}_a = f(H_g) - \xi(H_a) \cdot H_a \qquad (9)$$

$$\tau \cdot \dot{H}_g = f(H_a) - \xi(H_g) \cdot H_g \qquad (10)$$

where H_a is the activity of the HPA axis, and H_g is the activity of the HPG axis, τ is the time constant, and $\dot{x}$ represents the time derivative of x. The functions $f(\cdot)$ are decreasing Hill functions with values ranging in the interval (0-100] and having these forms:

$$f(x) = \frac{100}{1 + \left(\frac{x}{e_x}\right)^{h_x}} \qquad (11)$$

where e_x and h_x represent the Hill function parameters, as defined above. The self-limiting functions $\xi(\cdot)$ are shifted decreasing Hill functions whose values belong to the interval (1,5]:

$$\xi(x) = 1 + \frac{4}{1 + \left(\frac{\alpha \cdot x}{e_\xi}\right)^{h_\xi}} \qquad (12)$$

where $\alpha \in (0,1)$ is a coefficient representing the modulation of the self-limiting effect.

3.2.2. Realization of a questionnaire for FM patients

3.2.2.1. Participant Recruitment and Ethical Approval

The recruitment of participants was realized thanks to an Italian association of fibromyalgic patients (Fibromialgia Comitato Assoutenti Liguria, http://fibromialgiaediritti.altervista.org, accessed on March 8, 2021). The association members received an information letter with the link to the survey and joined the survey anonymously and freely. Each participant had to be provided with a diagnosis of FM established by a qualified healthcare professional (symptoms for at least 3 months) [77]. Participants had to fill a full informed consent to start the survey. In addition, to enter

the study, different exclusion criteria were adopted such as difficulty to speak and write the Italian language, breastfeeding or pregnancy, substance abuse and psychiatric alterations, including psychotic disorders and disturbances such as schizophrenia. Subjects were invited to respond to an extensive pre-enrollment questionnaire which was reviewed by our professional team to eventually exclude any ambiguity from the study.

The Ethics Committee of the University of Genova approved the study and FM recruitment (Assent N.2021/32) while the principles of the Helsinki Declaration were satisfied. The survey was opened from April to June 2021, accessible through a link on the Microsoft Office365 Platform of the University of Genova (Microsoft Forms®, https://www.office.com, Microsoft, Redmond WA, USA, accessed on February 22, 2021). Furthermore, to investigate the possible correlations between FM symptoms and vestibular disorders, data collected in a previous vestibular study were re-analyzed in this context. This vestibular study was led by Drs. Viviana Mucci and Cherylea J. Browne and was conducted in 2019–2022 upon Western Sydney University Human Ethics Committee ethical approval (H11962). A total of 80 subjects recruited online from all over the world, out of the 197 control respondents, provided informed consent for the use of their deidentified data in the current study.

3.2.2.2. Questionnaires

A cross-sectional study was designed by using validated questionnaires. A total of 344 answers from previously diagnosed FM patients were collected. The first section of the survey concerned socio-demographic features such as gender, age, educational status, working and family status. Clinical data included age of disease onset, diagnostic delay, disease duration, and biometric parameters.

To evaluate pain, participants were asked to report their average global pain intensity on a 11-point numerical rating scale (0 = "no pain"; 10 = "worst imaginable pain") [109]. The specific kind of pain mostly experienced was evaluated on a scale from 1 to 5, including numbness, tingling, pressure pain, sudden pain, light contact, burning, and occasional pain. The prevalence of central pain was investigated by using the Italian translation of the painDETECT questionnaire (PD-Q). The PD-Q questionnaire allowed to classify pain perception into nociceptive or neuropathic/nociplastic pain [110]. A PD-Q score ≤ 12 indicates prevalence of nociceptive pain, a PD-Q score ≥ 19 indicates neuropathic or nociplastic pain, and values in between represent intermediate conditions.

Secondary symptoms other than pain were also recorded, including migraine, fatigue, and sleep disturbances. Self-perceived effectiveness of treatments was also investigated by recording (null, low, average, good, and excellent) pharmacological treatments (non-steroidal anti-inflammatory drugs, steroids, antidepressants, and analgesics) and non-pharmacological strategies (psychotherapy, relaxation therapy, non-invasive instrumental treatments, massage, acupuncture, and diet therapy). Childhood and adolescence were investigated by asking participants to define these periods of life on a scale from 1 to 5 (very bad, bad, average, good, excellent). Experienced traumatic events were also recorded.

A section of the survey aimed at the evaluation of cognitive and behavioral management, by using Italian translations of two questionnaires: the Self-Related Emotional Intelligence Scale (SREIS) [111], and the Cognitive Behavioral Assessment-Hospital (CBA-H) [112]. The SREIS test is used to investigate emotional intelligence, emotion perception, and management. The questionnaire is made up of specific questions organized on a 5-point Likert scale (ranging from 1 = "not at all", to 5 = "very much"). The CBA-H questionnaire is used to evaluate psychological distress, stable personality traits, fear, well-being, and anxiety. The CBA-H is composed of 3 parts (A, B, C) organized in true/false questions.

To specifically evaluate vestibular problems, a second section of the questionnaire was designed. A total of 277 FM patients out of 344 completed this section of the survey. Participants answered the validated Italian versions of the Dizziness Handicap Inventory (DHI) [113], and the Situational Vertigo Questionnaire (SVQ) [114]. The DHI is composed of 25 items with yes/no/sometimes questions, corresponding to 0, 2, and 4 score values, respectively. The following four cutoffs are defined based on total score: ≤14: no handicap, 16–34: mild handicap, 36–52: moderate handicap, and ≥54: severe handicap. The 25 items of the DHI are divided into three domains, regarding functional, emotional, and physical aspects of dizziness. The physical component contains questions regarding movements that increase patients' symptoms, the emotional component concerns how the patient feels to be perceived by other people, and the functional component is focused on the ability of performing various activities and tasks. The SVQ consists of 19 items discriminating visual vertigo, with a score ranging from 0 (not at all) to 4 (very much) for each item. For control subjects, a 49-item questionnaire was distributed using the online survey platform Qualtrics (https://www.qualtrics.com/qualtrics/xm, Seattle, WA, USA, accessed on February 1, 2021).

3.2.2.3. Statistical Analyses

Clinical data and sociodemographic characterizations were analyzed by descriptive statistics. Inference and correlation analyses were conducted using the Pearson's chi-squared and Wilcoxon rank sum tests for inference analysis, and the Spearman's rank coefficient for correlations. These analyses were applied to PD-Q, CBA-H, and SREIS scores, and to the intensities of pain. Data distributions for semiquantitative scores were analyzed by the Mann-Whitney test, while the goodness of fit for categorical variables was assessed by the chi-squared test. Questionnaire scale reliability was assessed by the Cronbach's alpha index (0-1). Computational analyses and statistics were performed by using MATLAB (see above) and R software (version 4.0.5, https://www.r-project.org/, accessed on April 6, 2022).

3.3. FM pathogenesis model: Results

3.3.1. The thalamocortical loop

3.3.1.1. Arrangement of the thalamocortical loop

As reported in section 3.2.1.2, by our literature search a loop network was identified involving thalamocortical regions, i.e. the thalamic ventroposterolateral nucleus (VPL), the primary somatosensory cortex (SC), and the thalamic reticular nucleus (TRN) [115]. These regions are connected with each other by different fibers, including: first order excitatory glutamatergic fibers projecting from VPL to TRN and to the SC, glutamatergic connections of SC projecting to first order neurons of VPL and to TRN, and inhibitory GABAergic projections connecting TRN to VPL [116]. SC is targeted on its layer 4 (L4) by the VPL first order neurons, while SC glutamatergic connections from layer 6 project to both VPL and TRN [117]. However, it has been shown that L4 acts as a distributor of intracortical excitation thus making L4 and L6 excitatorily coupled [118]. Therefore, the SC can be considered as a single functional element in the loop system.

Considering the arrangement of this neural network, three loops can be identified, a positive one: VPL-SC-VPL, with excitatory steps only, and two negative ones: VPL-SC-TRN-VPL and VPL-TRN-VPL, both having one inhibitory step (Figure 2). Depending on the kind of dominating loop, which depends on the strength of the various interactions, the system globally behaves as a candidate multistable system or as a candidate oscillator. When the negative loop prevails (GABAergic transmission), the system has a single stable equilibrium point (candidate oscillator), whereas if the positive loops dominate (glutamatergic transmission), the system behaves as a multistationary system with different stable equilibrium points [29].
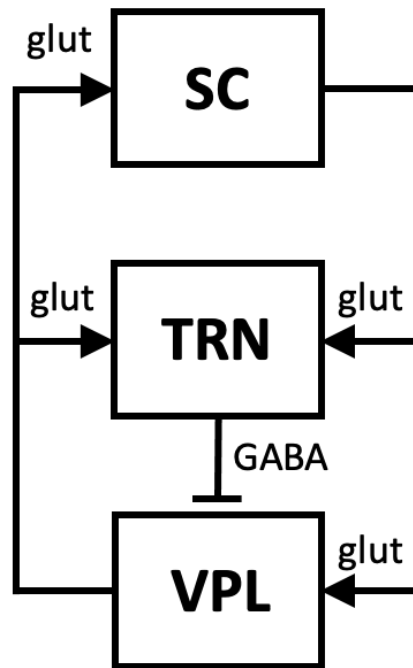
Figure 2. Schematic diagram representing the system of thalamocortical loops involved in the hypothetic pathophysiological mechanisms leading to FM. The loop system includes the primary somatosensory cortex (SC), and the reticular (TRN) and ventroposterolateral (VPL) nuclei of the thalamus. These different brain districts are connected by excitatory glutamatergic (glut) or inhibitory GABAergic (GABA) pathways. The system is of a positive loop: VPL-SC-VPL, including only excitatory steps, and two negative loops: VPL-SC-TRN-VPL and VPL-TRN-VPL, both including one inhibitory step in their pathway. The dynamical behavior of the system is dominated by negative loops or by positive loops, depending on the relative strength of glutamatergic vs. GABAergic transmission. Reproduced with permission from J Comput Neurosci [107], Creative Commons Attribution (CC BY) license (https://creativecommons.org/licenses/by/4.0/).

An imbalance between the strengths of the GABAergic and glutamatergic transmissions would tend to abolish the negative loop influence, inducing the positive loop contribution to dominate the system and consequently causing the emergence of a multistable behavior. Multistationary systems are known to have at least two stable equilibrium points and the possibility of shifting between these two equilibria makes these systems of interest in pathogenesis [119]. So, the thalamocortical loop could shift from a healthy state condition to a pathological one by an inbalance in neurotransmission.

3.3.1.2. Mathematical model of the thalamocortical loop

The thalamocortical network assumed to be involved in the FM pathogenesis can be described mathematically. In particular, the activities of the different neuron populations can be represented

by differential equations describing their time evolution. Each differential equation was used to quantify the variation through time of the mean firing rate (i.e. the number of spikes per second) of neurons belonging to a specific area. As reported in the Methods (section 3.2.1.2.1) the following system of differential equations represent the time variation of the neuronal activity of SC, TRN, and VPL:

$$\tau \dot{S} + S = f(bV) \qquad (6)$$

$$\tau \dot{T} + T = f(bV + bS) \qquad (7)$$

$$\tau \dot{V} + V = \frac{g(aT) \cdot bS^h}{h(aT)^h + bS^h} \qquad (8).$$

The variables S, T, and V denote the mean firing rate of neurons belonging to SC, TRN and VPL, respectively, $\dot{S}$, $\dot{T}$, and $\dot{V}$, represent the time evolution of these variables, the coefficient a represents the strength of the GABAergic transmission, and the coefficient b represents the strength of the glutamatergic transmission. All the functions have Hill-type expressions, with f(•) and h(•) representing increasing Hill functions, while g(•) represents a decreasing Hill function. As reported in section 3.2.1.2.1, Hill type functions are commonly used to model the input-output relationships between different neural populations [46, 55, 97].

In our system, the effects of many neurons are replaced by a single overall characteristic, as a schematic representation of the biological phenomenon. From a mathematical standpoint, this simplification does not affect the conclusions, so far as the essence of the phenomenon is captured. The instability we are analyzing, leading to bistability, remains qualitatively unaffected if we consider a "lumped" effect instead of a cascade of individual effects. Simple models that capture the essential aspects of the phenomenon are useful because they are amenable for analysis and can provide explanations and insight into the functioning of the system. [56]

3.3.1.3. Acquisition of bistability upon weakening of the inhibitory GABAergic transmission

The dynamics of the system described above have been analyzed by using the MATLAB software. A shift in the dynamics has been identified, revealing the emergence of a bistable behavior in the thalamocortical network. In loop systems, monostability is associated to the presence of a unique steady state. In our thalamocortical loop, this steady state is characterized by low firing rate for all the elements involved (Figure 3A-C). Such monostability is maintained so far as the strength of the inhibitory GABAergic transmission is sufficiently high. To explore the role of GABAergic transmission, we maintained a fixed value of $b = 1$, while letting a to assume different values. As reported in the phase portraits diagrams (Figure 3D-F), for values of a close to 1, the system presents a single large

basin of attraction associated to the unique equilibrium point, so that all the system's trajectories, induced by different kinds of excitation in each single element, end up converging to the steady state characterized by low firing rate. However, if the efficacy of the GABAergic fibers scales down, then for $a = 0.265$ the system reaches a bifurcation point and acquires two different steady states: high- and low-firing-rate steady states. Such a value of a represents a bifurcation point, i.e. the shift from a monostable to a bistable behavior. In the phase portraits (Figure 3D-F) two attraction basins are shown, representing the areas within which the system inevitably fall on either of the two stable equilibrium points. In addition, when the GABAergic transmission weakens (decreasing a value), the attraction basin related to the high-firing-rate steady state enlarges. By this way, the probability for the system to converge to a high-firing-rate steady state becomes higher (Figure 3D). Considering the mean firing rates of the different regions: for values of a immediately smaller than the bifurcation value, the variable *V* results relatively low (40 Hz) at the high equilibrium point, while the variable *S* results higher (about 80 Hz) (Figure 3A-C). Hence, for values of a smaller than the bifurcation value, the threshold for the activation of VPL, e.g. by spinothalamic input, is very low, and sufficient for inducing SC to reach a permanent high-excitation status. This ultrasensitive behavior is a typical feature of biological bistable switches [27].

The mathematical analysis shows that the system always admits the equilibrium at zero, which is always stable and corresponds in our model to baseline activity for all neuron populations. The system may overall admit an odd number of equilibria, which are always ordered and are typically three: the low-firing-rate stable equilibrium at zero, which corresponds to basal activity, the high-firing-rate stable equilibrium, which can be related to a pathogenic pain processing activity, and an unstable equilibrium with intermediate neuron activity. If such a bistability pattern emerges for $a = 0$, we show that it is preserved for values of a below a certain threshold a^*, $0 < a < a^*$. We also prove that there exists a threshold value $\hat{a}$ for a (associated with the bifurcation value observed in our numerical simulations) such that, for all $a > \hat{a}$, the only admissible equilibrium is the one at zero (associated with basal activity), which is stable and hence has the whole state space as a basin of attraction. From a qualitative point of view, our model shows robust prediction of the system's behavior, even considering different kinds of functions and parameters. For example, the substitution of one of the Hill functions appearing in equation (13) with a constant value, does not modify the behavior of the system, with the same transition from monostability to bistability, but shifted to a higher value for the bifurcation point. This corresponds to a higher tendency of the system to acquire bistability. Moreover, it is known that the GABAergic transmission can reverse its

activity from inhibitory to excitatory, if an inversion of the transmembrane chloride gradient occurs [120]. In this case, equation (12) would be modified as follows:

$$\tau\dot{V} + \theta V = f(bS + aT) \qquad (13).$$

The system behaves as a bistable system for any value of a and is more likely to fall within the attraction basin of the high-firing-rate steady state [29]. The possibility for the system to shift among different stable equilibrium points is assumed to be an essential prerequisite for the development of FM. The GABAergic transmission is a key element whose reduction in strength induces the switching of the system from monostable to bistable.

3.3.1.4. Variations of the thalamocortical loop dynamics by varying the strength of the interactions

The system monostability has been demonstrated for b and for $a > 0.265$ with the existence of a single attraction basin corresponding to the low-firing-rate steady state. We have shown the existence of a bifurcation point at $a = 0.265$, meaning that when a decreases, the system acquires bistability with the possibility to shift to an additional steady state corresponding to high firing rate. The reduction of a is correlated to the enlargement of the attraction basin of the high-firing-rate steady state. Under this condition the system results more prone to fall on the high-firing-rate steady state, which is representative of the chronic pain symptom reported by FM patients. The relationship between the bifurcation value of a, indicated as $\hat{a}$, and b was also analyzed, finding that for decreasing values of b, $\hat{a}$ decreases according to a sigmoid curve (Figure 4). In addition, for changing values of θ the above $b/\hat{a}$ relationship is maintained but the curve steepness lowers for decreasing values of θ.
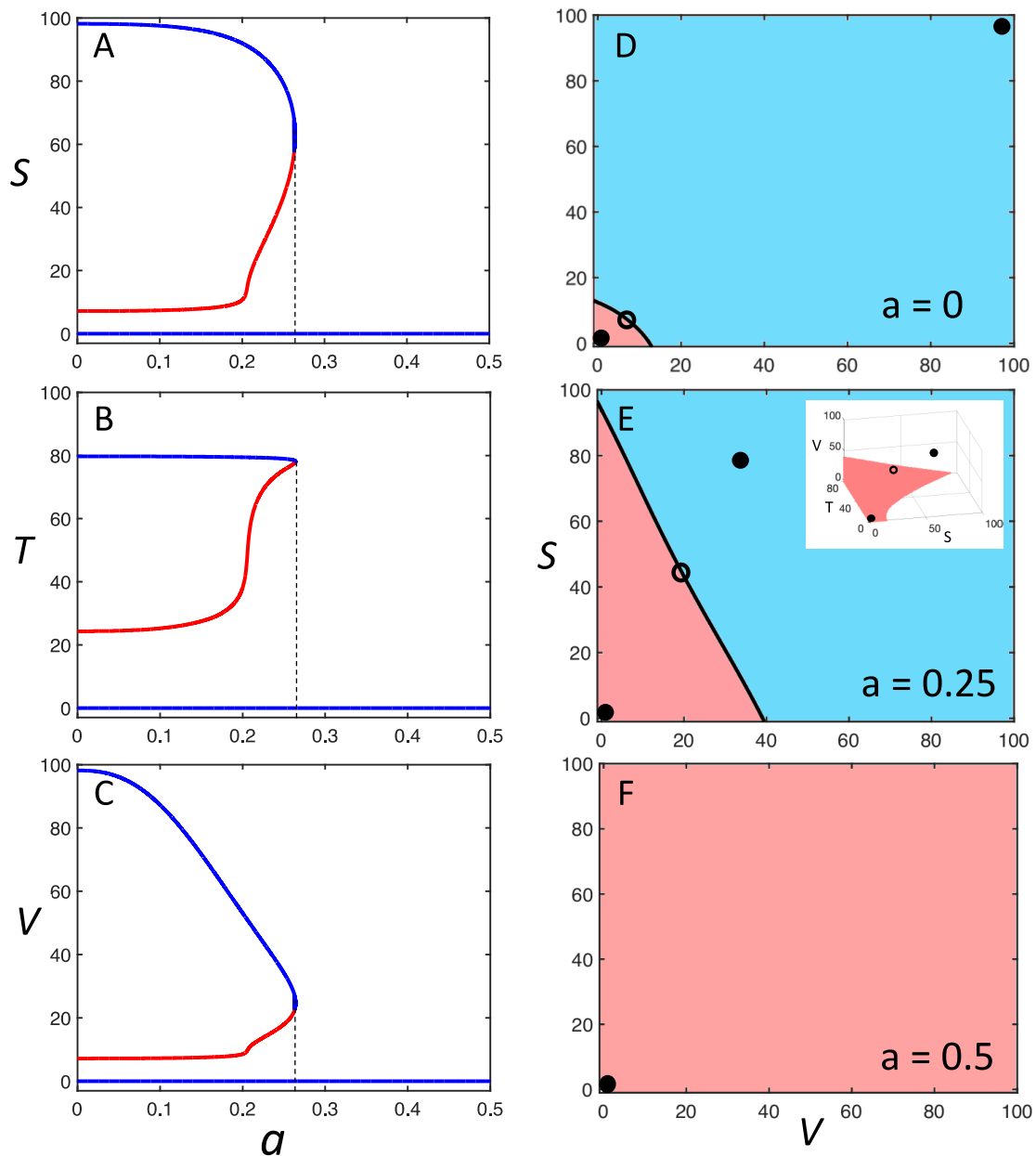
Figure 3. Thalamocortical loop: bifurcation diagrams and related phase portraits. (A, B, C) Bifurcation diagrams: curves showing the steady states of the three variables (S, T, V) plotted against the bifurcation parameter a, representing the strength of GABAergic inhibition. The variables are expressed as mean firing rate (Hz), and a is a dimensionless parameter ranging in the interval [0,1]. Glutamatergic strength is set to the maximal value, $b = 1$. Stable steady states (stable equilibrium points) are represented by curve branches in blue, while unstable ones are represented by curve branches in red. For decreasing values of a the system reaches a bifurcation point $\hat{a}$ (dashed vertical lines) shifting to bistability and acquiring two stable equilibrium points and an unstable one. The steady state characterized by low firing rate represents the physiological condition, while the steady state associated with a high firing rate corresponds to the pathogenic condition. (D, E, F) Diagrams of phase portraits representing projections in the V/S plane of the system 3-dimensional phase portrait. The diagrams show, for different values of a and for a fixed value of $T = 80$, the basins of

attraction of the stable equilibrium points indicated as black filled dots. In light blue is reported the basin of attraction related to the high-firing-rate steady state, while in light red the low-firing-rate steady state. Unstable equilibrium points are indicated as open dots. Panel E shows a condition in which a is just below $\hat{a}$, while its inset reports the whole 3-dimensional phase portrait in the S/T/V space [107]. Reproduced with permission from J Comput Neurosci [107], Creative Commons Attribution (CC BY) license (https://creativecommons.org/licenses/by/4.0/).
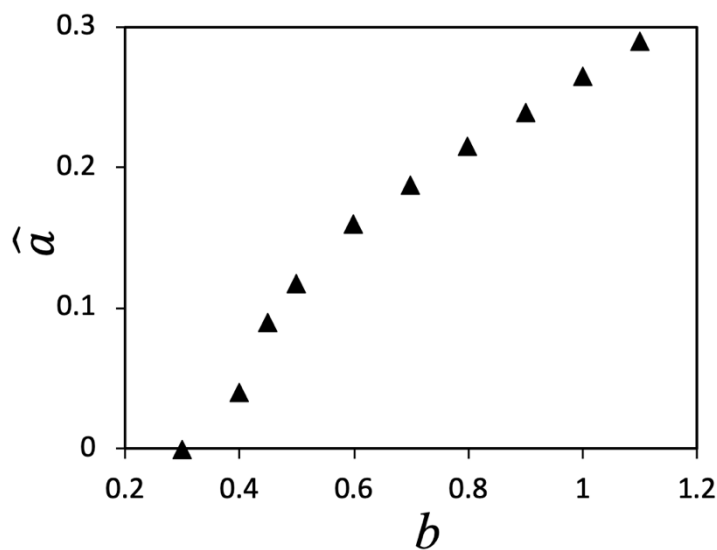
Figure 4. Positive, non-linear correlation between b, the coefficient measuring the glutamatergic transmission strength, and $\hat{a}$, the bifurcation value of a, the coefficient measuring the GABAergic transmission strength.

3.3.1.5. Effects of the endocrine axes on the dynamics of the thalamocortical loop

The thalamocortical loop model offers a possible explanation for FM chronic pain, but it does not account for the causes of GABAergic weakening. However, literature data argues for a role of the HPA and HPG axes in FM insurgence [121]. This body of evidence can be harmonized within our model because both endocrine axes are known to influence glutamatergic and GABAergic neurotransmissions in the brain. The HPA axis involves the hypothalamus, the anterior pituitary, and the adrenal glands, which are sequentially connected by specific interactions. By releasing corticosteroids into the plasma, HPA has a regulatory role concerning the responses to different stress conditions. HPA is relevant not only during acute stress conditions, but also under chronic stress conditions, producing consequent changes in response to persistent traumatic agents [122]. The HPG axis involves the hypothalamus, the anterior pituitary, and the gonads, with mutual

interactions. HPG has a regulatory role in both male and female reproductive functions through the release of gonadal steroids into the plasma [123].

3.3.1.5.1. Influence of the HPG axis on the thalamocortical loop

Many studies have reported gonadal hormone modulatory effects on glutamatergic and GABAergic neurotransmissions. Also, progesterone and testosterone levels observed in female FM patients during the menstrual cycle have shown an inverse correlation with pain intensity [124]. Furthermore, testosterone has a role in the upregulation of the α2 subunit of the $GABA_A$ receptor in the rat cerebral cortex, inducing higher GABAergic ion currents [125]. Also, depressed women treated with testosterone have benefited of antidepressant and anxiolytic effects, possibly related to increased concentration of GABA in the posterior-cingulate cortex [126].

A series of steroids, known as neurosteroids, have been found to affect neurotransmission in the brain, in an exclusive, or more efficient mode with respect to gonadal hormones [127]. Among neurosteroids, the progesterone derivative allopregnanolone ($3\alpha,5\alpha$-tetrahydroprogesterone) (Allo), and androstanediol (5α-androstane-$3\alpha,17\beta$-diol), which derives from testosterone and shares Allo structure, are known to act on $GABA_A$ receptors as positive allosteric modulators [128]. In relation to this kind of activity, these neurosteroids induce anxiolytic, antiepileptic, and sedative effects [129, 130]. Their brain level is the result of de novo synthesis and/or brain penetration by themselves or their precursors. Neurosteroid brain levels depend more closely on gonadal hormone blood levels for wide variations of these latter [131, 132].

To investigate the role of HPG in the modulation of the thalamocortical loop system in our model of FM pathogenesis, we firstly analyzed Allo effects, because of the wider fluctuations of female progesterone with respect to male testosterone along the reproductive cycle. To this aim, we derived a quantitative relationship between Allo brain levels and GABAergic strength. Allo and other neurosteroids exert their positive allosteric modulation on both synaptic, γ-type, and extra-synaptic, δ-type, $GABA_A$ receptors. By this way, they enhance both phasic and tonic GABAergic inhibition [133]. However, in our model based on a schematic description of neural network activity, we considered the total effect of neurosteroids on GABAergic transmission. We then derived, which, as shown above, is represented by the parameter a in the differential equations of the thalamocortical model. We then derived brain and plasma levels of Allo at different woman reproductive phases from previous studies [120, 134], or alternatively, we estimated these values from the ratio between the known values of Allo brain and plasma levels at the luteal phase (Table 2).

Table 2. Gonadal steroid concentrations in the woman at different phases of the cycle and at pregnancy.

Reproductive period	Gonadal steroid	Body district	Level (ng/mL)
Follicular phase	Progesterone	Plasma	1.5
		Brain tissue	–
	Allopregnanolone	Plasma	0.15
		Brain tissue	2.4*
Luteal phase	Progesterone	Plasma	10
		Brain tissue	41
	Allopregnanolone	Plasma	1.2
		Braintissue	20
Late pregnancy	Progesterone	Plasma	204
		Brain tissue	–
	Allopregnanolone	Plasma	16
		Brain tissue	256*

* = proportionally derived from the ratio of brain and plasma values at luteal phase

Thereafter, we derived from literature data the parameters of dose-response curves representing the effect of Allo on GABA$_A$ receptors. All the considered curves showed a good fit to Hill functions, allowing to obtain median values for the Hill function parameters (Table 3). A couple of studies also reported baseline values of the activity of GABA$_A$ receptors, allowing to estimate the maximum possible increase of activity induced by Allo on these receptors, resulting to be 100% and 200% of baseline, respectively [135, 136].

Table 3. Parameters of the Hill functions derived from the fitting of Allo modulatory effects on GABA$_A$ receptors.

Experimental model	N	h^1	e^2 (ng/mL)	e^3 (%)	Threshold dose eliciting max effect (ng/mL)	Refs.
Bovine chromaffin cells	5	2	15	20	–	[137]

Rat hippocampus/cortex	6	2	45	8	600	[135]
Xenopus oocytes	6	2	300	2	1500	[138]
Rat neurons	5	2	18	5	150	[139]
Mouse L-tk cells	8	1.2	9	0.3	300	[140]
Rat dentate granule cells	7	1.15	3.9	5	90	[136]
Rat embryo hippocampus	7	2.8	300	4.8	900	[141]
Median values		2	18	5	450	

[1]Value of the Hill coefficient. [2]Value of the half-saturation constant of the Hill function, obtained from original data. [3]Value of the half-saturation constant obtained by rescaling data on a [0,100] interval. The parameter e corresponds to the EC_{50}, representing the Allo dose inducing a 50% effect.

Considering the above dataset, we quantify $GABA_A$ activity in response to Allo at different phases of the female reproductive cycle. The maximum activity of $GABA_A$ receptors was set at $a = 1$, corresponding to the activity observed when allopregnanolone is at the highest pharmacological doses (possible range 90–1500 ng/mL, median value 450 ng/mL, Table 3). Conversely, the minimum effect of Allo was assumed to occur at its follicular brain levels of 2.4 ng/mL (Table 2). At the follicular phase, the strength of GABAergic connections was assumed to be like the one in the absence of Allo (Table 3). Hence, assuming a maximum increase of 150% in the activity of the $GABA_A$ receptor, on average, the value of a at the follicular phase (a_f) was obtained from the equation $a_f + 1.5a_f = 1$, yielding $a_f = 0.4$. Consequently, the EC_{50} of Allo, taken as the median value of the parameter e in Table 2 (18 ng/mL), should correspond to $a = 0.7$, i.e. the midpoint of the interval [0.4,1]. The value of $a = 1$ is never reached around the female cycle, since luteal Allo brain levels are around 20 ng/mL, i.e. definitely below the doses inducing maximum $GABA_A$ activation, as observed in experimental studies (Table 3). From the follicular to the luteal phase, Allo brain levels correspond to a values that are always above the bifurcation point of our thalamocortical systems, i.e. $\hat{a} = 0.265$ for a maximum value of $b = 1$.

However, a depressive effect on $GABA_A$ receptors due to very low Allo levels drives GABAergic strength below basal follicular levels. Progesterone fall at perimenstrual and post-partum phases has been found to induce a sharp reduction of the Allo in the brain, denoted as "Allo withdrawal". This condition has been associated to premenstrual syndromes, such as seizure susceptibility and anxiety [142-144]. In a rat model of this kind of syndromes, very low Allo levels are correlated to an increase of the expression of the $GABA_A$ $\alpha4$ subunit, inducing a reduction in $GABA_A$ activity [145].

This effect has been shown to depend on the upregulation of the transcription factor early growth response factor-3 (Egr3), resulting in a 6-fold decrease in the GABA$_A$ current time constant [146]. Hence, a corresponding reduction of GABA$_A$ ion current can be calculated. This estimate has been derived by us from the ion current decay equation:

$$C = C_0 * e^{\frac{t}{tau}} \qquad (14)$$

where C = current at time t, C_0 = current at time t = 0 (set to C_0 = 1), tau = time constant. Integrating for tau = 1 and tau = 1/6 as follows:

$$C_{TOT} = C_0 \int_0^{\infty} e^{-\frac{t}{tau}} dt \qquad (15),$$

an about 3-fold decrease of GABA$_A$ currents was inferred. Hence, by applying a 3-fold decrease to the previously derived follicular value of $a = 0.4$, a value of $a \cong 0.13$ was inferred for Allo withdrawal. We then derived Allo brain levels at withdrawal by considering an animal model of catamenial epilepsy obtained by exposure to the 5α-reductase inhibitor finasteride [147]. In female rats, finasteride has induced the decrease of Allo plasma concentration from 9 to 6 ng/mL. Hence, assuming a proportional reduction of brain Allo in the woman, and considering a brain follicular level of 2.4 ng/mL, we estimated Allo withdrawal at 1.6 ng/mL, that was put in correspondence with the above-derived value of $a = 0.13$. To summarize, the Allo effect on GABAergic transmission was modeled by considering two independent actions:

- Allo ranging from follicular to luteal and pregnancy levels, inducing a dose-dependent increase of the GABAergic transmission in response to positive allosteric modulation on GABA$_A$ receptors;

- Allo sub-follicular, withdrawal levels reducing the strength of GABAergic transmission because of a rearrangement of the α subunits of GABA$_A$ receptors.

Mathematically, two increasing Hill functions are used to model such a combined effect:

$$a = f_u(Allo) + f_p(Allo) \qquad (16),$$

where $f_w(A)$ is the withdrawal component:

$$f_u(Allo) = a_f * \frac{Allo^{h_u}}{\left(e_u^{h_u} + Allo^{h_u}\right)} \qquad (17),$$

$f_p(A)$ is the positive allosteric component:

$$f_p(Allo) = \left(1 - a_f\right) * \frac{Allo^{h_p}}{\left(e_p^{h_p} + Allo^{h_p}\right)} \qquad (18),$$

$Allo$ is the brain concentration of the neurosteroid, a is GABAergic strength, a_f is the value of a at the follicular value of $Allo$, e_u and h_u are the EC$_{50}$ and Hill coefficient for the genomic effect induced

by Allo withdrawal on the GABA$_A$ α subunit, and e_p and h_p are the EC$_{50}$ and Hill coefficient for the positive allosteric effect of Allo on GABA$_A$. For computational analysis, we adopted e_p and h_p values corresponding to the median values reported in Table 3. The parameters e_u and h_u are not available in the literature, except that steroid hormone genomic effects fit a Hill function. Therefore, considering that the withdrawal effect emerges at Allo sub-follicular levels, we used a Hill function with maximum at $a = 0.4$, asymptotically approaching this value from a value of *Allo* $\cong 2.4$, and admitting a solution for the above-reported values, *Allo* = 1.6, $a = 0.13$. The derived values for the parameters of the (17) and (18) Hill functions are reported in Table 4.

Table 4. Parameters of the Hill functions of equation (16).

Type of Allo effect	Range of Allo variation	Function	e (ng/mL)	h	a_f (ng/mL)
GABA$_A$ currents	Follicular-to-luteal	$f_p(A)$	18	2	0.4
Expression of the α4 subunit	Withdrawal-to-luteal	$f_u(A)$	1.8	6.5	0.4

The symbols are as in Table 3.

The equation (16) describes the predominance of the withdrawal effect of Allo on GABAergic strength for subfollicular brain levels, i.e. concentrations ranging between 0 – 2.4 ng/mL, while the positive allosteric GABA$_A$ modulation is predominant for Allo concentrations above 2.4 ng/mL. As shown in Figure 5, Allo withdrawal drives the coefficient a down to an estimated value of 0.13. To understand possible pathogenic consequences of such a decrease, this value must be related, on one side, to the bifurcation value $\hat{a}$, as determined by our computational model, and on the other side to the strength of glutamatergic transmission.

3.3.1.5.2. Influence of the HPA axis on the thalamocortical loop

Indirect data on N-methyl-D-aspartate receptor (NMDAR)-dependent cytosolic Ca^{2+} rise suggest that glutamate-induced excitotoxicity involves an about 100% increase of glutamatergic transmission [148], which can be assumed as maximum glutamatergic strength, corresponding to $b = 1$ in our model. Hence, we can assume that in our model a value of $b = 0.5$ represents physiological glutamatergic strength. According to the $b/\hat{a}$ relationship depicted in Figure 2, $b = 0.5$ corresponds to $\hat{a} = 0.116$, i.e. a bifurcation point that is close to, but still below, the value of $a = 0.13$ appraised for Allo withdrawal. However, if b reaches a value of 0.6, the bifurcation value

becomes $\hat{a} = 0.16$. Hence, a 20% increase of glutamatergic strength would be sufficient to drive the bifurcation point above the reduction of GABAergic strength imposed by Allo withdrawal.
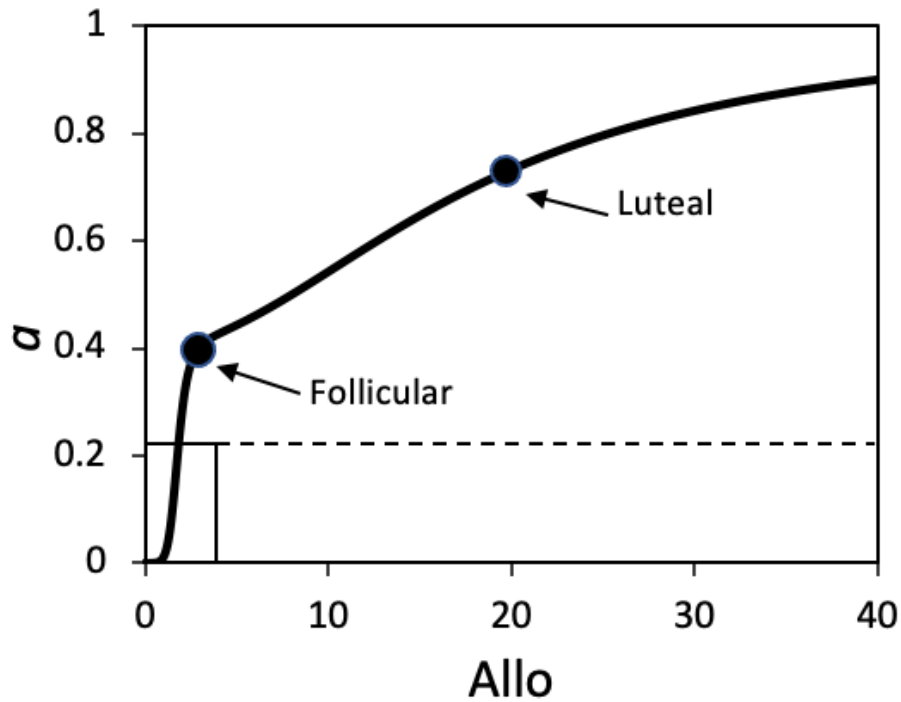
Figure 5. Plot of the variation of the coefficient a, representing GABAergic transmission strength, as a function of brain Allo levels, according to equation (16). The curve is the combination of two Hill functions representing two effects of Allo on GABA$_A$ receptors: in the lower Allo range an effect on the GABA$_A$ α subunit expression, while in the higher Allo range the positive allosteric effect on GABA$_A$ currents. The dashed horizontal line indicates the value of a corresponding to the bifurcation point $\hat{a}$ at the max glutamatergic strength ($\hat{a} = 0.265$, $b = 1$). The inset indicates the zone corresponding to Allo withdrawal, which includes the values assumed by $\hat{a}$ for $b = 0.5$ ($\hat{a} = 0.116$,), and for $b = 0.6$ ($\hat{a} = 0.16$).

It should be noted that the numerical values of our analysis have been estimated from indirect data, and therefore, they are not expected to exactly quantify real pathophysiological processes. However, we can conclude that a combination of strong GABAergic reduction and mild glutamatergic rise are likely to create a pathogenic functional state in the thalamocortical loop system. We then explored possible causes of an increase of glutamatergic transmission able to

induce an FM pathogenic condition. Consistent with the correlation between FM and acute or chronic stress, these causes should be looked for in the activation of the HPA axis.

Various data indicate that activation of the HPA axis under stress response has repercussions on GABAergic transmission, being part of the homeostatic mechanisms that limit the impact of HPA on the body's physiology [149]. Pituitary ACTH stimulates adrenals to release Allo and THDOC, both passing the brain barrier and acting as positive allosteric GABA$_A$ modulators [150]. Dehydroepiandrosterone (DHEA) and its sulphated derivative DHEA-S are also released by adrenals, acting as negative modulators of GABA$_A$ and positive modulators of NMDA glutamate receptors [150]. Hence, the panel of corticosteroids released upon HPA activation seems to induce a complex effect on central neurotransmission, in which the weights of the single components are difficult to evaluate due to the scarcity of quantitative data. However, it has been found that the first global effect of acute stress is a rapid decrease of GABAergic transmission together with an increase of glutamate transmission in brain areas involved in cognitive functions, such as prefrontal cortex and hippocampus [151, 152]. Moreover, chronic stress has a strong enhancing impact on the glutamatergic function possibly leading to excitotoxicity and neurodegeneration [153]. Hence, despite the existence of different endocrine homeostatic mechanisms that limit in time or moderate the stress response, a central GABA/glutamate unbalance in favor of brain network excitability can be considered a distinctive consequence of HPA activation. Such an effect can also be exacerbated under specific conditions, as reported by studies about a mental stressor test on humans. These experiments showed that the homeostatic Allo response to HPA activation was absent in postpartum women [154], and was negatively correlated with baseline Allo levels in men [155], thus possibly exacerbating the GABA/glutamate unbalance.

3.3.2. The endocrine loop
3.3.2.1. Double-inhibitory interplay between the HPG and HPA axes

In the arguments above, HPG and HPA axes have been considered to operate as single units, each affecting neurotransmission independently. However, evidence argues for the possibility that under specific conditions these axes behave as a unique system characterized by reciprocal inhibition on each other [108]. The consideration of the two endocrine axes as a unique system should not be considered as a universally valid paradigm as confirmed by inter-age and inter-subject endocrine variations [156, 157]. Literature data reported weak correlations between these axes in circadian or follicular-to-luteal fluctuations, while conversely, significant negative correlations were observed

for higher hormones fluctuations under perimenstrual, pregnancy, and stress conditions, or after pharmacological treatments [158]. Such a mutual inhibition of the endocrine axes has been reported to be involved in physiological processes [159, 160], but under specific conditions it could trigger pathogenic processes.

The inhibition of HPA is mediated by gonadal hormone activities. Androgens, progesterone, estrogens, and their metabolites modulate neurons belonging to the hypothalamic periventricular and paraventricular nuclei and the anterior pituitary. On the other hand, HPG repression is mediated by inhibitory activities of corticosteroids exerted on hypothalamic kisspeptin neurons, gonadotropin-releasing-hormone (GnRH) neurons, the anterior pituitary, and the gonads [159]. By analyzing progesterone and cortisol circadian levels in cycling and postmenopausal women, absent or slight correlations have been observed [161, 162]. Conversely, the HPG-HPA inhibitory interplay has emerged in case of higher hormone fluctuations. In gilt pigs, treatments inducing elevated concentration of cortisol, but not acute elevation, have inhibited the luteinizing hormone (LH) surge, and consequently estrus and ovulation [163]. Experiments on female monkeys have revealed decreased progesterone availability to target organs after cortisol tissue infusion [164]. By considering progesterone variations in pregnant women, an inverse correlation with cortisol has been found [165, 166], while intravenous cortisol infusion has caused transient progesterone, estrogen, and androgen suppression [167]. Studies performed on eumenorrheic women treated with hydrocortisone at early follicular phases have shown a scaling down of the pulse frequency of hypothalamic gonadotropin-releasing hormone (GnRH) and pituitary LH [168]. Allo and cortisol levels have been investigated in the premenstrual dysphoric disorder (PMDD), finding higher Allo and lower cortisol nocturnal levels compared with healthy controls [169]. In an *in vitro* cell culture-based study, cortisol has been found to cause pre-labor progesterone withdrawal in pregnant women, confirming its anti-progestinic effect [170]. The HPG-HPA interplay can also arise from an indirect mechanism due to the decreased availability in pregnenolone for progesterone synthesis during increased cortisol production [157].

In mammal males, interactions between the two endocrine axes have also been observed. In rams and bulls, after treatment with synthetic dexamethasone, lowering effects on testosterone and circulating LH have been observed [171, 172]. Pharmacological treatment in human adult males inducing plasma cortisol rise has shown a reduction on circulating testosterone concentrations [173]. Similarly, in human males the cortisol increase due to endurance exercise has induced a

reduction of testosterone, whereas conversely, testosterone replacement has lowered the cortisol excursion induced by corticotropin-releasing hormone (CRH) stimulation tests [174].

3.3.2.2. Molecular mechanism involved in the double-inhibitory interaction between HPG-HPA

The HPG-HPA inverse correlation can be explained by different mechanisms. In vertebrate models, HPG axis repression is due to stress-induced glucocorticoids which act by stimulating gonadotropin-inhibitory hormone (GnIH) neurons or by inhibiting GnRH neurons [175-177]. In experiments on castrated male rats, the release of CRH has been found to inhibit the LH release following electroshock-induced stress [178]. On the other side, in pregnant women and female rats HPA inhibition has been shown to depend on GABAergic inhibition induced by high Allo levels [179-181]. One of the widest hormones fluctuations in humans is plasma progesterone induced by LH surge at ovulation and during the luteal phase [182]. Pituitary LH secretion has been finely reconstructed in rodents [183, 184]. Two neural populations, one is located rostrally in the preoptic area (POA) and the other one more caudally in the arcuate nucleus (ARC), release the neurotransmitter kisspeptin which is known to activate GnRH neurons, thereby stimulating the pituitary [185]. The POA kisspeptin neurons induce the large GnRH and LH surge before ovulation and are modulated by a positive estradiol feedback [184]. The ARC kisspeptin neurons are responsible for the pulsatile, small GnRH and LH release and receive negative feedback by estradiol. Sexual dimorphism has been found in both neural populations in humans and sheep, while lower kisspeptin neurons were observed in male rodents in the rostral periventricular area of the third ventricle, possibly explaining male inability of mounting the estrogen-induced LH surge [186]. Even though gonadotropin release is modulated by estradiol, many GABA and glutamate receptors are expressed on GnRH and kisspeptin neurons, suggesting a relevant modulatory role for these neurotransmitters [187, 188]. GABA was reported to exert both excitatory and inhibitory effects on GnRH neurons [183, 189, 190], but only inhibitory effects on kisspeptin neurons [191, 192], while glutamate generally induces excitation on the same neurons [186, 193, 194]. However, the emerging effect is a GABAergic inhibition of LH surge [190, 195] and its stimulation by glutamate [103, 108]. The LH surge has also been found to occur concomitantly with a decline of GABAergic transmission, involving both GnRH neurons and POA kisspeptin neurons [193, 196].

By considering the HPA axis, CRH neurons of the hypothalamic paraventricular nucleus belong to an intricate neural circuit involving limbic, cortical, and brainstem areas, which modulate the endocrine response to psychosocial and environmental inputs. In addition, regulation orchestrated

by glutamate, GABA, and norepinephrine, is required to guarantee proper CRH neuron activity [197-199]. Glutamate exerts excitatory effects on CRH neurons, whereas GABA induces tonic and phasic inhibition by acting through extrasynaptic or synaptic receptors, respectively [200]. The CRH release is modulated by noradrenergic inputs which originate from the brainstem and act on peri- and paraventricular glutamatergic and GABAergic interneurons, respectively. Norepinephrine has been found to either suppress or enhance the GABAergic inhibitory activity, while the norepinephrine excitatory effect on the HPA axis mainly occurs via a glutamate release on CRH neurons [199].

The modulation of CRH neurons is the result of a complex polysynaptic route involving different brain regions that integrate social and psychogenic stressor stimuli. These pathways include the amygdala, prefrontal cortex, hippocampus, peri-paraventricular neurons, medial preoptic area, and the bed nucleus of the stria terminalis. The converging site of these routes is the GABAergic regulation of CRH neurons, which is stimulated by inputs deriving from the prefrontal cortex and the hippocampus (downregulating the stress response), and inhibited through the amygdala activation (stimulating the stress response) [201]. However, after acute and chronic stress, the GABAergic synapse shows different kinds of plasticity. For example, after norepinephrine increase due to stress conditions, the GABA synapse on CRH neurons becomes excitatory because of the disruption of the chloride gradient. This phenomenon attenuates the inhibition of GABA on the HPA axis [202].

3.3.2.3. Quantitative evidence of the double-inhibitory HPG-HPA interaction

To develop a mathematical model describing the interplay between HPG and HPA, we started by analyzing literature data about the correlation between plasma levels of gonadal hormones and glucocorticoids. As stated above, in studies on humans and animals, hormone measurements revealed positive correlations or weak correlations for hormone circadian oscillations [203-205]. On the other hand, significant negative correlations were shown by studies reporting the following data:

- glucocorticoid plasma concentrations after stress condition, together with the reciprocal gonadal hormone fluctuations

- gonadal hormone plasma concentrations induced by pharmacological treatments or by pregnancy, together with the reciprocal alterations of glucocorticoids (Table 5).

Dose-response relationships were obtained by using as input (independent) variable the plasmatic concentration of the hormone whose variations have been induced by reproductive,

environmental, or pharmacological effects, and as output (dependent) variable the values of the other hormone (Table 5).

Table 5. Parameters of the Hill functions obtained from different matched samples of gonadal hormone plasma levels and the corresponding corticosteroid plasma levels.

x^1	y^2	e^3	h^4	n^5	p^6	Species	Refs.
Corticosterone	Progesterone	1	4.2	6	< 0.001	chicken	[206]
Corticosterone	Testosterone	5	3.9	4	< 0.001	chicken	[206]
Cortisol	Testosterone	28	5.2	6	< 0.001	rabbit	[207]
Cortisol	LH	28	2.4	13	< 0.001	swine	[163]
Cortisol	Progesterone	23	8	8	< 0.001	humans	[208]
Cortisol	Testosterone	22	6	10	< 0.001	men	[209]
Cortisol	Testosterone	48	2.4	71	< 0.001	men	[173]
Progesterone	Corticosterone	32	3.5	11	< 0.001	chicken	[210]
Testosterone	Cortisol	17	7.3	6	< 0.001	rabbit	[207]
Testosterone	Cortisol	58	7.5	12	< 0.001	rabbit	[207]
LH	Cortisol	50	7.5	6	< 0.001	rabbit	[207]
LH	Cortisol	51	4.1	12	< 0.001	rabbit	[207]
Testosterone	Cortisol	23	1.5	71	< 0.001	men	[173]
Progesterone	Cortisol	64	3.8	23	< 0.001	women	[165]
Progesterone	Cortisol	65	8	6	< 0.001	women	[211]
		28^7	4.2^7				

[1]Variable used as input (hormone plasma levels standardized according to a [0,100] interval); [2]variable used as output (see input variable); [3]half-saturation constant of the Hill function; [4]Hill coefficient, [5]number of observations; [6]p-value of the correlation; [6]median values of half-saturation constants and Hill coefficient.

By considering the median value of the Hill coefficient for the endocrine axis interplay $h = 4.2$ (Table 5), and the Hill coefficient representing the allopregnanolone genomic effect on $GABA_A$, $h = 6.5$ (Table 4), it is worth noting that these values are higher than those belonging to the input-output neuron firing rate relationship of our thalamocortical model $h = 2.5$ [107], and the modulatory effect of allopregnanolone on $GABA_A$, $h = 2$ (Table 4). The Hill coefficient measures

the cooperativity between interacting systems [212]. Hence, the lower values of h reported for neuron electrophysiology with respect to that described for endocrine axes interplay can be taken as a confirmation that the Hill function is a suitable fit for the herein analyzed interactions, consistent with the notion that the Hill function fits stimulus-response data in a wide set of biological systems [46, 97, 213-216].

3.3.2.4. Dynamical model of the HPG-HPA interaction

After the estimation of the parameter values to be used in the mathematical expression of the inhibitory interplay between the HPG and HPA axes, we developed a mathematical model of the dynamical system. As reported from literature data, the activation of HPA and HPG is due to hypothalamic neurons receiving various inputs from different brain regions which are modulated, among others, by HPA and HPG hormones or their brain derivatives. Due to the paucity of quantitative and qualitative data for this set of interactions, we considered a schematic model including two macroscopic effects:

- the self-inhibition of each axis due to negative feedback loop;

- the double-inhibitory interaction between the two axes (mutual inhibition) emerging during wide fluctuations of corticosteroid and/or gonadal hormones.

We therefore considered a loop system made up of two elements, each representing one of the axes, as described in section 3.2.1.2.2, and illustrated in Figure 6.
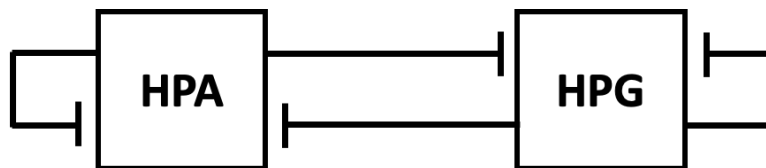
Figure 6. Simplified schematic diagram representing the double inhibitory and self-inhibitory loop system formed by the HPA and HPG endocrine axes. Line ends are as in Figure 1.

The system dynamics were mathematically described by two differential equations with two state variables representing the axis activities on a (0–100] scale (see section 3.2.1.2.2):

$$\tau \cdot \dot{H}_a = f\left(H_g\right) - \xi(H_a) \cdot H_a \qquad (9)$$

$$\tau \cdot \dot{H}_g = f(H_a) - \xi(H_g) \cdot H_g \qquad (10).$$

Such a mathematical model accounts for both the negative feedback of each axis (self-limiting factor) and the mutual inhibition between axes (double-inhibitory, positive loop). For each axis, the variation of activity over time depends on the activity of the other axis (mutual inhibition), according to a decreasing Hill function, and on itself, including a multiplying factor consisting of another decreasing Hill function (self-limiting element). The self-limiting functions $\xi(\cdot)$ are decreasing Hill functions that take values within the interval $(1,5)$ (section 3.2.1.2.2). When $\xi \to 5$, the self-limiting effect of each axis becomes dominant over mutual inhibition and the two axes behave as independent systems modulated by their own self-inhibition. On the other hand, when $\xi \to 1$, the mutual inhibition between the axes emerges and the system behaves as a double-inhibitory positive loop admitting two stable equilibrium points represented alternatively by high H_a and low H_g, or low H_a and high H_g. In the differential equations describing mutual inhibition both axes share the same parameters, which were set equal to the median values of data shown in Table 5. The time constant τ, representing the timescale of the response of each element, was set to 30 min, a common delay in endocrine responses. The parameters of the self-limiting Hill function were set so to obtain a system behavior consistent with the observed correlation pattern between HPA and HPG at different intensities of their activity. The parameter values are shown in Table 6.

Table 6. Parameter values adopted in the system of differential equations representing the interactions between the endocrine axes (see Section 3.2.1.2.2).

Interaction type	Form of the Hill function	Parameter value	Dimension
Double inhibitory interaction	$f(x) = \dfrac{100}{1 + \left(\dfrac{x}{e_x}\right)^{h_x}}$	$e_x = 28$ $h_x = 4.2$	ng/mL dimensionless
Limiting self-interaction	$\xi_x = 1 + \dfrac{4}{1 + \left(\dfrac{\alpha \cdot x}{e_\xi}\right)^{h_\xi}}$	$e_\xi = 25.57$ $h_\xi = 6.6$ $\alpha = 0.48$	ng/mL dimensionless dimensionless

The computational analysis of the system dynamics revealed the existence of three different stable equilibrium points, as represented by the phase portrait of Figure 7. As for FM pathogenesis, it is worth to consider the system behavior for extreme values of the variables *HPG* and *HPA*. When

both variables assume high values (upper-right corner in the phase portrait), $\xi \rightarrow 1$ for each axis, mutual inhibition between axes is stronger, and a positive loop is then established, which should drive the system trajectories towards either of the steady states at the upper-left or lower-right corner of the phase portrait. However, the mutual inhibition initially induces the decrease of both variables, which makes the value of ξ to increase, so that the self-limiting effect of each axis becomes stronger. Hence, the trajectories of the system end up converging to the steady state characterized by a low activity of both axes (lower-left corner in the phase portrait). More evidently, at low or medium activity of both axes the system falls on the same lower-left equilibrium point, having the widest basin of attraction (Figure 7).

Such a convergence of the system should not be a fixed point since endocrine axes undergo circadian fluctuations and never reach a constant level of activity. Hence the system trajectories should converge on a limit cycle having the form of a Lissajous figure, i.e. the combination of two independent cycles with different periods, describing the HPA and HPG circadian fluctuations. However, with the aim of building a pathogenesis model, these circadian fluctuations can be neglected because their range is confined with respect to the wide fluctuations expected to be relevant for FM pathogenesis.

On the other hand, when one variable is high and the other is low, the self-limiting loops do not dominate over the double-inhibition loop and the system tends to fall on either of the equilibrium points at the lower-right or upper-left corners of the phase portrait (Figure 7). The attraction basin of the lower-right equilibrium point is representative of a functional zone in which the HPG activity is very low, e.g. due to Allo withdrawal, whereas HPA has a high level of activity, e.g. due to stressful conditions.
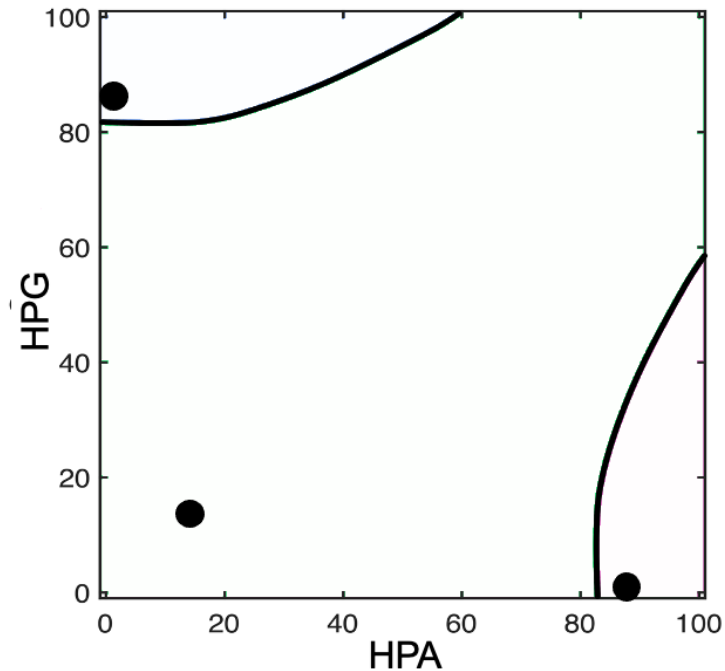
Figure 7. Diagram of the phase portrait of the loop system describing the mutual interaction between HPG and HPA, as reported in Figure 6. The diagram shows the basins of attraction (black lines) of three stable equilibrium points (black dots), derived through computational analysis by using equations (9) and (10) with the data of Table 6. The equilibrium point leading to FM pathogenesis is the point of convergence of the basin of attraction at the bottom right, corresponding to high HPA and low HPG values.

3.3.3. Comprehensive multistable model of FM pathogenesis

The HPA-HPG mutual inhibition gives rise to a positive loop and therefore, the dynamical system can be considered a candidate multistable system admitting multiple equilibrium points [29]. So, like the thalamocortical loop, the endocrine loop can behave as a switch giving rise to pathophysiological processes [44]. As previously reported, the switching of the endocrine loop to the steady state with high-HPA and low-HPG levels could induce sustained GABAergic weakening and glutamatergic strengthening in the thalamocortical loop involved in the pain processing pathway. These conditions increase the probability of the thalamocortical loop to cross the bifurcation point, with the result of a transition to bistability and an immediate tendency to fall on a steady state characterized by hyperexcitation, which is presumed to cause the development of FM (Figure 8). To conclude, the pathogenesis model that we have hypothesized, consisting of two dynamical systems interconnected with each other, explains the insurgence of FM by starting from the primary causes that perturbate the endocrine mechanisms. The resulting high-firing-rate activity

of the thalamocortical loop is assumed to induce disturbed pain processing accompanied by the insurgence of chronic pain. Moreover, cascade events depending on the pain processing disorder, or alternatively, a parallel occurrence of GABA/glutamate unbalance in other brain networks, could explain the set of symptoms that characterize, besides pain, the FM syndrome.
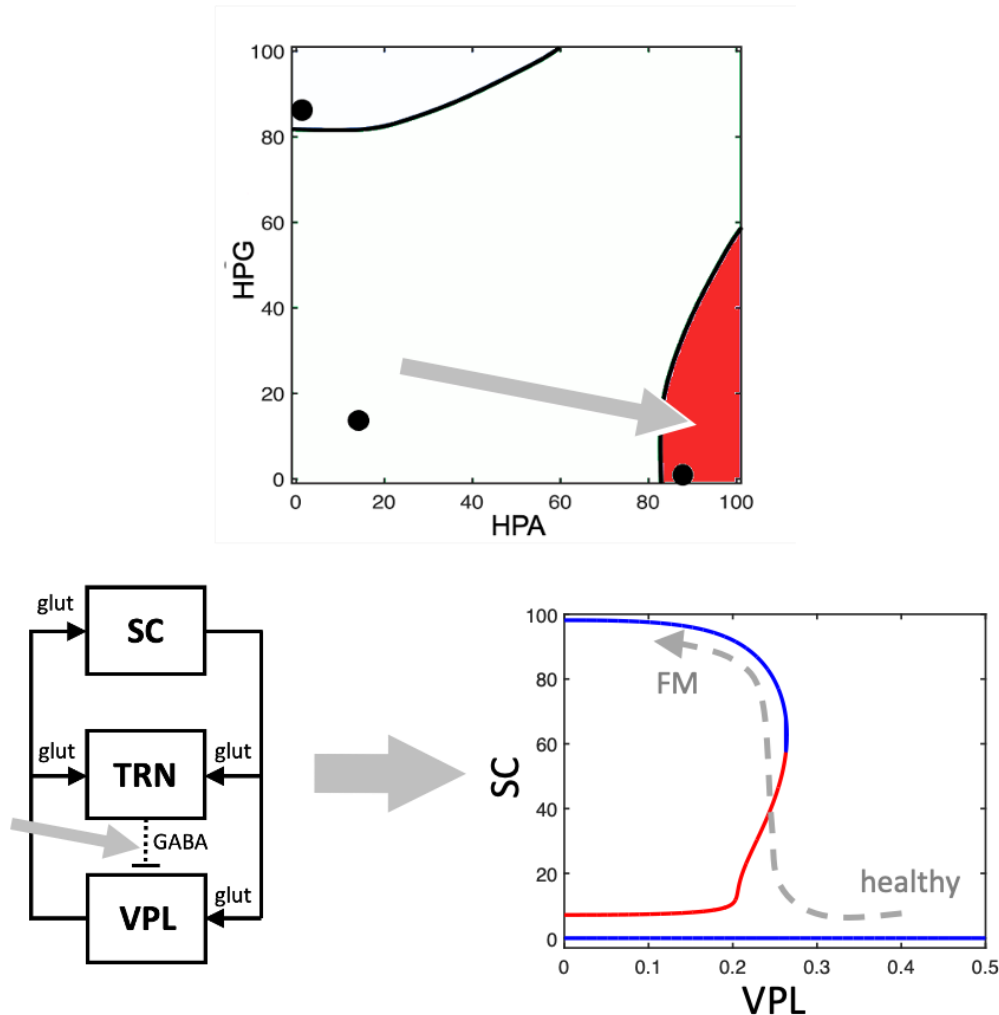
Figure 8. Schematic representation of the FM pathophysiological process based on the dynamics of our multistable model. If the endocrine dynamical system formed by the HPA-HPG mutual inhibitory interaction crosses the boundary of the basin of attraction with high HPA/ low HPG equilibrium point (top diagram, red area), then the GABAergic branch of the thalamocortical loop becomes weakened (left-bottom diagram). This functional state characterized by stress response corresponds to an increased value of b in the differential equations representing the thalamocortical system (see section 3.2.1.2), e.g. increasing from $b = 0.5$ to $b = 0.6$. The functional state also involves a value of $a < \hat{a}$ in the same equations, e.g. $a = 0.13, \hat{a} = 0.16$ (see section 3.3.1.5.2). Hence, the combination of GABAergic weakening and glutamatergic strengthening leads the thalamocortical system to cross a bifurcation point and to acquire bistability, with a tendency to jump to a high-firing-rate equilibrium point (right-bottom diagram). Top diagram: *HPA* and *HPG* are variables representing the percent activities of the HPA and HPG endocrine axes, e.g. cortisol (HPA) and

progesterone (HPG) plasma concentrations. Right-bottom diagram: bifurcation diagram showing curves reporting the steady states of variables S (primary somatosensory cortex) as a function of the bifurcation parameter a (see Figure 3), and depicting the transition of the thalamocortical loop from low-firing-rate equilibrium to high-firing-rate equilibrium for decreasing values of a.

3.3.4. First validation of the FM pathogenesis model by questionnaire data

3.3.4.1. Sociodemographic characteristics

The questionnaire survey received a total of 352 answers by FM patients. Only 324 participants expressed about the gender and 88% of these respondents were females. The average age was 47.9 years. Other main features were high education level (81% academic degree/upper secondary, PhD or equivalent), grey-collar or white-collar job (about 50%), and married or cohabitant (about 60%). Also, half of participants had children (Table 7).

Table 7. Demographic data (percent distribution) in the population of questionnaire respondents (n = 352)**.**

Gender	Female	Male	No answer			
	88.1	4.0	7.9			
Education	Primary	Lower secondary	Upper secondary	Academic degree	PhD or equivalent	No answer
	1.4	17	55.7	18.5	7.1	0.3
Marital status	Single	Married/ cohabitant	Separated / divorced	Widowed		
	22.2	59.9	15.6	2.3		
N. of sons	0	1	2	3	> 3	
	37.2	28.4	25.9	6.8	1.7	
Employment	Grey-collar	White-collar	Blue-collar	Shopkeeper	Unemployed	No answer
	39.8	11.9	8.8	3.4	35	1.1

3.3.4.2. Clinical features

Data showed diagnostic delay and age of onset consistent with statistics from similar studies. The obesity prevalence was confirmed by the body mass index (BMI > 30) (Table 8). FM participants reported symptoms other than pain and comorbidities as follows: brain fog, fatigue, sleep

disturbance, dizziness, anxiety, headache, photophobia, irritable bowel, depression, and diplopia. These symptoms are shown in Figure 9 together with their relative frequencies.

Table 8. Clinical characterization of participants (n = 352)**.**

	Min	Q1	Median	Mean ± s.d.	Q3	Max
Height (cm)	147	160	163	164 ± 6	168	193
Weight (Kg)	39	57	65	67.9 ± 15.4	76	125
BMI	15.6	21.3	24.2	25.3 ± 5.4	28.3	45.9
Patient age (years)	18	41	50	47.9 ± 10.8	56	86
Age-of-onset (years)	13	36	44	42.3 ± 10.1	50	83
Disease duration (years)	< 1	5	9	11.7 ± 9.3	15	49
Diagnostic delay (years)	< 1	1	3	6.35 ± 6	8	48
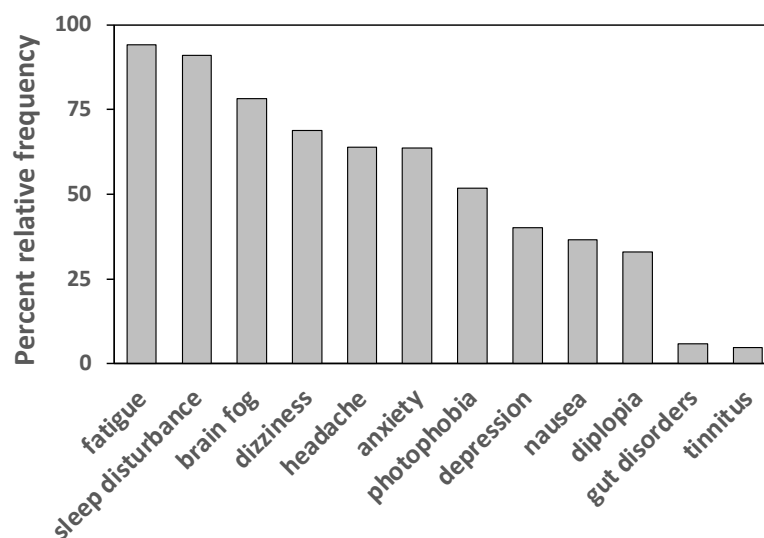
Figure 9. Symptoms aside from pain reported by questionnaire respondents and expressed as percent relative frequencies. (n= 352). Frequencies lower than 4% were not considered [217]. Reproduced with

3.3.4.3. Psychological profile

Concerning the psychological profile of the studied population, the clinical cutoffs of CBA-H scores showed the emergence of anxiety state, low mood, and excessive emotional involvement (Figure 10). The SREIS test indicated a high probability of emotional instability due to the ability of perceiving emotions, but with a low capacity of self-managing them (Figure11).
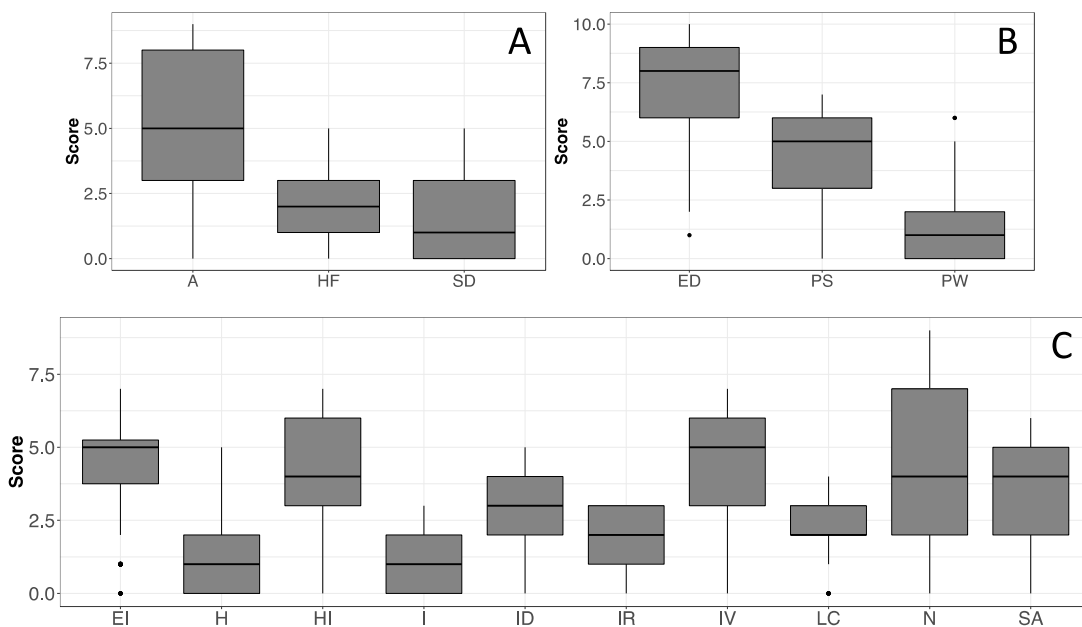
Figure 10. Boxplot of the CBA-H test score distribution, A, B and C sections. Scale legend, Part A: A = Anxiety state; HF = Fears associated with health-care routine; SD = Situational depression. Part B: PS = Psychophysical stress; PW = Perceived wellbeing; ED = Depression. Part C: HI = Haste and impatience; I = Irritability; H = Hostility; ID = Difficulties in interpersonal relationships, EI = Excessive emotional involvement; IV = State of introversion, IR = State of inability to relax; N = State of neuroticism; LC = leadership and competitiveness; SA = State of social anxiety (n = 352) [217]. Reproduced with permission from Healthcare [217], Creative Commons Attribution (CC BY) license (https://creativecommons.org/licenses/by/4.0/).
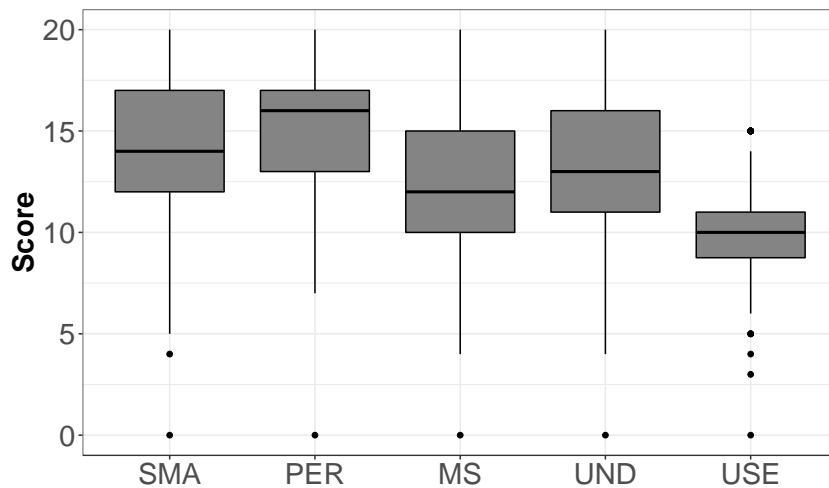
Figure 11. Boxplot of the different scores of the SREIS test. Scale legend: PER = Ability of perceiving emotions; SMA = Ability of social management of emotions; USE = Use of emotions; MS = Ability of managing emotions "self"; UND = Ability of understanding emotions (n = 352) [217]. Reproduced with permission from Healthcare [217], Creative Commons Attribution (CC BY) license (https://creativecommons.org/licenses/by/4.0/).

3.3.4.4. Evaluation of Pain

Participants reported an average pain intensity of 6.4 ±1.8, on a scale ranging from 0 to 10. This value refers to the week before the questionnaire compilation. A large portion of patients reported a pain level above 6, meaning moderate-to-severe pain. Among the values of the different types of pain, pressure pain emerged as the most frequent. In dendrogram analysis, pressure pain resulted the most uncorrelated from the other pain types, which in contrast formed correlated clusters (Figure 12).
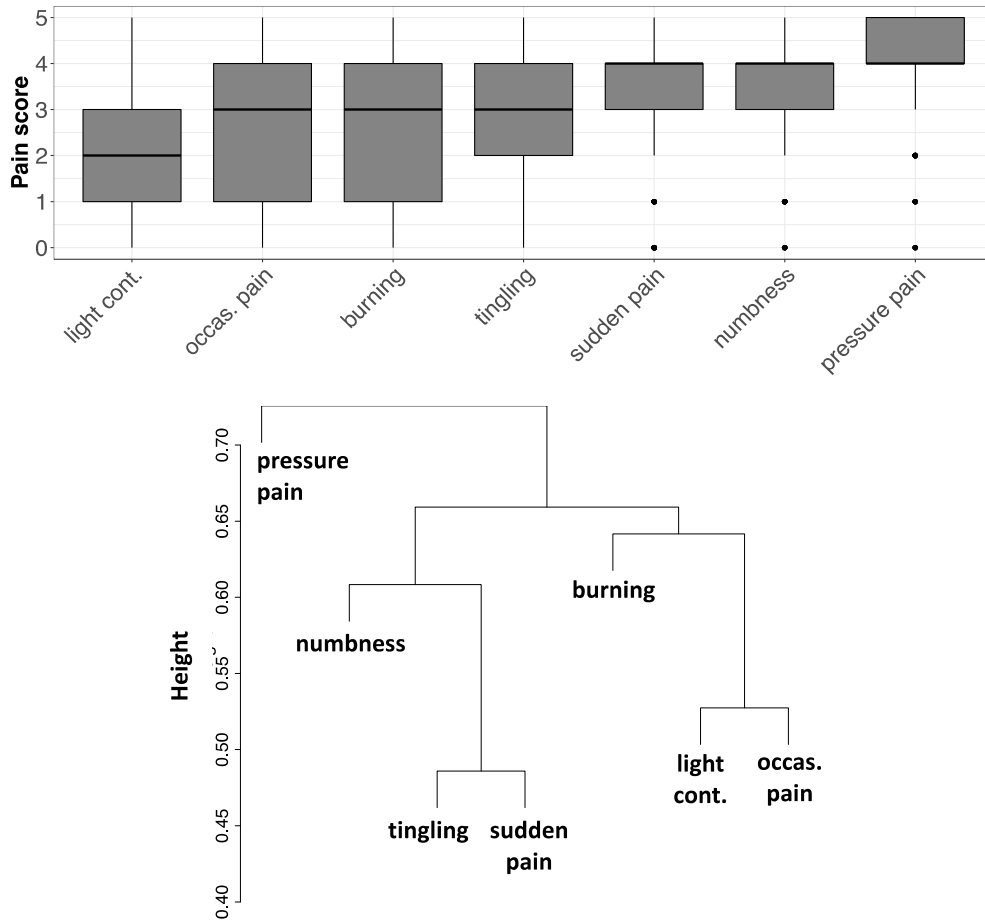
Figure 12. Scores of each pain type reported by patients (n = 352). (Top) Boxplots of each pain type experienced by subjects during the last week before answering the questionnaire. (Bottom) Pain type cluster dendogram obtained by average linkage of pairwise correlations (distance = 1 − correlation coefficient). Legend: occas. pain = occasional pain, light cont. = light contact [217]. Reproduced with permission from Healthcare [217], Creative Commons Attribution (CC BY) license (https://creativecommons.org/licenses/by/4.0/).

The PD-Q test (Cronbach's alpha= 0.78), characterizing peripheral or central pain, highlighted the prevalence of elevated scores, with a mean value of 21.48, a median of 22, and an interquartile ranging from 17 to 27. Participants were subdivided into three specific pain categories, defined by the test cutoffs: high, low, and intermediate levels (Figure 13). From this analysis, a marked prevalence of high scores emerged, meaning a prevalence of pain associated to central pain processing [110]. Such a result is consistent with the notion of nociplastic pain used to characterize FM painful symptoms [218].
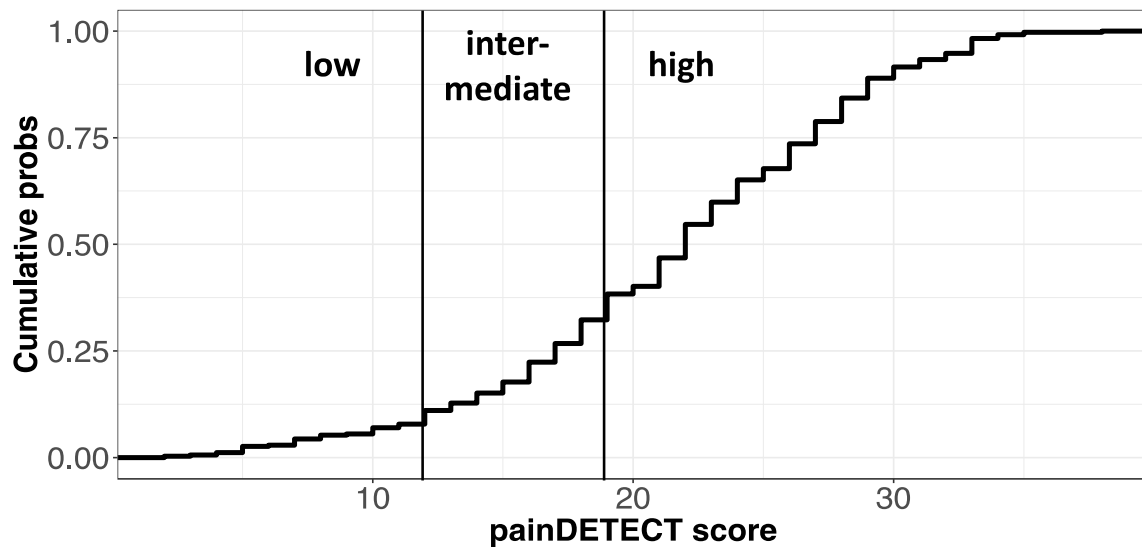
Figure 13. PD-Q score cumulative frequency, including cut-offs (vertical lines) for pain categories indicating increasing likeliness for central pain (n = 344). Score classification into three groups according to pain categories revealed a significant divergence from uniform distribution (χ-squared test, $p < 0.001$) [217]. Reproduced with permission from Healthcare [217], Creative Commons Attribution (CC BY) license (https://creativecommons.org/licenses/by/4.0/).

A correlation analysis between PD-Q scores and CBA-H cut-offs showed that when CBA-H indicated a clinical concern in a specific category, the PD-Q score was higher (Figure14). Significantly higher PD-Q scores were found associated to health-care related fears, inability to relax, interpersonal difficulties, situational depression, impatience, and haste. Consistently, an opposite trend was found for psychophysical wellbeing.
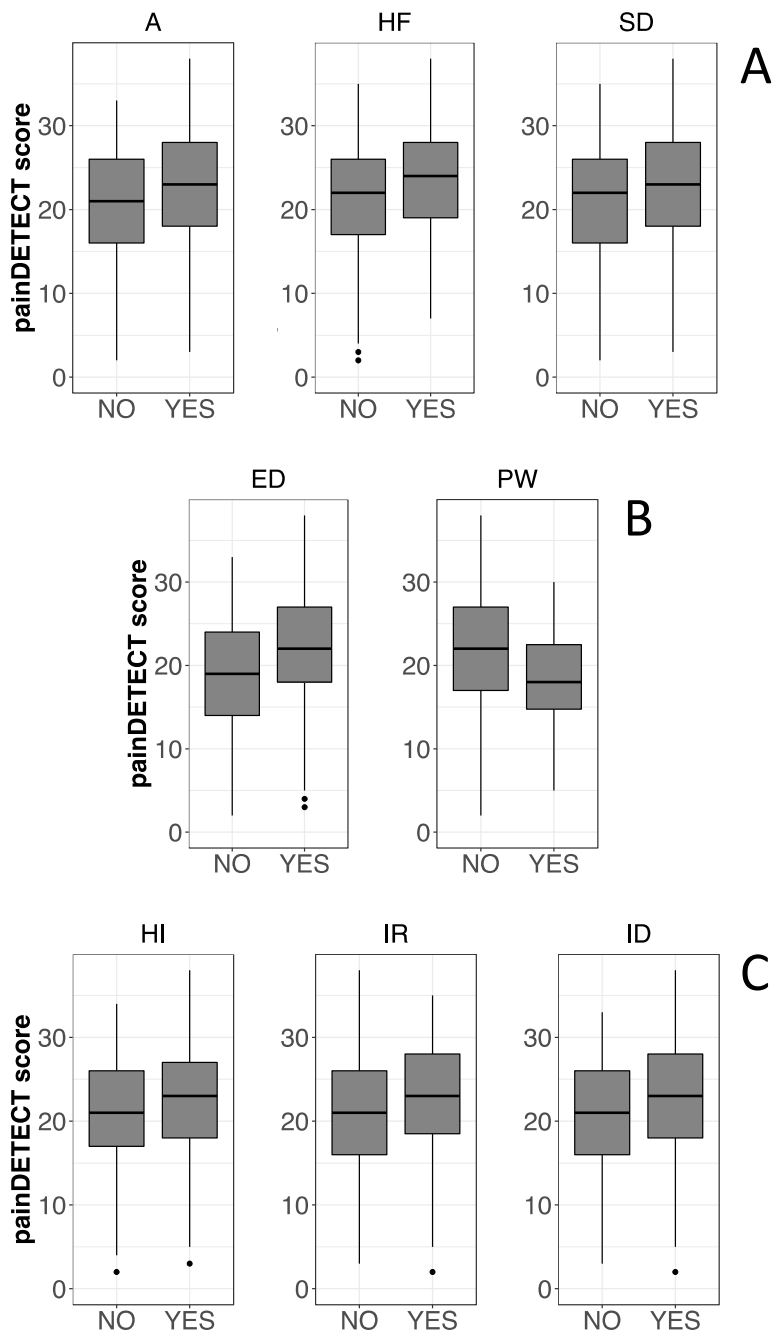
Figure 14. Correlations between CBA-H categories and PD-Q. For each CBA-H category, PD-Q scores were classified according to the related cut-off and the obtained two data groups were represented by boxplot diagrams. The two groups are indicated by the labels YES (altered condition), and NO (unaltered condition), except for Psychophysical wellbeing (PW) where YES represents the unaltered condition. The boxplots are relative to the categories for which significant differences were observed (p < 0.05. Mann Whitney). (A): HF = Fears related to health care; SD = State of situational depression; A = State of anxiety. (B) ED = State of depressive mood; PW = State of psychophysical wellbeing. (C) HI = State of haste and impatience; IR = State of inability to relax; ID = Difficulties in interpersonal relationships [217]. Reproduced with permission from

3.3.4.5. Effectiveness of treatments

The effectiveness of therapies that was reported by participants showed prevalently a better response to non-pharmacological than to pharmacological treatments (Figure 15). Such a difference was confirmed by a dendrogram analysis that revealed the clustering of most non-pharmacological treatments (Figure 15). PD-Q test categories were used to further explore the patterns of the perceived therapy effectiveness. Each therapy was reported in terms of average effectiveness perceived by subjects who were classified as "high" or "low" in the PD-Q test. The related plot confirmed the higher efficacy of non-pharmacological treatments with respect to pharmacological ones, except for instrumental physical therapy and acupuncture. Also, subjects rating as "low" in the PD-Q test were associated to higher effectiveness for most therapies, suggesting a negative correlation between the degree of pain and the effectiveness of treatments (Figure 15). Statistical comparisons by the Wilcoxon test showed that non-pharmacological treatments were judged more effective than pharmacological ones by the whole population of patients (n = 344, p = 2.03e-11). The same result was obtained by analyzing separately "high" subjects (n = 233, p = 5e-08) or "low" subjects (n = 38, p = 0.018). Mind-body therapies were reported as the most effective in absolute.
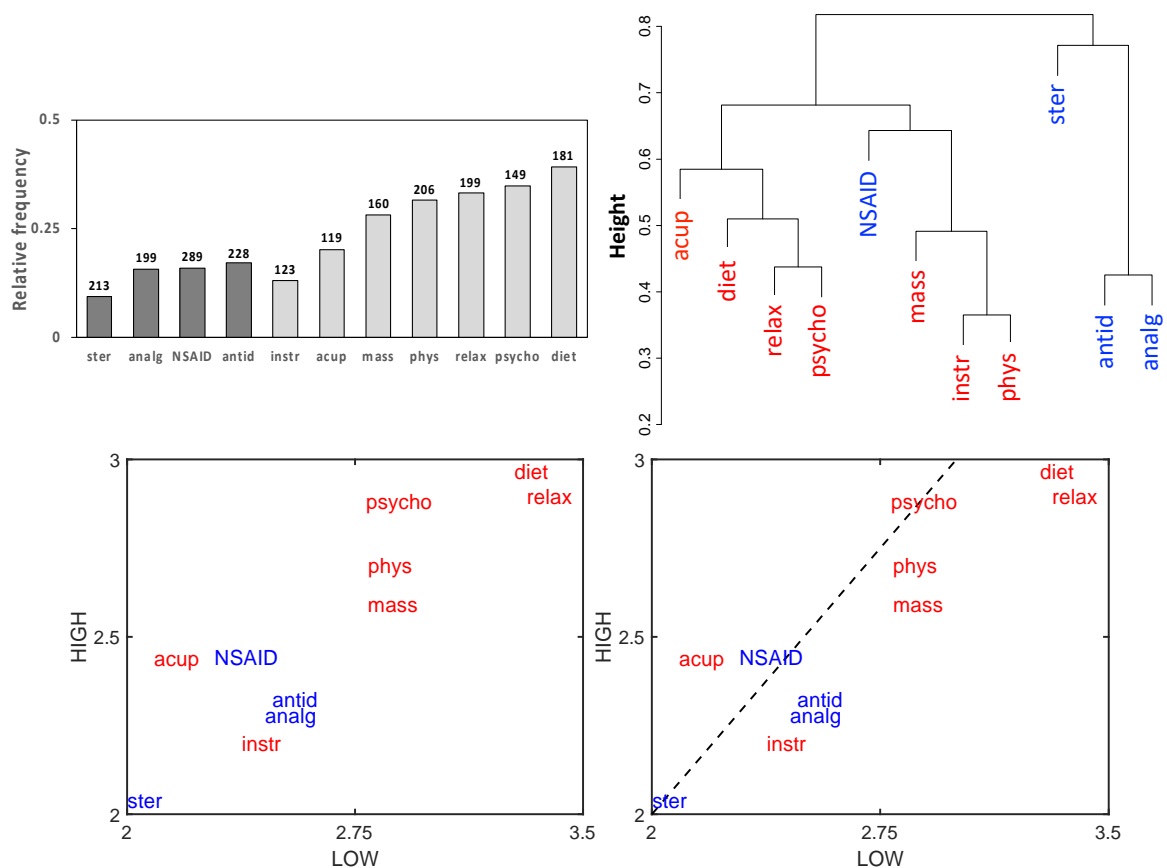
Figure 15. Efficacy of therapies as classified by FM patients. (Top left chart) Bars indicate the sum of the relative frequencies of the 2 top ratings (namely 'good' and 'excellent') out of 5. The number above each bar indicates valid responses. Lighter bars: non-pharmacological therapies; darker bars: pharmacological therapies. (Top right chart) Average-linkage dendrogram based on pairwise correlations among therapies. Pharmacological therapies = blue; non-pharmacological therapies = red (see Figure 12). (Bottom charts) Plots of the averages of therapy efficacies calculated from the values reported by subjects classified as 'low' or 'high' in the PD-Q test. In the left bottom chart, the perpendicular dotted lines intersect the axes at global average values. In the right bottom panel, the dotted line is the axes bisector. Non-pharmacological therapies: mass = treatment with massage; acup = treatment with acupuncture; psycho = treatment with psychotherapy; phys = treatment with physical therapy; diet = treatment with diet; relax = treatment with relaxation; instr = treatment with non-invasive instruments. Pharmacological therapies: NSAID = non-steroid anti-inflammatories; analg = analgesic drugs; antid = antidepressant drugs; ster = steroid drugs. Reproduced with permission from Healthcare [217], Creative Commons Attribution (CC BY) license (https://creativecommons.org/licenses/by/4.0/).

By considering the intensities of the different pain types, the higher effectiveness of non-pharmacological therapies with respect to pharmacological ones was confirmed, even though increased pain severity was often associated to a reduction of non-pharmacological prevalence (Figure16).

The correlation between the perceived effectiveness of non-pharmacological and pharmacological treatments and the CBA-H clinical cutoffs showed that the efficacy of non-pharmacological treatments could depend on the psychological profile of patients, with lower effectiveness perceived by patients with introversion, interpersonal difficulties, inability to relax, and emotional instability (Figure17).
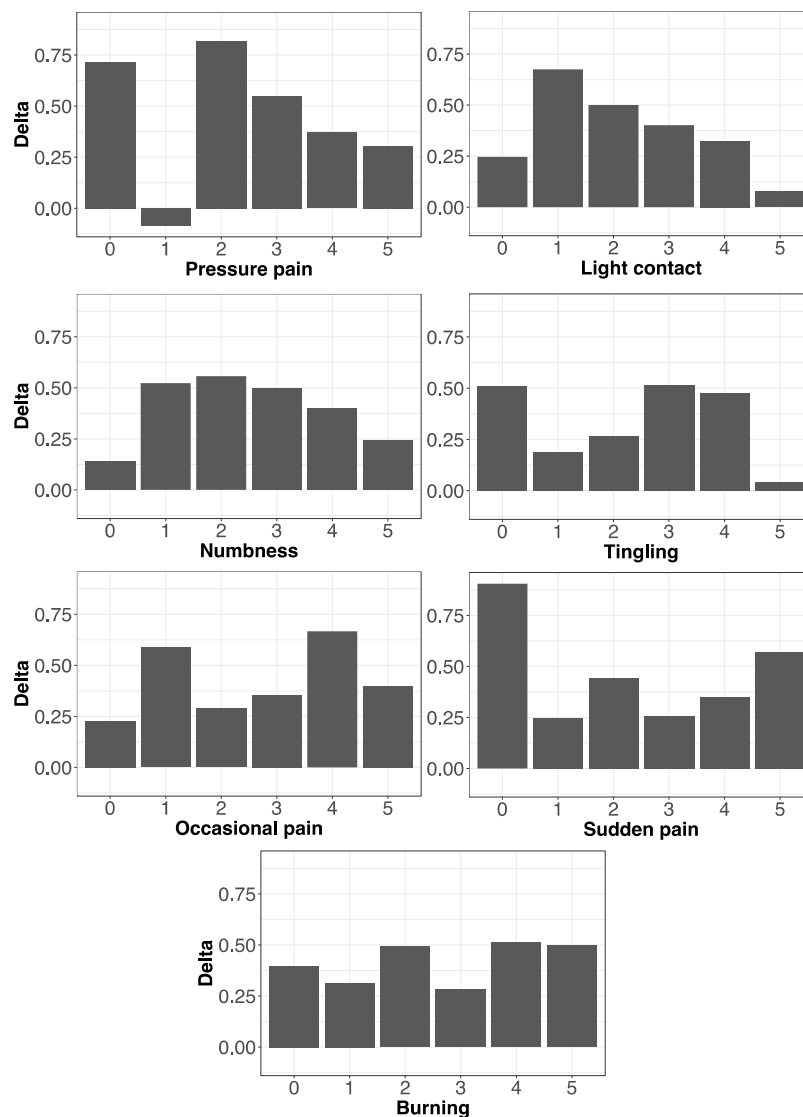
Figure 16. Efficacy of treatments classified by the intensity of pain types. The delta between the average efficacies of non-pharmacological and pharmacological therapies is calculated for each pain type at different
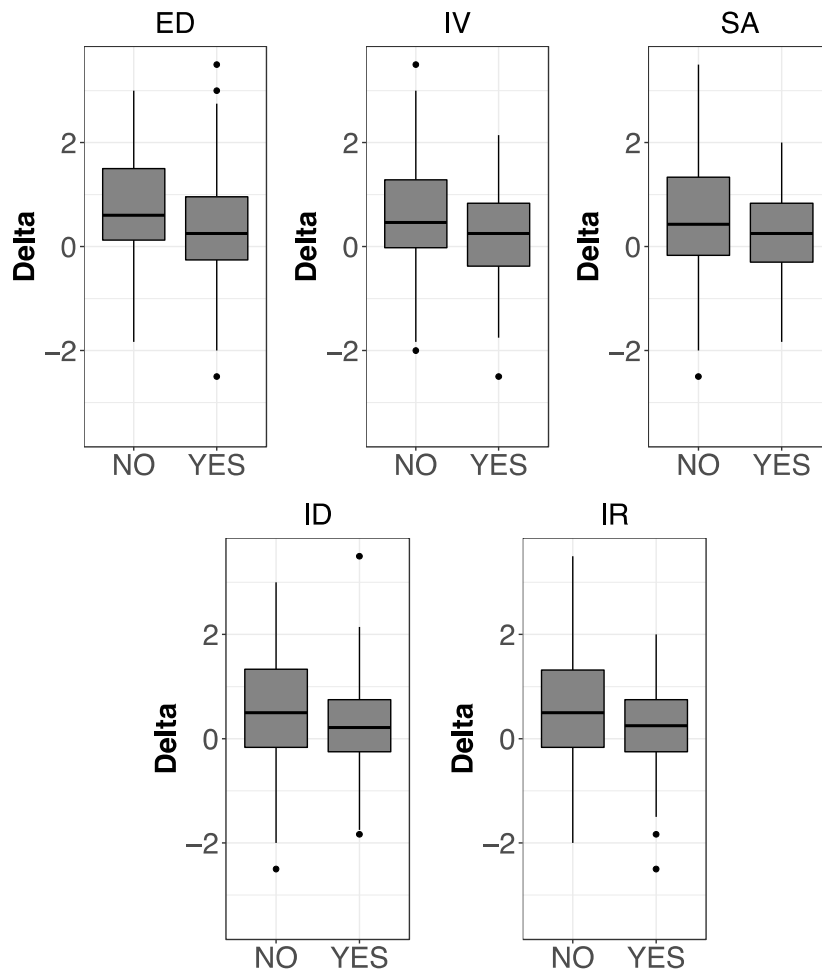
Figure 17. Boxplots of the delta between the average efficacies of non-pharmacological and pharmacological treatments (see Figure 16) for different categories of the CBA-H test. The YES and NO conditions are based on the cutoffs of the CBA-H categories (see Figure 14). Only categories showing significant differences between YES and NO conditions are reported (Mann Whitney, $p < 0.05$). ED = State of depressive mood; ID = Difficulties in interpersonal relationships; SA = State of social anxiety; IV = State of introversion; IR = Inability to relax. Reproduced with permission from Healthcare [217], Creative Commons Attribution (CC BY) license (https://creativecommons.org/licenses/by/4.0/).

3.3.4.6. Correlations between pain scores and vestibular symptoms

The statistical analysis of SVQ and DHI scores showed higher values in FM patients with respect to control subjects (Figure 18). These differences were statistically significant ($p < 0.01$) according to the Wilcoxon rank sum test, revealing a higher incidence of vestibular symptoms in FM patients.

In addition, the correlation between DHI and PD-Q scores was measured by the Spearman's rank correlation coefficient, finding a value of $\rho_s = 0.443$. The correlation between DHI scores and pain intensity in the last week showed a Spearman's rank coefficient of about 0.346. Similarly, SVQ scores were correlated with pain intensity and the PD-Q test, with $\rho_s = 0.253$ and $\rho_s = 0.349$, respectively. These correlations revealed higher scores of DHI and SVQ are associated higher intensities of perceived pain.
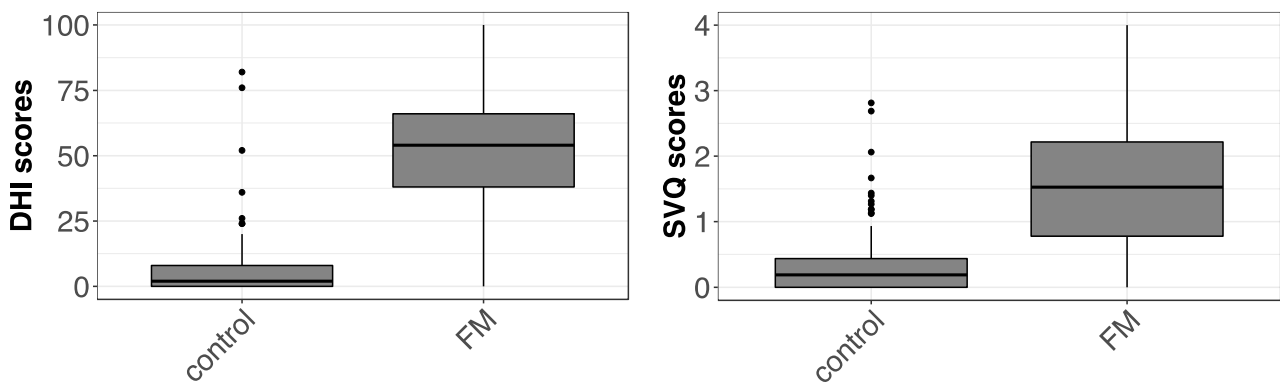
Figure18. Boxplot charts of the Dizziness Handicap Inventory (DHI) scores, and the Situational Vertigo Questionnaire (SVQ) scores recorded in control subjects and FM patients participating in the questionnaire.

3.4. FM pathogenesis model: Discussion

3.4.1. Consistency between the model and clinical data

We have explained a pathogenesis model of FM supported by experimental evidence reported in the literature. This model starts from previous studies from our laboratory, concerning a thalamocortical loop network system [107], and a literature review of FM during pregnancy [219]. The new model explains the link between FM brain network dysfunctions and constitutive or environmental conditions such as sex and stressful stimuli, which are strictly correlated to FM insurgence. The link between these elements consists in the modulation performed by the HPG and HPA axes on pain-processing pathways, possibly causing disorders also in other brain regions through cascade or parallel processes, and supposed to give rise to the wide cluster of FM symptoms.

Our model predicts that low HPG activity is an essential condition for the development of FM. This is supported by epidemiological data about the higher incidence of FM symptoms in women with suspected or proven infertility caused by gynecological disorders. Also, the model is based on the mutual inhibition between HPG and HPA, and this view is supported by evidence that some gynecological disorders, including ovarian dystrophy, ovarian cysts, uterine disorders, menstrual

alterations, miscarriage, and stillbirth, have been related to HPG depression caused by HPA hyperactivation [220]. Furthermore, our model is confirmed by data about the alleviating effect of progesterone and testosterone, but not estradiol, on FM pain severity [124].

The model also provides an explanation for FM female prevalence. In females, progesterone and Allo levels sharply decrease in prepartum and premenstrual phases, causing Allo withdrawal in the brain. Therefore, the possible combination of stress conditions, inducing HPA upregulation, with an abrupt neurosteroid fall is expected to amplify the unbalance between HPG and HPA activity, thus creating the thalamocortical hyperexcited state that is considered pathological according to our model. In males, Allo levels also undergo variations but with lower fluctuations [155], thus reducing the probability of FM insurgence. Female prevalence could also be explained by considering the positive modulation of estradiol on the NMDAR glutamate receptor [221], acting in antagonism to progestin positive modulation of $GABA_A$. Moreover, in women the maximum efficacy of the HPA activator ACTH occurs between 30-60 years of age [222], corresponding to the age range of maximum FM incidence. Conversely, in men ACTH efficacy has been found to decrease in the same period [222]. Finally, a reduction of the negative feedback of HPA induced by cortisol has been observed in aging women [223].

The explanation of a new mechanism of FM pathogenesis by our model suggests the identification of new therapeutic targets. Neurosteroids are hypothesized to be the factors mediating the effects of HPG and HPA variations on the central nervous system. This prediction is supported by correlations between neurosteroids and neurological alterations including epilepsy, psychiatric disorders, anxiety, and post-partum depression [146, 224]. The most studied condition from this point of view is catamenial epilepsy, consisting in the exacerbation of perimenstrual seizure. The pathogenic mechanism of this disease involves the alteration of various steroids, such as THDOC, DHEA-S, cortisol [225], and/or premenstrual Allo withdrawal [226]. The above-cited PMDD is another example of disorder involving an increased sensitivity to stress during the late luteal phase caused by low Allo levels, involving a reduced GABA control of the HPA axis [227].

Even though the pathogenic mechanisms of these disorders have not been fully disclosed yet, neurosteroids seem to be unquestionably involved, suggesting the development of therapies based on these compounds or their synthetic analogues. Many neurosteroids acting as positive allosteric modulators of $GABA_A$ receptors have shown anticonvulsant effects in preclinical studies performed on catamenial epilepsy models in the rat [228]. Progesterone has been tested in preclinical studies, as well as its synthetic progestin norethisterone and the gonadotropin antagonist goserelin [144,

226]. Neurosteroids with positive GABA$_A$ modulation have both antidepressants and anxiolytic properties, while their targets include both γ-type and δ-type GABA$_A$ receptors, whereas benzodiazepines act only on γ-type ones, possibly explaining the absence of antidepressant effects of these latter [229]. The efficacy of neurosteroids has been confirmed in different psychiatric alterations, such as insomnia and essential tremor [229], in accordance with the hypothesis that these syndromes could share similar neural alterations [230]. Different neurosteroids have been already tested in clinical trials, among which brexanolone has been already approved by FDA for the treatment of post-partum depression. The administration of this drug is complicated by the need of infusion and by relevant side effects, including nausea, somnolence, and dizziness [231]. Zuranolone (SAGE-217), an analogous of brexanolone with good oral bioavailability and lower side effects, has been tested for severe depression conditions [232, 233], and has been approved by FDA for post-partum depression [234].

3.4.2. Consistency between the model and questionnaire results

By using an online validated questionnaire, we aimed at obtaining information about FM patients, consistent with the idea of FM as a central, multisensorial syndrome. The analysis of the main clinical and sociodemographic features of participants confirmed the standard profile of FM patients. A significant female prevalence emerged, with symptoms generally starting at adult age prior to menopause. Aside from pain, other symptoms were reported by patients, in accordance with current FM diagnostic guidelines [61]. Difficulties in the clinical management of patients were confirmed by the diagnostic delay (mean = 6.35 ± 6 years) and the poor outcome of pharmacological treatments, in most cases less efficient than body-mind applications. These drawbacks are possibly linked to poor knowledge of etiology and lack of clinical biomarkers. According to the EULAR recommendations (European League Against Rheumatism), a prompt diagnosis is fundamental to select the correct treatments and for a better patient management in terms of symptoms such as pain and also from the psychosocial point of view [235].

Overall, the questionnaire data provide support to our model, suggesting the nature of FM as a central problem with sharp female prevalence.

3.4.3. FM as a multisensory disorder

The known pattern of pain perceived by FM patients was confirmed by our data. Pressure pain resulted the dominant pain type, consistent with the diagnostically relevant presence of tender

points in the disease. The CBA-H test indicated the absence of true psychopathological disorders, but nevertheless, the significant presence of low mood, anxiety, and emotional discomfort related to pain. Hence, high pain scores could reflect an overestimation deriving from pain catastrophizing [236]. These results are consistent with the revised pain definition established in 2020 by the International Association for the study of Pain: "An unpleasant sensory and emotional experience associated with, or resembling that associated with, actual or potential tissue damage", highlighting that pain is a personal experience influenced by physiological and psychosocial factors, and that individuals develop the concept of pain through their life experiences [237].

Aside from pain, other symptoms are consistent with typical FM patterns, while problems concerning vestibular perception, vision, and tinnitus suggest that a hypothesis of FM as a multi-sensory disorder deserves to be considered [238]. The emergence of different sensory alterations suggests the possible relevant role of the thalamus in FM insurgence, also considering the similarities in the thalamocortical arrangement of visual and pain processing [115, 239]. In conclusion, our data confirmed the new idea of FM as a multisensory, central disorder, in contrast with the idea of chronic pain disorder, and more in line with that of a central sensitivity syndrome [240].

3.4.4. Better efficacy of non-pharmacological therapies compared to pharmacological ones

The higher scores recorded for the efficacy of non-pharmacological treatments with respect to pharmacological ones highlights that the FM central disorder also involves the emotional spheres [241]. The preference for non-pharmacological treatments could indicate that these therapies alleviate the side effects of drugs. However, the apparent higher efficacy of diet, relaxation, and psychotherapy suggests that these treatments could act closer to the factors responsible for the onset of the disease [242, 243]. By contrast, the drugs that at present obtain the greatest consensus among physicians, including the antidepressants duloxetine, minalcipran, and amitriptyline, and the gabapentinoids gabapentin and pregabalin, have scarce effects on FM critical targets [244].

3.5. FM pathogenesis model: Conclusions

As shown above, the management of FM is disappointing, as confirmed by the low efficacy of both pharmacological and non-pharmacological strategies [217, 244-246]. According to our model, it is possible to envisage that neurosteroids could be a new pharmacological option because of their modulatory activity on $GABA_A$ receptors. Benzodiazepines share the same target of neurosteroids

but they have no effect in FM patients [247]. On the other hand, neurosteroids are characterized by different pharmacological properties on $GABA_A$ receptors. Moreover, they are suitable to contrast the endocrine conditions that according to our model would trigger the disease. Neurosteroids are known for the treatment of neuropathic pain [248], but they have never been considered as a therapeutic option for FM. Conversely, our model predicts that neurosteroids could have a role in reverting the process of FM pathogenesis, thus providing insight for a link between this disease and different central disorders that are also prevalent in females. Consequently, our analysis suggests the use of synthetic or natural $GABA_A$-active neurosteroids, or compounds with similar targeting properties, as a possible new horizon for the treatment of FM.

4. DEVELOPMENT OF AN *IN VITRO* MODEL OF BRAIN NETWORK AND ANALYSIS OF ITS FUNCTIONAL FEATURES

4.1. *In vitro* brain network: Background

Brain networks are the high-order units of the human brain, consisting of a system of neural networks, i.e. dense networks of synaptically interconnected neurons. Hence, the human brain is characterized by an enormous complexity both from the biochemical and the morphological points of view. This poses strong limits to the understanding of the basic processes that rule the functioning of our brain. Investigating and analyzing these processes is therefore fundamental to understand how brain networks can move from a state of good functioning to a state of altered functioning. Our goal is therefore to build unifying models able to explain and predict the development of these neural processes.

By following the Loopomics hypothesis [44]**,** in neural network disorders the pathogenic process can be modeled as an alteration of brain or neural networks arranged as loop systems. Therefore, the pathophysiological events leading to the disease should be studied by analyzing the dynamics of suitable network loop models. However, the optimal modeling of these loop systems requires to achieve detailed knowledge of the pattern of signal transmission among different neurons in neural networks, and among different neuron populations in brain networks. Such a goal can be pursued experimentally by reconstructing *in vitro* a system of different, interconnected neuron populations simulating a brain network, and then studying its dynamics through MEA devices.

Neural and brain networks are made up of different cell types, but the electrophysiological signals of neurons are a preferential readout since they can be accurately measured at different time and space scales. Various signals of neurons, including spikes, bursts, and local field potentials, can be recorded and analyzed [249]. Moreover, at the level of area subdivision, there is functional segregation for different stimuli. These properties are fundamental to obtain the rapid extraction of information and the generation of correspondent brain states [250].

Studies on the architecture of structural and functional brain networks have revealed that brain areas are not randomly and completely interconnected with each other [251]. Specific interconnections are generated by following a rather organized order where network communities interlinked by hub regions mediate communications processes between modules [251]. Literature data revealed significant evidence for modularity in neural systems and this property is of particular interest because blocks or subnetworks that are densely connected often correspond to specialized functional components. The correspondence between the functioning of brain processes and the

underlying connectivity dynamics is crucial not only for a basic knowledge of physiological processes but also for a targeted intervention on these processes in case of dysfunction [252, 253].

The MEA technology can be used to study neural networks and to map the propagation of the electrophysiological activity among different neural populations. This technique allows to explore the possible interplay between connectivity and patterns of spontaneous [254], and stimulus-evoked activity [255]. Questions about brain circuitry, dynamical states, and their interactions can be satisfied thanks to these *in vitro* models representing an optimal compromise between real brain and theoretical models. We have developed an *in vitro* model of brain network, by growing a system of different neuron populations on a MEA device and recording the electrophysiological activity of the system at multiple sites. This experimental model has allowed to disclose the essential elements of the activity pattern of the brain network, which realize the characteristic nonrandom features of its functioning.

4.2. *In vitro* brain network: Materials and methods

4.2.1. Realization of polymeric devices to be used on Micro-Electrode Arrays

Multiple network systems were realized *in vitro* by shaping network connectivity with polydimethylsiloxane (PDMS) polymer constraints. Circle masks and cross-shaped masks were fabricated from a mixture of PDMS prepolymer and the curing agent (Syligard 184, Sigma Aldrich) at a 10:1 (w/w) ratio and polymerized in an oven at 80 °C for 20 min. Circle masks were used to prepare one-network systems (1N). Cross shaped masks were used to separate four different interconnected regions and consist of cross-shaped plastic separators able to realize four compartments, obtaining four-network systems (4N) (Figure 19). The cross arms were about 2 mm long, 0.6 mm wide, and 0.3 mm thick. Both PDMS masks were sterilized in 70% ethanol for 20 min before being positioned on the active area of MEAs in a reversibly and perfectly aligned way.
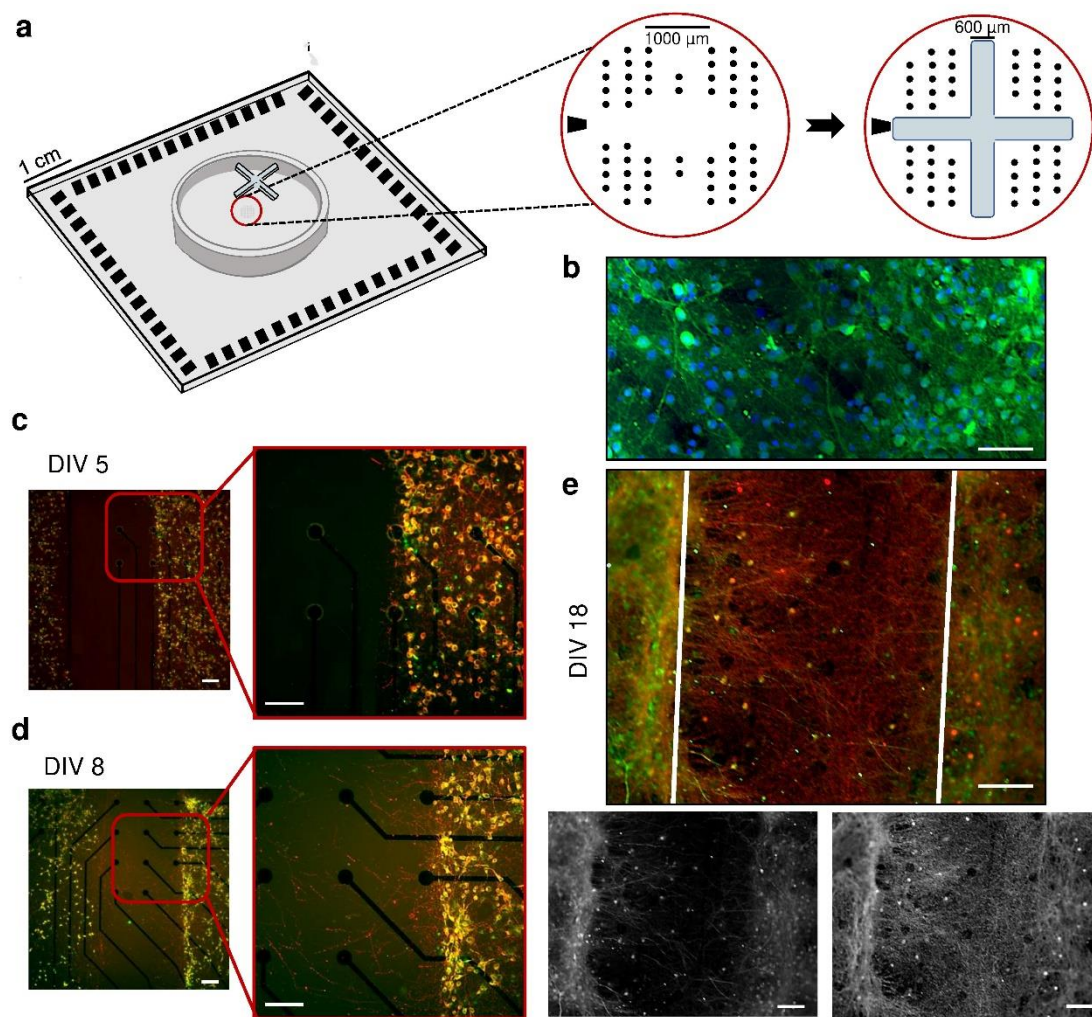
Figure 19. a) Position of the PDMS cross mask on the MEA device. Electrode positions are indicated by black dots and the reference electrode is indicated by the black trapezoid on the left. b) Immunofluorescence microscopy micrographs of rat embryo cortical neurons at 18 days *in vitro* (DIV 18), showing nuclei (DAPI, blue) and microtubule-associated proteins (MAP2, green). c, d, e) Immunofluorescence micrographs of a 4N assemblies at DIV 5, DIV 8, and DIV 18, showing axons extending between different clusters (Tau protein, red), and dendritic microtubule-associated protein (MAP2, green). The vertical white lines indicate the area previously occupied by the cross mask. Scale bars: 100 µm. Reproduced with permission from Scientific Reports [256], Creative Commons Attribution (CC BY) license (https://creativecommons.org/licenses/by/4.0/).

4.2.2. Use of animals

Pregnant female Sprague-Dawley rats (175–200 g in weight at the beginning of the protocol, 350–450 g at the end) were housed two per cage with a 12/12 h light/dark schedule (lights on at 7 a.m.), free access to food and water, controlled humidity, and temperature of 22 ± 1 °C. After 18-19 days of embryo development, the animals were anesthetized and sacrificed by beheading. Brain cortex tissue was excised and used for obtaining dissociated cell cultures. Experiments involving animals were carried out according to the ARRIVE guidelines established by the European Council (EU Directive 114 2010/63/EU) [257], and the Italian D.L. n. 26/2014. Experiments were approved by the University of Genova Ethical Committee and by the Italian Ministry of Health (Project authorization No. 2018-75f11.N.POG, 512/2015-PR and 140/2014-B-DGSAF24898). All experiments were carried out by minimizing the number of animals and their suffering.

4.2.3. *In vitro* culture of primary neurons from rat embryo cortex

Cerebral cortices of E18-19 rat embryos were used to prepare primary cultures of neurons. First, under a stereotaxic binocular (Nikon SMZ-2T), cerebral cortices were isolated from embryos, deprived from meninges, and putted into cold Hank's balanced salt solution (HBSS, Sigma Aldrich, W/O calcium and magnesium). Aliquots of cortices from 3 embryos were pulled together and exposed to an enzymatic digestion in 0.125% trypsin (Gibco Invitrogen) and 0.05% DNAse (Sigma-Aldrich) in Hanks' solution, for 18-20 min, in a water bath at 37 °C. The enzymatic digestion was stopped with Neurobasal medium (Gibco Invitrogen) complemented with 10% fetal bovine serum (FBS, Sigma-Aldrich) for 5 min, and then the tissue pellet was finely dissociated with a fine-tipped Pasteur pipette, until a milky suspension of cells was apparent. The resulting cell suspension was diluted in Neurobasal medium supplemented with 2% B-27 Supplement (Gibco Invitrogen), 1% stable L-Glutamine (GlutaMAX 100x, Gibco Invitrogen) and 1% PenStrep (Penicillin-Streptomycin Solution, Gibco Invitrogen), without serum. Finally, cells were plated on 4Q-MEA devices (Multi Channel Systems, Reutlingen, Germany, MCS), pre-sterilized and precoated with poly-L-ornithine (100 µg/ml, Sigma Aldrich). Aliquots of 10 µl cell suspension were put in each sector defined by the cross-shaped masks (4N systems), and aliquots of 50 µl cell suspension in circle masks (1N systems), realizing a final density of 1500 cells/µL. After about 2.5 h, Neurobasal medium was added to MEA to favor cell adhesion to the substrate, reaching a final volume of 1500 µL. Proliferation of glia cells was not prevented with any drug, to allow for healthy development of neurons [258]. Cell cultures

were grown in incubator with 5% CO_2 and 95% humidity, at 37 °C. The cross-shaped masks were removed after 5 days from cell plating to permit the extension of neural fibers among the four different sectors. Also, half volume of Neurobasal medium was replaced with BrainPhys medium (StemCell Technologies) supplemented with 1% GlutaMAX, 2% NeuroCult SM1 (StemCell Technologies), and 1% PenStrep solution. Thereafter, half of the medium was changed twice a week to allow the development of mature neural networks with respect to morphology and function (Fig. 19b).

4.2.4. Protocol of immunofluorescence staining

For immunofluorescence analysis, cells were grown on coverslips as described above. After obtaining mature neural networks, cells were washed twice with phosphate buffer solution (PBS, Sigma-Aldrich) and fixed with a solution of 4% paraformaldehyde (Sigma-Aldrich) in PBS, pH 7.4, for 15 min at room temperature. Cells were then permeabilized with 0.1% Triton-X100 (Sigma-Aldrich) in PBS, for 15 min at room temperature, and blocked with blocking buffer solution (BBS) consisting of 3% FBS in PBS for 40 min at room temperature, to avoid non-specific binding of antibodies. Afterward, cells were incubated overnight with primary antibody diluted in BBS, in a humified atmosphere at 4 °C. The following primary antibodies were used: Tau (axon microtubule-associated protein, mouse monoclonal, 1:500, Synaptic System), MAP2 (dendritic microtubule-associated protein, rabbit polyclonal, 1:500, Synaptic System). In addition, fluorescent labeling of nuclei was obtained with DAPI (1:1000, Synaptic System). Finally, cells were rinsed three times with PBS, exposed for 40 min at room temperature to either of the secondary antibodies: Alexa Fluor 488 (1:700, Invitrogen), Alexa Fluor 549 (1:1000, Invitrogen), goat anti-mouse or goat anti-rabbit, and images were acquired with a fluorescence microscope (Olympus BX-51), equipped with a CCD camera (Orca ER II, Hamamatsu), and digitized with Image ProPlus software (Media Cybernetic).

4.2.5. Protocols of data recording

A total of 6 biological preparations allowed us to plate cell cultures on a total of n = 35 MEAs, obtaining both 1N and 4N network systems. All 4N and 1N assemblies were recorded at day *in vitro* DIV = 18. To characterize the spontaneous electrophysiological activity of neural networks, we recorded the activity of n = 16 4N systems, and n = 11 1N systems used as controls.

To analyze the role of hyperpolarization-activated cyclic nucleotide-gated (HCN) channels (section 4.3.3) the HCN inhibitor ivabradine (IVB) was used. A total of n = 3 1N systems were used

to derive IVB dose-response curves of mean firing rate (MFR) inhibition, thus finding the IC_{50} (section 4.2.8.4) and obtaining the suitable IVB concentration to be used in experiments. In addition, n = 5 1N systems were treated with IVB at the concentration of 15 µM, derived from dose-response curves, to investigate neural network responses (section. 4.3.3). The summary of the entire dataset is reported in Table 9.

Table 9. Summary of the dataset used in the MEA experiments.

Experiment	DIV	n of MEAs	Session duration
Spontaneous electrophysiological activity of 4N	18	16	20 min
Spontaneous electrophysiological activity of 1N	18	11	20 min
Ivabradine dose-response curves on 1N and IC_{50}	18	3	1 h
Ivabradine effects induced on 1N	18	5	10 min baseline + 10 min ivabradine + 10 min washout

4.2.6. Recording of electrophysiological activity

Recordings of the spontaneous electrophysiological activity of neural networks were performed outside the cell culture incubator and started 5 min after the positioning of MEAs on the heated (37 °C) amplifier location, used to prevent cell cultures from mechanical and thermal stress. During recordings, MEA were maintained under constant slow flow of humified gas (5% CO_2, 20% O_2, 75% N_2). All recordings were performed at the sampling frequency of 10 kHz, using a MEA 2100 system (MCS). Each session lasted 20 minutes. MC_Rack software (MCS) and MATLAB (see above) were used to acquire and analyze data, respectively.

4.2.7. Protocol of *in vitro* culture treatments

The effect of ivabradine (IVB, Sigma-Aldrich) on the spontaneous network activity was evaluated by injecting directly into the culture medium increased concentrations of the drug. The derivation of the dose-response curves was performed by pipetting increasing concentrations of IVB solution into the culture medium and recording the neural networks activity for 10 min. A wide administration scale (300 nM – 30 µM), with logarithmic scale, was chosen to quantify IVB effects

on the neuronal activity. The first 2 min of each phase were discarded to avoid bias due to drug diffusion into the medium.

4.2.8. Data processing and statistical analysis

4.2.8.1. Spike and burst detection

The Precision Time Spike Detection (PTSD) algorithm was used for the detection of spike occurrence [259]. To obtain this specific detection the following three parameters had to be set:

- specific threshold of electrodes, set at 8 times the standard deviation of signal noise;

- spike duration, set at 2 ms;

- period of refractoriness, set at 1 ms.

The sorting of spikes was not performed, since a bursting event can produce a fast sequence of spikes with overlapping shapes, which makes sorting difficult and unreliable [260]. After the identification of a spike train, burst detection was obtained with the string method [261], by setting:

- minimum number of spikes to define a burst event (set at 5);

- maximum time period occurring between two different spikes inside a burst event (set at 100 ms).

4.2.8.2. Detection of network burst activities

To detect the activity of the whole network, i.e. network burst (NB) events, a self-adaptive algorithm was employed [262]. The following parameters were set:

- maximum time interval between sequential burst events in a network burst;

- minimum percentage of active electrodes involved in the NB (set at 20%).

4.2.8.3. Spiking and bursting statistics

The characterization of the network activity level was performed by computing firing and bursting statistics. First, the number of spikes per second, defined Mean Firing Rate (MFR), was evaluated together with the number of active electrodes in a MEA. MFR values lower than 0.1 spikes/s were discarded from the analysis. Second, the bursting activity was analyzed in terms of Mean Bursting Rate (MBR) and Burst Duration (BD). Instantaneous firing rate (IFR) was used to analyze the activation sequences of each cluster involved in a network burst event. The IFR was obtained subdividing the number of revealed spikes by the bin width in a specific time frame of 100 ms. By using a Gaussian kernel of width equal Δt, such a window was realized. The IFR of the whole

network was obtained by calculating this parameter for each electrode, and then identifying the time of activation of a single cluster (*i*) for each NB (*k*) as the IFR time to reach the maximum value during the NB:

$$t_{start(i,k)} = t_{\max\left(IFR_i(t_{start(k)}-t_{end(k)})\right)}$$ (19),

where $t_{start(k)}$ and $t_{end(k)}$ are the starting and ending times of the *k-th* NB, respectively.

4.2.8.4. Dose-response curve (IC$_{50}$)

In experiments with increasing doses of IVB, to compare the MFR values of the different experiments, firstly the basal MFR was calculated based on the number of active electrodes during electrophysiological recordings without IVB. Then for each experiment MFR values were normalized considering the basal activity values. Normalized MFR values were fitted to a Hill curve as a function of the delivered IVB concentration (see equation 20). The Hill function is known to be the best model for the relationship between drugs concentration and consequent responses [263]:

$$MFR_{norm}([IVB]) = MFR_{norm}^{max} + \frac{MFR_{norm}^{min} - MFR_{norm}^{max}}{1 + 10^{HC(\log(IC_{50}-\log([IVB]))}}$$ (20),

where MFR_{norm}^{min} and MFR_{norm}^{max} are the highest and the lowest normalized MFR values, and [*IVB*] is the delivered concentration of ivabradine, respectively. *HC* is the Hill coefficient, which provides the largest absolute value of the curve slope. Finally, the *IC$_{50}$* is the half-maximal inhibitory concentration observed.

4.2.8.5. Statistical analysis

The MATLAB platform was used for descriptive and inference analyses. In order to investigate significant differences among data, different statistic tests were used:

- ANOVA and Student's *t* test, with Bonferroni's correction for multiple pairwise comparisons, for mean comparisons of normalized (log conversion) or normal quantitative data;

- Chi-squared test to analyze the distribution frequency of qualitative classes;

- Kolmogorov Smirnov test to investigate cumulative frequency distributions;

- Wilcoxon Signed-Rank test for paired frequencies.

The diversity of cluster activation sequences was analyzed by using the Shannon diversity index [264], defined as:

$$H = -\Sigma p_i * \ln(p_i) \qquad (21),$$

where p_i is the relative frequency of the ith type of activation sequence. The index H spans between a minimum of 0 (if there is only one type of activation sequence with a relative frequency equal to 1), to a maximum of $\ln(N)$, where N is the number of different activation sequence types (if all types have the same frequency). The H values were then normalized by applying the Shannon equitability index [264]:

$$E = \frac{H}{\ln N} \qquad (22),$$

which transforms the Shannon index into a normalized value in a interval [0,1].

All statistical tests were performed by applying a significant threshold of p = 0.05. The reported box plots represent the mean (square), the median (line), the standard deviation (whiskers) and the percentile interval 25-75 (box) values.

4.3. *In vitro* brain network: Results

Interconnected sub-populations (4N) were investigated and characterized in terms of spontaneous activity resulting from the interactions among neuron clusters. This kind of assembly was then compared to simple cortical networks without modular connectivity (1N).

4.3.1 Spiking and bursting features depend on the degree of modularity

Spontaneous electrophysiological activity was exhibited by both 1N and 4N networks. The activity showed the same main features, including spiking and bursting signals, and in addition global network activities indicated as network bursts (NB). These results indicated that both single [265], and multiple [254], neural networks share comparable spiking and bursting behavior when coupled to MEAs. However, the spiking and bursting activity patterns of 1N and 4N showed quantitative differences in terms of specific parameters. The values of MFR (Figure 20a), MBR (Figure 20b), and BD (Figure 20c) were significantly higher in 1N networks, while IBI was lower in 1N with respect to 4N (Figure 20d). Table 10 reports the values of the mean, median, and standard error of the mean, as well as the first (Q1) and third (Q3) quartiles, detected on the complete datasets of 4N and 1N networks. To evaluate statistical differences between the two network assemblies, the Student's *t*

test was applied to log-transformed data and the corresponding *p* values are shown in the last column of Table 10.

Comparing the two different kinds of assemblies, no significant differences were found considering the collective network activity, evaluated in terms of numbers of network burst (NB, Figure 20e) and network burst duration (NDB, Figure 20f).
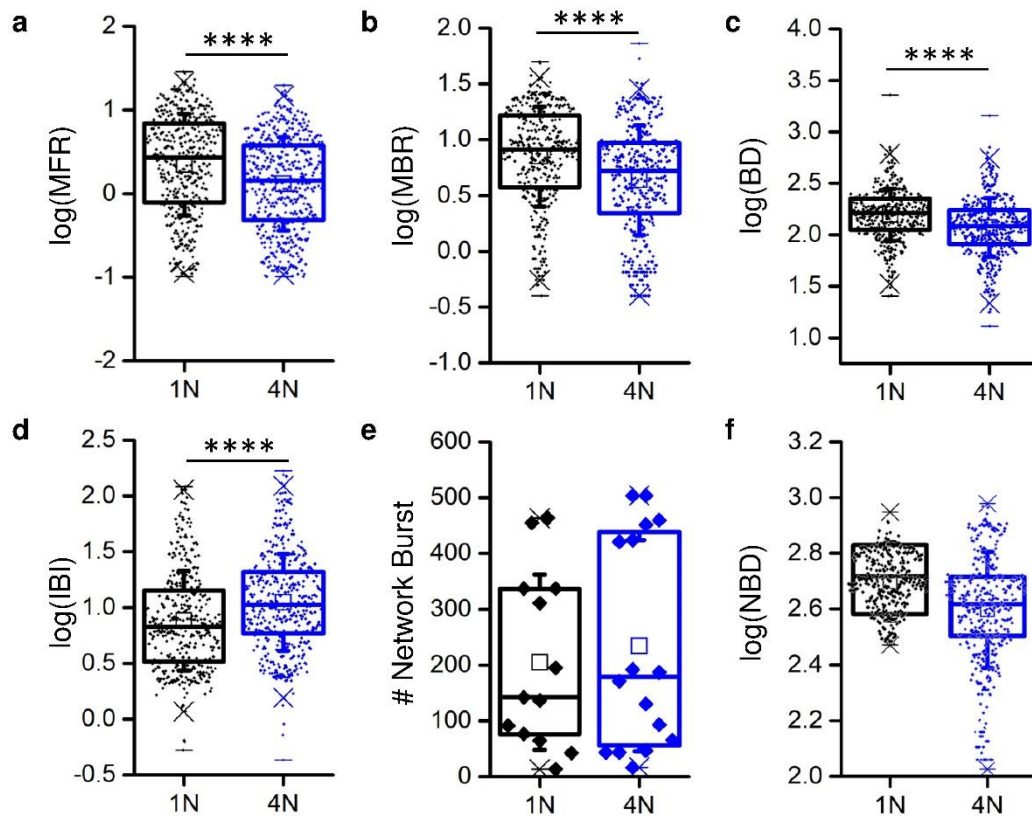
Figure 20. Electrophysiological activity of one-network assemblies (1N) and four-network assemblies (4N). a) Values of Mean Firing Rate (MFR), b) Values of Mean Bursting Rate (MBR), c) Values of Burst Duration (BD), d) Values of Inter Burst Interval (IBI), e) Numbers of network burst occurrence (# Network Burst), f) Values of Network Burst Duration (NBD). ****: p < 0.0001, *t* test. Reproduced with permission from Scientific Reports [256], Creative Commons Attribution (CC BY) license (https://creativecommons.org/licenses/by/4.0/).

Table 10. Summary statistics of basic measurements of neural network functioning.

Par.	Unit	Assembly	Q1	Median	Q3	Mean	S.E.M.	p*
MFR	spikes/s	1N	0.77	2.71	6.89	4.66	0.24	$7.3 \cdot 10^{-13}$
		4N	0.48	1.43	3.78	2.63	0.14	
MBR	bursts/ min	1N	3.75	8.21	16.5	10.7	0.42	$1.6 \cdot 10^{-10}$
		4N	2.23	5.23	9.36	7.44	0.37	

BD	Ms	1N	112	163	225	187	7.18	1.9·10^{-10}
		4N	81.4	122	173	147	5.61	
IBI	s	1N	3.29	6.79	14.2	13.8	0.93	1.4·10^{-7}
		4N	5.87	10.6	21.0	18.7	1.13	
NB	NBs/min	1N	15.2	28.4	67.4	41.0	39.4	0.66
		4N	12.1	35.8	86.2	46.9	47.4	
NBD	ms	1N	392	521	646	524.5	52.6	0.17
		4N	333	415	495	431.9	44.8	

*Student's t-test. Reproduced with permission from Scientific Reports [256], Creative Commons Attribution (CC BY) license (https://creativecommons.org/licenses/by/4.0/).

4.3.2. The rhythmic patterns of activity are shaped by the assembly of neuron clusters

4.3.2.1. Patterns of activation sequence propagation

The activities of 1N and 4N networks showed the same macroscopic features, demonstrating that different topologies or structures do not influence the intrinsic network functioning (Figure 20e, 20f). By contrast, the modes of propagation of network activation resulted to differ depending on the network topology. The activity propagation of the network was quantified by estimating the IFR (section 4.2.8.3). Considering only the active electrodes, the cumulative firing rate was determined for each cluster in both 4N and 1N experiments. In 4N experiments the study was performed by subdividing the electrodes into 4 groups, representing real neuron clusters defined by the cross-shaped mask. In 1N experiments the electrodes were subdivided into 4 virtual clusters, topologically corresponding to the real clusters of 4N assemblies. Figure 21a shows an example of a 4N control network. The four colored traces are representative of the 4 virtual clusters used to study the activity of the network. The IFR profile and raster plot (Figure 21a) highlight a repetitive and rhythmic pattern of activity. The network burst in 4N starts from the purple cluster and then propagates sequentially to the cyan, green, and red cluster.

In the example concerning the 1N network (Figure 21b) a specific pattern of propagation does not emerge. The clusters involved in the network burst are less stereotyped and not predictable. The IFR profiles of three network bursts of 1N are represented (Figure 21b): the first one showed a propagation involving all 4 interconnected populations (cyan-purple-red-green), the second network burst involves only three clusters (cyan is missing), and the third one involves all the clusters in a random sequence.
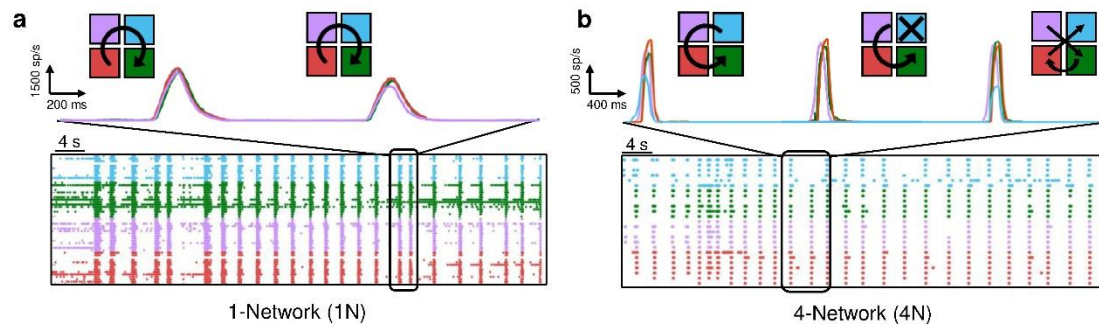
Figure 21. Raster plots of the electrophysiological activity recorded in 1N (a), and 4N systems (b), along 60-s periods. On the top, instantaneous firing rate profiles of 5-s time windows are visible, accompanied by color maps showing the sequential propagation (arrows) of activation sequences among virtual clusters (1N) or real clusters (4N). Reproduced with permission from Scientific Reports [256], Creative Commons Attribution (CC BY) license (https://creativecommons.org/licenses/by/4.0/).

To obtain quantitative evaluations of cluster activation, we firstly considered the number of clusters involved in each activation sequence. In both 1N and 4N, the sequences of 4 clusters are more frequent with respect to those consisting of 3 and 2 clusters, showing that all 4 clusters tend to be involved in the activation sequence. In 1N networks, the relative frequency of sequences of 4 clusters was about 0.8 (Figure 22a), while the relative frequencies associated to sequences of 3 and 2 clusters were 0.18 and 0.03, respectively. In 4N networks (Fig. 22a) the sequences of 4 clusters had a relative frequency of 0.58, while the relative frequencies of 3-clusters, 2-cluster, and 1-cluster activation sequences were 0.30, 0.15, and 0.05, respectively. Hence, by analyzing the relative frequencies of the number of recruited clusters during network bursts, we demonstrated a similar behavior for 1N and 4N, where the involvement of all the clusters in the activation sequences was the most likely occurrence. The lower frequency of 4-cluster activation sequences in 4N probably depended on the gaps among clusters allowing the extensions of inter-cluster connecting fibers in a wider range of directions.

Figure 22. a) Frequencies of categories based on the number of clusters involved in a network burst (1, 2, 3, or 4 clusters), as derived from IFR profiles. b) Boxplots of the distributions of the numbers of observed circular activation sequences (Observed) compared with the numbers obtained from simulated samplings under randomness (Expected), having the same total number of activation sequences (in random conditions circular activation sequences are 1/3 of total). Statistical analys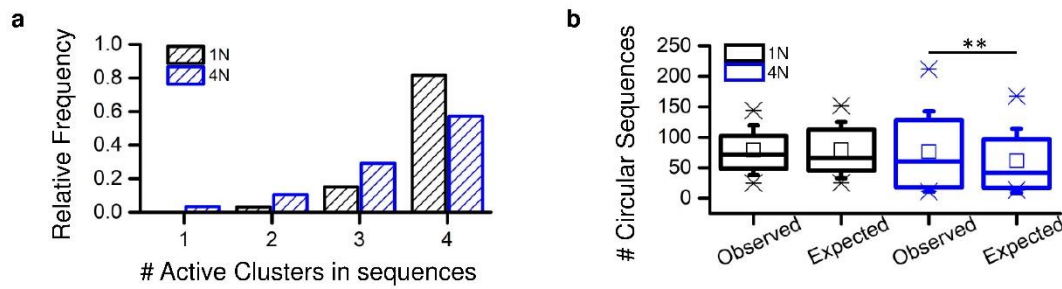is revealed significant difference for 4N, Wilcoxon Signed-Rank test, ** p < 0.01. Reproduced with permission from Scientific Reports [256], Creative Commons Attribution (CC BY) license (https://creativecommons.org/licenses/by/4.0/).

The 4N spatial organization could be relevant for the generation of the propagation pathways of network bursts among clusters. Different connectivity directions could be followed by the network bursts, including circular propagation paths (CP) that could be clockwise or counterclockwise, and cross-diagonal paths (DP). For a better understanding of these propagation phenomena, we considered the probability of CP and DP in the 4-cluster topology under aleatory condition (expected dataset), being respectively 1/3 and 2/3. For each experiment, the number of observed CPs, out of the total number of sequences (S), was considered, and it was compared to the number of the expected CPs, corresponding to S/3. By comparing the observed CPs with the expected CPs in 1N, no statistical difference was found according to the Wilcoxon Signed-Rank test. By contrast, for 4N the number of observed CPs resulted significantly higher than that of expected CPs (Figure 22b).

4.3.2.2. Pacemaker activity: clusters acting as preferential initiators of activation sequences

The different propagation modes appeared to be associated with the emergence of dominant clusters from which network bursts arise and expand to the entire network. Both *in silico* and *in vitro* studies support the existence of leader neurons, firing at the beginning of a network burst more often than expected by chance [266, 267]. In our 1N and 4N experiments, the frequency of initiator clusters was unequally distributed among the 4 real or virtual clusters. To show this pattern, for each experiment the highest relative frequency of an initiator cluster was attributed to "frequency class 1". This operation was repeated for the next most frequent initiator cluster, until

each cluster was assigned to a specific frequency class (classes 2, 3, and 4). Next, the median value of each frequency class out of all experiments was found, obtaining four median values that were compared with those of a uniform distribution of clusters among the four frequency classes, corresponding to a value of 0.25 for each frequency class. A comparison with the Chi-squared test (p < 0.01) showed significant differences for both in 1N and 4N networks (Figure 23a). This result showed that both 1N (black line) and 4N (blue line) shared a similar behavior, with the emergence of a specific hierarchy among clusters involving the predominance of two initiator clusters, i.e. those with a frequency higher than the expected frequency under random distribution.

4.3.2.3. Nonrandom composition and repetitive series of activation sequences

To better investigate the patterns of activation exhibited by 1N and 4N, the observed activation sequences in real experiments (Observed) were compared to Monte Carlo samples of activation sequences (Expected). For each experiment, a Monte Carlo sample of activation sequences, numerically equivalent to the sample of observed activation sequences, was obtained by drawing sequences of clusters from a uniform frequency distribution. Thereafter, the diversity of the activation sequences in the Observed and Expected experiments were measured by the Shannon equitability index. In this analysis, the index should approach the value of $E = 1$ for datasets of random sequences (Expected), while it should be equal to $E = 1$ in the presence of a unique sequence of activation (section. 4.2.8.5). Our analysis showed a significantly lower diversity in the Observed activation sequences with respect to the Expected ones, for both 1N (p = 3.6·10^{-7}, Wilcoxon Signed-Rank Test) and 4N (p = 3.2·10^{-9}, Wilcoxon Signed-Rank Test). These results showed a prevalent occurrence of specific activation sequences in contrast to a completely random occurrence (Figure 23b).

Besides the non-random diversity of activation sequences, the time series of identical consecutive activation sequences were also of interest. To quantify this pattern, the length of the series of identical consecutive sequences was considered. Moreover, a different weight was attributed to the series depending on their length: longer series have a higher impact than shorter ones of equal occurrence, while series that occur more frequently weight more than less frequent ones with the same length. For example, a series of 2 identical sequences that occurs 10 times will have a weighted absolute frequency of 2 x 10 = 20; a series of 4 sequences that occurs 5 times will have a weighted absolute frequency of 4 x 5 = 20. In this analysis, a different behavior was found between 4N and 1N, as highlighted by the cumulative distributions of relative frequencies derived

from weighted absolute frequencies. In 1N, the longer detected sequence consisted of 7 identical sequences with a relative frequency of 0.03. In 4N, the longer detected sequence consisted of 14 repeated sequences, with a relative frequency of 0.01. Accordingly, a significant difference between the 1N and 4N frequency distributions was found with the Kolmogorov-Smirnov test (Figure 23c). Also, the 4N cumulative frequency distribution was significantly different from a dataset of repeated activation sequences generated by Monte Carlo sampling (p = $3.3 \cdot 10^{-4}$, Kolmogorov-Smirnov test).
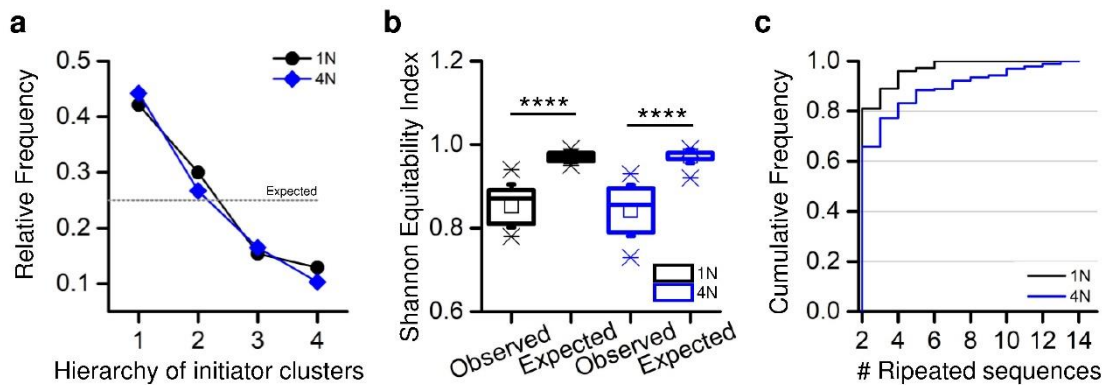
Figure 23. a) Median values of the data sets obtained by considering the frequency of the most frequent starting cluster in each experiment (indicated as 1), the frequency of the second most frequent starting clusters in each experiment (indicated as 2), etc. b) Box plots obtained from two couples (1N and 4N) of matched data sets. Each matched data set was obtained by calculating, for each experiment, the Shannon equitability index (section 4.2.8.5) of the recorded activation sequences (Observed), and of a Monte Carlo simulation with the same total number of activation sequences (Expected). Wilcoxon Signed-Rank Test, **** p < 0.001. c) Cumulative frequency distributions of data sets obtained by considering the numbers of activation sequences forming series of identical consecutive elements, in 1N and 4N assemblies. By comparing the cumulative frequency distributions between 1N and 4N, significant differences were found. Kolmogorov-Smirnov test, p < 0.01. Reproduced with permission from Scientific Reports [256], Creative Commons Attribution (CC BY) license (https://creativecommons.org/licenses/by/4.0/).

4.3.3. The rhythmic activity involves HCN channels and glutamate-dependent excitability

HCN channels are known to generate rhythmic patterns of activity in excitable cells, with various examples reported in different regions of the central neuron system [268, 269]. Therefore, the spontaneous electrophysiological activity of 1N networks was analyzed in the presence and in the absence of the specific HCN channel inhibitor ivabradine (IVB) [270] (Figure 24a).

To perform this set of recordings, a concentration of 15uM IVB was used, that is close to the IC50 value obtained by deriving dose-response curves for MFR in preliminary experiments (Figure 24b).
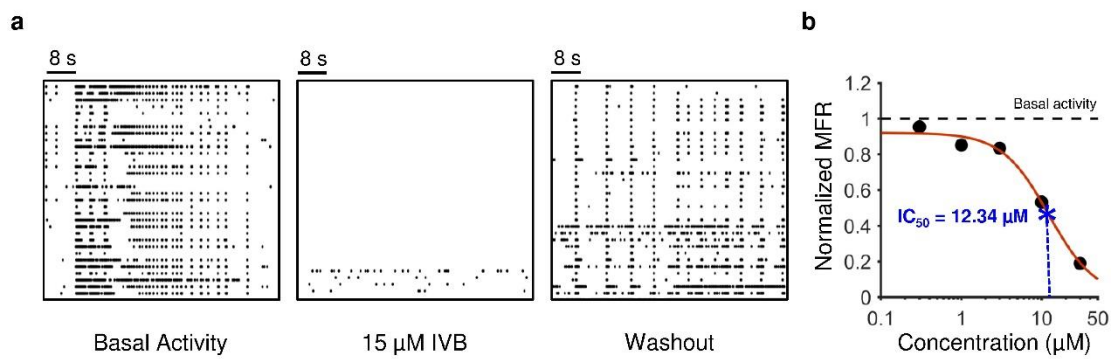
Figure 24. Ivabradine (IVB) effect on the electrophysiological activity of 1N. a) Raster plots representing 60-s periods of representative samples. b) Dose dependency of mean firing rate inhibition by IVB, obtained by the injection of IVB concentrations ranging between 0.3–30 μM, Hill fitting curve (see Equation 20), and estimated IC_{50} (blue star and dotted vertical line). Reproduced with permission from Scientific Reports [256], Creative Commons Attribution (CC BY) license (https://creativecommons.org/licenses/by/4.0/).

The effect of IVB on the electrophysiological activity of neural networks was a marked decrease of global activity, as shown by the significant reduction of active electrodes (Figure 25a), as well as of MFR and MBR (Figure 25b, 25c). These effects were transient and disappeared after washout, with a return of MFR and MBR to basal values. The effect of IVB did not affect the BD but increased the IBI and its standard deviation (Figure 25d, 25e, 25f). In summary, IVB induced a global reduction of the network activity, reducing the number of bursts and increasing the delay between them. These data strongly suggest that HCN channels are essential for the rhythmic spontaneous activity of the network.
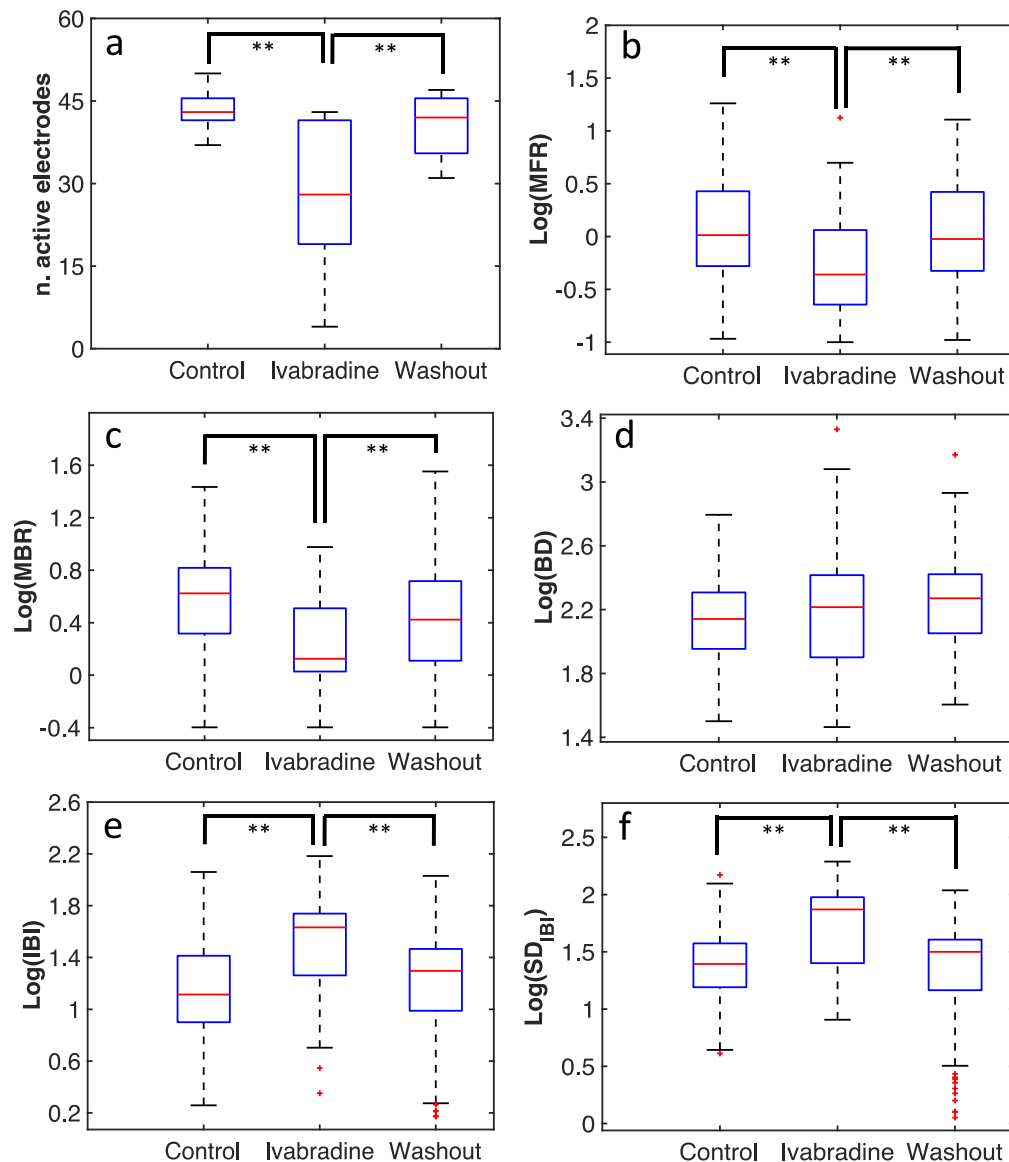
Figure 25. Inhibition of electrophysiological activity induced by exposure of 1N to 15 µM ivabradine (IVB). Recordings were performed at three different timepoints: before IVB injection (controls), during IVB diffusion, and after washout. a) Number of active electrodes; b) values of Mean Firing Rate (MFR); c) values of Mean Bursting Rate (MBR); d) values of Burst Duration (BD); e) values of Inter Burst Interval (IBI); f) values of IBI Standard Deviation (SD_{IBI}). ANOVA, Bonferroni post-hoc test, ** $p < 0.01$. Reproduced with permission from Scientific Reports [256], Creative Commons Attribution (CC BY) license (https://creativecommons.org/licenses/by/4.0/).

We then considered the contribution of excitability to the spontaneous activity of the network. Glutamate is the main excitatory neurotransmitter in the CNS, and therefore, we used MK801, a known blocker of the glutamate NMDA receptor [271]. The drug administration protocol was identical to that described above for ivabradine, while a concentration of 15 µM MK801 was

selected after a series of preliminary tests. Like the results obtained with IVB, the effect of MK801 on 1N networks was a significant decrease of spontaneous activity (Figure 26a). We then compared the activation of the whole network in the presence of IVB and MK801, quantified as the total number of network bursts (NB) during each experimental session. Under both treatments, a significant reduction of NB was observed, but the treatment with ivabradine was followed by a significant recovery upon washout (Figure 26b). In experiments with MK801, even though a partial recovery of network activity was observed (Figure 26a), there was no statistical recovery for what concern NB (Figure 26c). The absence of recovery of global network activity upon MK801 treatment is consistent with electrophysiological and ligand binding studies showing that the blockade of NMDARs by MK-801 persist long after drug washout [272].

The experiments with IVB and MK801 indicate that the spontaneous rhythmic activity observed in our experiments requires a combination of network excitability and pacemaker activity. These essential properties seem primarily due to the presence of HCN channels and ionotropic glutamate receptors.

Figure 26. Effect of the delivery of MK801 on the activity of 1N assemblies. a) Raster plots showing 180-second intervals of electrophysiological activity in a representative cortical network before (*basal*), during (*MK801*), and after the delivery (*washout*) of 15 μM MK801. b) Boxplot showing the logarithm of total network burst reco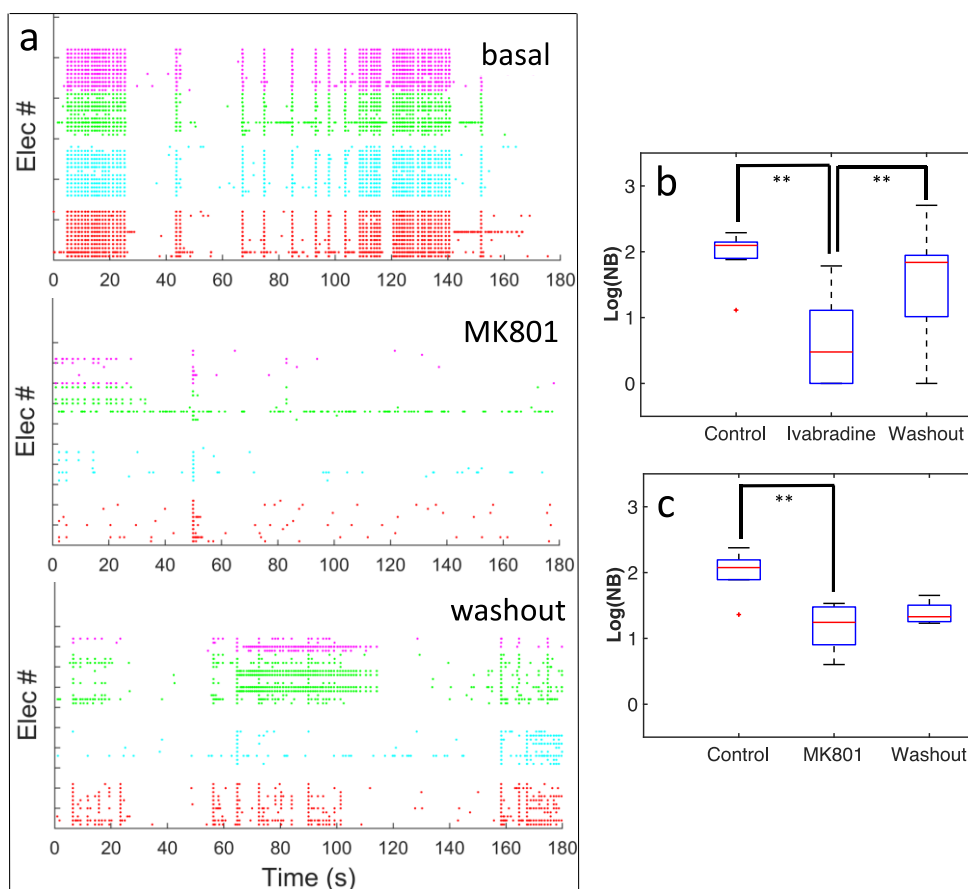rded before, during, and after administration of 15 μM ivabradine (n = 7). c) Boxplot showing the logarithm of total network burst recorded before, during, and after administration of 15 μM MK801 (n = 6). ANOVA, Bonferroni post-hoc test, ** p < 0.01.

4.4. *In vitro* brain network: Discussion

By using an *in vitro* experimental model consisting of reconstructed networks of cortical neurons, the electrophysiological activity patterns in different modular network organizations were investigated. To build the *in vitro* experimental set-up, MEA devices and physical polymeric constraints were used. Rhythmic bursts and isolated spikes are known to characterize the electrophysiological activity of *in vitro* dissociated cortical networks [260]. The characterization of these dynamics has been achieved by different routes, such as chaos theory, inferential statistics, or self-organized criticality, showing that similar activation patterns are displayed by different experimental systems. Different cell preparations, including human models derived from pluripotent stem cells [273], and rodent neuronal primary cultures [265], reproduce the same patterns of electrophysiological activity, sharing the main features of neural networks. These data are relevant to develop standard neural network models because they show that the electrophysiological spontaneous activity can be considered as a general reference system, not influenced by biological or experimental conditions.

Our experiments support these considerations since the main features of neural activity were maintained in both single-network systems and cultures engineered as interconnected neuronal networks. In both 1N and 4N assemblies, the activity of burst propagation in the whole network represented a distinctive feature and supported the idea of the existence of burst initiation points and consequent propagation [274]. In previous studies, burst initiation points have been associated to network inhomogeneities [274]. In contrast, our results revealed a non-random distribution of these initiation points due to the presence of dominant clusters. Independently from the modular topology, dominant clusters acted as starting points of activation sequences behaving as "network pacemakers". Some sequences of spontaneous sequential cluster activation resulted more frequent with respect to a purely random set of sequences.

Moreover, departure from randomness of time series of identical sequences was observed in 4N assemblies. In these systems, longer series of identical activation sequences than under randomness

were found, suggesting that the 4N configuration realizes phenomena of synaptic plasticity. Literature data have reported *in vitro* synaptic plasticity both in hippocampus slices and in dissociated cortical networks [275], induced experimentally by high-frequency tetanic stimulation [276]. Interestingly, our results seem to reveal effects associated to neuroplasticity without electrical stimulation of the network system, but as an emergent property of spontaneous electrophysiological activity. As said above, such a behavior was stronger in the 4N configuration, which is more representative of the *in vivo* arrangement of brain networks. The 4N configuration was used to simulate the topological connectivity of complex patterns of activation. By contrast, the 1N experimental model was not able to reproduce the dynamics of high-order patterns of spontaneous activity such as modularity [277], and small-worldness [278].

The presence of network pacemakers was confirmed through the inhibition of hyperpolarization-activated cyclic nucleotide-gated (HCN) channels [268]. In our experiments, IVB was used to inhibit HCN currents, obtaining a strong decrease of the electrophysiological activity such as the propagation and rhythmicity of network bursts, thus confirming pacemaker activity. Many neurophysiological processes are known to be characterized by an intrinsic pacemaker activity. These processes have different brain localizations, including thalamocortical neurons [279], the respiratory central pattern generator [280], locus coeruleus noradrenergic neurons [281], neocortical neurons [282], medial septal neurons [283], and substantia nigra dopamine neurons [284]. Moreover, in some of these cases the involvement of HCN channels has been demonstrated [285, 286].

Overall, our *in vitro* experiments demonstrated that interconnected neural networks show spontaneous activity characterized by a rhythmic, synchronized pattern, depending on pacemaker elements. Also, specific network patterns become spatiotemporally consolidated, possibly due to neuroplasticity phenomena. Consolidated network patterns lasted on average from a few seconds up to a maximum of 20-25 seconds, suggesting a link to short-term synaptic plasticity [287]. Hence, the spatiotemporal consolidation of network activity in our experiments had features distinctly different from the neuroplasticity induced by tetanic stimulation [288]. Moreover, in our experiments the stronger consolidation of network activity, observed in 4N with respect to 1N assemblies, could be explained by signal channeling along distinct pathways. In repeated activation sequences, each neuron cluster is repetitively stimulated by the upstream cluster and operates similarly on the downstream cluster. In 4N, the interconnection between real neuron clusters is

more channeled, with fewer random side dispersions than in the virtual clusters of 1N assemblies. This accounts for the more consolidated, repeated activation sequences observed in 4N networks.

In conclusion, the key features of our *in vitro* neural networks are the presence of pacemaker centers, and the nonrandom repetition of distinct activation sequences along time, amenable to neuroplasticity. These activities have been observed also *in vivo* [282], thus possibly representing the basic elements of the electrophysiological activity of neural networks, both *in vivo* and *in vitro*. This seems also confirmed by computational simulations of cortical neural networks, in which optimized results have been achieved by combining together mathematical models of pacemaker activities and synaptic plasticity [289].

4.5. *In vitro* brain network: Conclusions

Our engineered experimental set-up consisting of multiple-neural networks was developed to simulate a brain network structure. Data suggest that pacemaker activity and synaptic plasticity are the key elements of the high-order activity of this system. These findings would be of interest for predicting the system behavior under different conditions by using computational simulations (Figure 27). Finally, the realization of *in vitro* neural network systems in different configurations, as well as the detection of their electrophysiological features, are the prerequisite for the development of brain network digital twins. This kind of strategy could lead to a better understanding and prediction of brain network dynamics, possibly allowing to improve the management of brain dysfunctions.
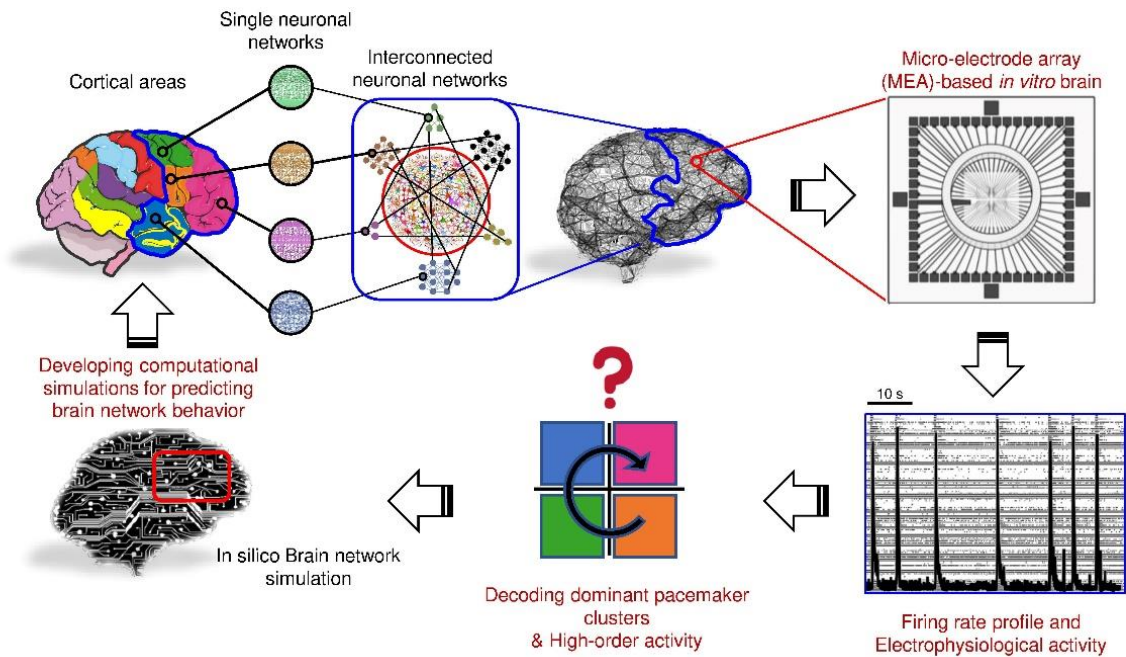
Figure 27. Future perspectives of MEA experiments. The first aim is to reproduce neural networks and their interconnections on Micro-Electrode Arrays (MEAs). Such an *in vitro* experimental model enables the extraction, examination, and quantitative analysis of neural network electrophysiological activities. This technique and analysis system could lead to the development of *in silico* models (digital twins) able to predict *in vivo* brain network dynamics. Computational simulations could help to understand the origin and development of neurological diseases. Reproduced with permission from Scientific Reports [256], Creative Commons Attribution (CC BY) license (https://creativecommons.org/licenses/by/4.0/).

5. CONCLUSIONS

5.1 Conclusions: Background

Progress in biomedical research is made difficult by the complexity of life, which obviously includes all aspects of human health and disease development. These drawbacks are made dramatically evident by the wide set of diseases that are still unclear for what concern causes, development, and treatments. Hence, disease management is frequently puzzling, while patient management is disappointing, involving heavy social and economics burdens.

The present study deepens its roots in a previously formulated idea that the above problems are primarily due to the unsuitability of current paradigms about the nature of living beings, and that a reconceptualization of the phenomenon of life is needed. Such a kind of hypothesis, named Loopomics, considers living beings essentially as a set of controls systems whose dynamics depends on the activity of loops, i.e. closed chains of interactions among functional elements [28]. Such hypothesis is still unproved, but it explains how living systems avoid the butterfly effect of chaotic systems, despite the enormous complexity of their processes. A non-chaotic behavior leading to predictable outcome is easily explained by loop dynamics characterized by equilibrium points, thus accounting for the two fundamental occurrences of living systems, on one side homeostasis (negative loops), and on the other side transformations (positive loops). The Loopomics hypothesis can be extended to the development of diseases, because these processes are themselves biological transformations, even though their progress involves dysfunction, damage, or degeneration [44].

5.2. Conclusions: FM pathogenesis model

Based on the above background, this study aims at developing models of neurological diseases consisting of loop systems, so to provide an explanation of pathogenesis and detect the critical therapeutic targets. We focused on the FM syndrome since it perfectly fits with the above considerations, urgently requiring to unveil the disease etiology and development by starting from the biological basis of pathophysiological mechanisms. Despite a wide set of biological and clinical studies, the body districts and triggering events involved in FM pathophysiology are still unknown, resulting in extremely difficult patient management and the absence of effective therapies. The neuroendocrine model of FM pathogenesis presented in this study provides an explanation of the disease from the primary causes up to the appearance of symptom. Our model could also be a guide for the development of pathogenesis models of other disorders potentially involving neuroendocrine mechanisms. The model is consistent with the following FM features:

- the new definition of nociplastic pain, i.e. pain depending on central neural disorders [218];

- accumulating evidence that FM involves multisensory alterations including vison and equilibrium sensory processing [107];

- the female prevalence, which in our model is related to two main pathophysiological events:

- the downregulation of the HPG axis;

- the upregulation of the HPA axis.

The HPG downregulation is an aleatory event if we consider hormonal fluctuations in males, but it is a periodic event in females because of wide hormonal fluctuations in the cycle or during pregnancy. By contrast, the HPA upregulation of chronic or post-traumatic stress can be considered an aleatory event in both sexes. Therefore, the probability of developing FM would be given by the product of two probabilities, of which both are small in males (the probability of HPG downregulation and of HPA upregulation), whereas only one in females (the probability of HPA upregulation), resulting in a higher overall probability for females.

5.3. Conclusions: *In vitro* brain network

In the FM model, brain network dynamics have been described by using differential equations whose variables represent mean firing rates of neuron populations. This method is generally used in the realization of dynamical systems of brain networks electrophysiological activities [290]. However, the firing rate is essentially a measure of neural network excitability and a model based only on this parameter could be an excessive schematization. Therefore, we designed experiments aimed to achieve a more complete characterization of the brain network electrophysiological activity. To do this, we chose to reconstruct *in vitro* a system of interconnected neural networks simulating a brain network under an experimental set allowing real-time recording. We therefore used MEA as the best technique for this kind of experiments, and realized, by using rat cortical neurons, *in vitro* neural network systems. The recorded data indicate that the electrophysiological activity of *in vitro* brain networks consist of three main components: excitability (mainly due to glutamatergic transmission, notably NMDAR), self-rhythmicity (mainly due to HCN channels), and possibly neuroplasticity. These functional components give rise to a spontaneous activity represented by rhythmic network bursts, with pathways of activation sequences that tend to persist along time. Similar to what occurs in engineered telecommunication systems [291], the spontaneous rhythmic activity of neural networks could represent some sort of "carrier wave" suitable to be modulated by input signals, so to provide

codified, predictable output signals. Such a behavior could represent the basis of brain network functioning, thus explaining the following:

- the fact that brain networks are permanently "on" and the functional meaning of this occurrence (realization of a carrier wave);

- the fact that brain networks realize a rhythmic activity as the best pattern to provide codified signals upon modulation;

- the prevalence of excitatory (glutamate) vs. inhibitory (GABA) neurotransmission in the brain according to the need of maintaining spontaneous activity in the absence of input.

These considerations suggest that the use of firing rate as the only system variable in brain network modeling could be a schematization sufficient to describe drastic pathophysiological changes, but insufficient for physiological transitions or disorders involving slighter modulations. The supplementary implementation of rhythmic activity and neuroplasticity could allow to realize more suitable digital twins of brain network electrical activities under both physiological and pathogenic conditions.

6. REFERENCES

1.   von Bertalanffy L. General System Theory: Foundations, Development, Applications. New York, NY, USA: George Braziller Inc; 1968.

2.   John E. Hall, Guyton AC. Textbook of Medical Physiology. 1990.

3.   John Reith, Young JZ. Doubt and Certainty in Science 1950.

4.   Frederick Chee, Fernando T. Closed-Loop Control of Blood Glucose. Springer. 2007;368.

5.   Abbassi-Ghanavati M, Greer LG, Cunningham FG. Pregnancy and laboratory studies: a reference table for clinicians. Obstet Gynecol. 2009;114(6):1326-31. doi: 10.1097/AOG.0b013e3181c2bde8. PubMed PMID: 19935037.

6.   Milsom JR. Biological Control Systems Analysis. McGraw-Hill. 1966.

7.   Riggs AD, Bourgeois S, Cohn M. The lac repressor-operator interaction. 3. Kinetic studies. J Mol Biol. 1970;53(3):401-17. Epub 1970/11/14. doi: 10.1016/0022-2836(70)90074-4. PubMed PMID: 4924006.

8.   Jones RW. Principles of Biological Regulation: An Introduction to Feedback Systems. Academic Press. 1973.

9.   Umbarger HE. Evidence for a negative-feedback mechanism in the biosynthesis of isoleucine. Science. 1956;123(3202):848. Epub 1956/05/11. doi: 10.1126/science.123.3202.848. PubMed PMID: 13324101.

10.   Cannon WB. Organisation for physiological homeostasis. Physiological Reviews 1929;9(3):399 - 431.

11.   Wall ME, Hlavacek WS, Savageau MA. Design of gene circuits: lessons from bacteria. Nat Rev Genet. 2004;5(1):34-42. Epub 2004/01/07. doi: 10.1038/nrg1244. PubMed PMID: 14708014.

12.   Alvarez-Vasquez FJ, Freyre-Gonzalez JA, Balderas-Martinez YI, Delgado-Carrillo MI, Collado-Vides J. Mathematical modeling of the apo and holo transcriptional regulation in Escherichia coli. Mol Biosyst. 2015;11(4):994-1003. Epub 2015/02/17. doi: 10.1039/c4mb00561a. PubMed PMID: 25683745.

13.   Ozbudak EM, Thattai M, Lim HN, Shraiman BI, Van Oudenaarden A. Multistability in the lactose utilization network of Escherichia coli. Nature. 2004;427(6976):737-40. Epub 2004/02/20. doi: 10.1038/nature02298. PubMed PMID: 14973486.

14.   Maamar H, Dubnau D. Bistability in the Bacillus subtilis K-state (competence) system requires a positive feedback loop. Mol Microbiol. 2005;56(3):615-24. Epub 2005/04/12. doi: 10.1111/j.1365-2958.2005.04592.x. PubMed PMID: 15819619; PubMed Central PMCID: PMCPMC3831615.

15.   Veening JW, Hamoen LW, Kuipers OP. Phosphatases modulate the bistable sporulation gene expression pattern in Bacillus subtilis. Mol Microbiol. 2005;56(6):1481-94. Epub 2005/05/27. doi: 10.1111/j.1365-2958.2005.04659.x. PubMed PMID: 15916600.

16.   Dubnau D, Losick R. Bistability in bacteria. Mol Microbiol. 2006;61(3):564-72. Epub 2006/08/02. doi: 10.1111/j.1365-2958.2006.05249.x. PubMed PMID: 16879639.

17.   Blauwkamp TA, Ninfa AJ. Physiological role of the GlnK signal transduction protein of Escherichia coli: survival of nitrogen starvation. Mol Microbiol. 2002;46(1):203-14. Epub 2002/10/09. doi: 10.1046/j.1365-2958.2002.03153.x. PubMed PMID: 12366843.

18.   Siegele DA, Hu JC. Gene expression from plasmids containing the araBAD promoter at subsaturating inducer concentrations represents mixed populations. Proc Natl Acad Sci U S A. 1997;94(15):8168-72. Epub 1997/07/22. doi: 10.1073/pnas.94.15.8168. PubMed PMID: 9223333; PubMed Central PMCID: PMCPMC21575.

19.   Pardee AB, Yates RA. Control of pyrimidine biosynthesis in Escherichia coli by a feed-back mechanism. J Biol Chem. 1956;221(2):757-70. Epub 1956/08/01. PubMed PMID: 13357469.

20.   Jacob F, Monod J. Genetic regulatory mechanisms in the synthesis of proteins. J Mol Biol. 1961;3:318-56. Epub 1961/06/01. doi: 10.1016/s0022-2836(61)80072-7. PubMed PMID: 13718526.

21. Paliwal S, Iglesias PA, Campbell K, Hilioti Z, Groisman A, Levchenko A. MAPK-mediated bimodal gene expression and adaptive gradient sensing in yeast. Nature. 2007;446(7131):46-51. Epub 2007/02/21. doi: 10.1038/nature05561. PubMed PMID: 17310144.

22. Pomerening JR, Sontag ED, Ferrell JE, Jr. Building a cell cycle oscillator: hysteresis and bistability in the activation of Cdc2. Nat Cell Biol. 2003;5(4):346-51. Epub 2003/03/12. doi: 10.1038/ncb954. PubMed PMID: 12629549.

23. Wykoff DD, Rizvi AH, Raser JM, Margolin B, O'Shea EK. Positive feedback regulates switching of phosphate transporters in S. cerevisiae. Mol Cell. 2007;27(6):1005-13. Epub 2007/09/25. doi: 10.1016/j.molcel.2007.07.022. PubMed PMID: 17889672; PubMed Central PMCID: PMCPMC2034509.

24. Freeman M. Feedback control of intercellular signalling in development. Nature. 2000;408(6810):313-9. Epub 2000/12/01. doi: 10.1038/35042500. PubMed PMID: 11099031.

25. Hernday AD, Braaten BA, Low DA. The mechanism by which DNA adenine methylase and PapI activate the pap epigenetic switch. Mol Cell. 2003;12(4):947-57. Epub 2003/10/29. doi: 10.1016/s1097-2765(03)00383-6. PubMed PMID: 14580345.

26. Sha W, Moore J, Chen K, Lassaletta AD, Yi CS, Tyson JJ, Sible JC. Hysteresis drives cell-cycle transitions in Xenopus laevis egg extracts. Proc Natl Acad Sci U S A. 2003;100(3):975-80. Epub 2003/01/02. doi: 10.1073/pnas.0235349100. PubMed PMID: 12509509; PubMed Central PMCID: PMCPMC298711.

27. Ferrell JE, Jr., Machleder EM. The biochemical basis of an all-or-none cell fate switch in Xenopus oocytes. Science. 1998;280(5365):895-8. Epub 1998/05/23. doi: 10.1126/science.280.5365.895. PubMed PMID: 9572732.

28. Burlando B. Loopomics: a new functional approach to life. J Appl Physiol (1985). 2017;123(4):1011-3. Epub 2017/04/22. doi: 10.1152/japplphysiol.00173.2017. PubMed PMID: 28428251.

29. Blanchini F, Franco E, Giordano G. A structural classification of candidate oscillatory and multistationary biochemical systems. Bull Math Biol. 2014;76(10):2542-69. Epub 2014/09/19. doi: 10.1007/s11538-014-0023-y. PubMed PMID: 25230803.

30. Bianconi E, Piovesan A, Facchin F, Beraudi A, Casadei R, Frabetti F, et al. An estimation of the number of cells in the human body. Ann Hum Biol. 2013;40(6):463-71. Epub 2013/07/09. doi: 10.3109/03014460.2013.807878. PubMed PMID: 23829164.

31. El-Samad H. Biological feedback control-Respect the loops. Cell Syst. 2021;12(6):477-87. Epub 2021/06/18. doi: 10.1016/j.cels.2021.05.004. PubMed PMID: 34139160.

32. Wolkenhauer O, Mesarovic M. Feedback dynamics and cell function: Why systems biology is called Systems Biology. Mol Biosyst. 2005;1(1):14-6. Epub 2006/08/02. doi: 10.1039/b502088n. PubMed PMID: 16880959.

33. Wolkenhauer O, Sreenath SN, Wellstead P, Ullah M, Cho KH. A systems- and signal-oriented approach to intracellular dynamics. Biochem Soc Trans. 2005;33(Pt 3):507-15. Epub 2005/05/27. doi: 10.1042/BST0330507. PubMed PMID: 15916553.

34. Laurent M, Kellershohn N. Multistability: a major means of differentiation and evolution in biological systems. Trends Biochem Sci. 1999;24(11):418-22. Epub 1999/11/05. doi: 10.1016/s0968-0004(99)01473-5. PubMed PMID: 10542403.

35. Olivenza DR, Nicoloff H, Sanchez-Romero MA, Cota I, Andersson DI, Casadesus J. A portable epigenetic switch for bistable gene expression in bacteria. Sci Rep. 2019;9(1):11261. Epub 2019/08/04. doi: 10.1038/s41598-019-47650-2. PubMed PMID: 31375711; PubMed Central PMCID: PMCPMC6677893.

36. Mochida S, Rata S, Hino H, Nagai T, Novak B. Two Bistable Switches Govern M Phase Entry. Curr Biol. 2016;26(24):3361-7. Epub 2016/11/28. doi: 10.1016/j.cub.2016.10.022. PubMed PMID: 27889260; PubMed Central PMCID: PMCPMC5196020.

37. Vigneron S, Sundermann L, Labbe JC, Pintard L, Radulescu O, Castro A, Lorca T. Cyclin A-cdk1-Dependent Phosphorylation of Bora Is the Triggering Factor Promoting Mitotic Entry. Dev

Cell. 2018;45(5):637-50 e7. Epub 2018/06/06. doi: 10.1016/j.devcel.2018.05.005. PubMed PMID: 29870721.

38.   Stallaert W, Kedziora KM, Chao HX, Purvis JE. Bistable switches as integrators and actuators during cell cycle progression. FEBS Lett. 2019;593(20):2805-16. Epub 2019/10/01. doi: 10.1002/1873-3468.13628. PubMed PMID: 31566708.

39.   Hutter LH, Rata S, Hochegger H, Novak B. Interlinked bistable mechanisms generate robust mitotic transitions. Cell Cycle. 2017;16(20):1885-92. Epub 2017/09/14. doi: 10.1080/15384101.2017.1371885. PubMed PMID: 28902568; PubMed Central PMCID: PMCPMC5638388.

40.   Nguyen LK, Kholodenko BN, von Kriegsheim A. Rac1 and RhoA: Networks, loops and bistability. Small GTPases. 2018;9(4):316-21. Epub 2016/08/18. doi: 10.1080/21541248.2016.1224399. PubMed PMID: 27533896; PubMed Central PMCID: PMCPMC5997137.

41.   Wang L, Walker BL, Iannaccone S, Bhatt D, Kennedy PJ, Tse WT. Bistable switches control memory and plasticity in cellular differentiation. Proc Natl Acad Sci U S A. 2009;106(16):6638-43. Epub 2009/04/16. doi: 10.1073/pnas.0806137106. PubMed PMID: 19366677; PubMed Central PMCID: PMCPMC2672527.

42.   Padmanabhan P, Goodhill GJ. Axon growth regulation by a bistable molecular switch. Proc Biol Sci. 2018;285(1877). Epub 2018/04/20. doi: 10.1098/rspb.2017.2618. PubMed PMID: 29669897; PubMed Central PMCID: PMCPMC5936722.

43.   Wackerhage H, Hoffmann U, Essfeld D, Leyk D, Mueller K, Zange J. Recovery of free ADP, Pi, and free energy of ATP hydrolysis in human skeletal muscle. J Appl Physiol (1985). 1998;85(6):2140-5. Epub 1998/12/08. doi: 10.1152/jappl.1998.85.6.2140. PubMed PMID: 9843537.

44.   Burlando B. A general hypothesis of multistable systems in pathophysiology. F1000Res. 2022;11:906. Epub 20220805. doi: 10.12688/f1000research.123183.2. PubMed PMID: 36226044; PubMed Central PMCID: PMCPMC9530619.

45.   Kim D, Rath O, Kolch W, Cho KH. A hidden oncogenic positive feedback loop caused by crosstalk between Wnt and ERK pathways. Oncogene. 2007;26(31):4571-9. Epub 2007/01/24. doi: 10.1038/sj.onc.1210230. PubMed PMID: 17237813.

46.   Huang B, Lu M, Jolly MK, Tsarfaty I, Onuchic J, Ben-Jacob E. The three-way switch operation of Rac1/RhoA GTPase-based circuit controlling amoeboid-hybrid-mesenchymal transition. Sci Rep. 2014;4:6449. Epub 2014/09/24. doi: 10.1038/srep06449. PubMed PMID: 25245029; PubMed Central PMCID: PMCPMC4171704.

47.   Kellershohn N, Laurent M. Prion diseases: dynamics of the infection and properties of the bistable transition. Biophys J. 2001;81(5):2517-29. Epub 2001/10/19. doi: 10.1016/S0006-3495(01)75897-3. PubMed PMID: 11606267; PubMed Central PMCID: PMCPMC1301721.

48.   Beutler B. Microbe sensing, positive feedback loops, and the pathogenesis of inflammatory diseases. Immunol Rev. 2009;227(1):248-63. Epub 2009/01/06. doi: 10.1111/j.1600-065X.2008.00733.x. PubMed PMID: 19120489; PubMed Central PMCID: PMCPMC2713013.

49.   Dominguez-Huttinger E, Christodoulides P, Miyauchi K, Irvine AD, Okada-Hatakeyama M, Kubo M, Tanaka RJ. Mathematical modeling of atopic dermatitis reveals "double-switch" mechanisms underlying 4 common disease phenotypes. J Allergy Clin Immunol. 2017;139(6):1861-72 e7. Epub 2016/12/10. doi: 10.1016/j.jaci.2016.10.026. PubMed PMID: 27931974.

50.   Mucci V, Indovina I, Browne CJ, Blanchini F, Giordano G, Marinelli L, Burlando B. Mal de Debarquement Syndrome: A Matter of Loops? Front Neurol. 2020;11:576860. Epub 2020/11/28. doi: 10.3389/fneur.2020.576860. PubMed PMID: 33244308; PubMed Central PMCID: PMCPMC7683778.

51.   De Caluwe J, Dupont G. The progression towards Alzheimer's disease described as a bistable switch arising from the positive loop between amyloids and Ca(2+). J Theor Biol. 2013;331:12-8. Epub 2013/04/26. doi: 10.1016/j.jtbi.2013.04.015. PubMed PMID: 23614875.

52.   Burlando B, Milanese M, Giordano G, Bonifacino T, Ravera S, Blanchini F, Bonanno G. A multistationary loop model of ALS unveils critical molecular interactions involving mitochondria and glucose metabolism. PLoS One. 2020;15(12):e0244234. Epub 2020/12/18. doi: 10.1371/journal.pone.0244234. PubMed PMID: 33332476; PubMed Central PMCID: PMCPMC7746301.

53.   Norwitz NG, Mota AS, Norwitz SG, Clarke K. Multi-Loop Model of Alzheimer Disease: An Integrated Perspective on the Wnt/GSK3beta, alpha-Synuclein, and Type 3 Diabetes Hypotheses. Front Aging Neurosci. 2019;11:184. Epub 2019/08/17. doi: 10.3389/fnagi.2019.00184. PubMed PMID: 31417394; PubMed Central PMCID: PMCPMC6685392.

54.   Freyer F, Roberts JA, Ritter P, Breakspear M. A canonical model of multistability and scale-invariance in biological systems. PLoS Comput Biol. 2012;8(8):e1002634. Epub 2012/08/23. doi: 10.1371/journal.pcbi.1002634. PubMed PMID: 22912567; PubMed Central PMCID: PMCPMC3415415.

55.   Ferrante M, Migliore M, Ascoli GA. Feed-forward inhibition as a buffer of the neuronal input-output relation. Proc Natl Acad Sci U S A. 2009;106(42):18004-9. Epub 2009/10/10. doi: 10.1073/pnas.0904784106. PubMed PMID: 19815518; PubMed Central PMCID: PMCPMC2764942.

56.   Blanchini F, Cuba Samaniego C, Franco E, Giordano G. Aggregates of Monotonic Step Response Systems: A Structural Classification. IEEE Trans Control Netw Syst. 2018;5:782–92.

57.   Angeli D, Ferrell JE, Jr., Sontag ED. Detection of multistability, bifurcations, and hysteresis in a large class of biological positive-feedback systems. Proc Natl Acad Sci U S A. 2004;101(7):1822-7. Epub 2004/02/10. doi: 10.1073/pnas.0308265100. PubMed PMID: 14766974; PubMed Central PMCID: PMCPMC357011.

58.   Scheffer M, Bascompte J, Brock WA, Brovkin V, Carpenter SR, Dakos V, et al. Early-warning signals for critical transitions. Nature. 2009;461(7260):53-9. Epub 2009/09/04. doi: 10.1038/nature08227. PubMed PMID: 19727193.

59.   Deb S, Bhandary S, Sinha SK, Jolly MK, Dutta PS. Identifying critical transitions in complex diseases. J Biosci. 2022;47(2). Epub 2022/10/11. doi: 10.1007/s12038-022-00258-7. PubMed PMID: 36210727; PubMed Central PMCID: PMCPMC9018973.

60.   Bazzichi L, Giacomelli C, Rossi A, Sernissi F, Scarpellini P, Consensi A, Bombardieri S. Fibromyalgia and sexual problems. Reumatismo. 2012;64(4):261-7. Epub 2012/10/02. doi: 10.4081/reumatismo.2012.261. PubMed PMID: 23024970.

61.   Sarzi-Puttini P, Giorgi V, Atzeni F, Gorla R, Kosek E, Choy EH, et al. Fibromyalgia position paper. Clin Exp Rheumatol. 2021;39 Suppl 130(3):186-93. Epub 2021/05/19. PubMed PMID: 34001303.

62.   Goldenberg DL. Pharmacological treatment of fibromyalgia and other chronic musculoskeletal pain. Best Pract Res Clin Rheumatol. 2007;21(3):499-511. Epub 2007/07/03. doi: 10.1016/j.berh.2007.02.012. PubMed PMID: 17602996.

63.   Kia S, Choy E. Update on Treatment Guideline in Fibromyalgia Syndrome with Focus on Pharmacology. Biomedicines. 2017;5(2). Epub 2017/05/26. doi: 10.3390/biomedicines5020020. PubMed PMID: 28536363; PubMed Central PMCID: PMCPMC5489806.

64.   Fink P, Rosendal M, Olesen F. Classification of somatization and functional somatic symptoms in primary care. Aust N Z J Psychiatry. 2005;39(9):772-81. Epub 2005/09/20. doi: 10.1080/j.1440-1614.2005.01682.x. PubMed PMID: 16168035.

65.   Bartels EM, Dreyer L, Jacobsen S, Jespersen A, Bliddal H, Danneskiold-Samsoe B. [Fibromyalgia, diagnosis and prevalence. Are gender differences explainable?]. Ugeskr Laeger. 2009;171(49):3588-92. Epub 2009/12/04. PubMed PMID: 19954696.

66.   Maurer AJ, Lissounov A, Knezevic I, Candido KD, Knezevic NN. Pain and sex hormones: a review of current understanding. Pain Manag. 2016;6(3):285-96. Epub 2016/03/18. doi: 10.2217/pmt-2015-0002. PubMed PMID: 26983893.

67.   Neumann L, Buskila D. Epidemiology of fibromyalgia. Curr Pain Headache Rep. 2003;7(5):362-8. Epub 2003/08/30. doi: 10.1007/s11916-003-0035-z. PubMed PMID: 12946289.

68.   Albert PR. Why is depression more prevalent in women? J Psychiatr Neurosci. 2015;40(4):219-21. doi: 10.1503/jpn.150205. PubMed PMID: WOS:000356934900001.

69.   Todd C, Lagman-Bartolome AM, Lay C. Women and Migraine: the Role of Hormones. Curr Neurol Neurosci Rep. 2018;18(7):42. Epub 2018/06/02. doi: 10.1007/s11910-018-0845-3. PubMed PMID: 29855724.

70.   Teggi R, Manfrin M, Balzanelli C, Gatti O, Mura F, Quaglieri S, et al. Point prevalence of vertigo and dizziness in a sample of 2672 subjects and correlation with headaches. Acta Otorhinolaryngol Ital. 2016;36(3):215-9. Epub 2016/05/24. doi: 10.14639/0392-100X-847. PubMed PMID: 27214833; PubMed Central PMCID: PMCPMC4977009.

71.   Jones KD, Horak FB, Winters-Stone K, Irvine JM, Bennett RM. Fibromyalgia is associated with impaired balance and falls. J Clin Rheumatol. 2009;15(1):16-21. Epub 2009/01/07. doi: 10.1097/RHU.0b013e318190f991. PubMed PMID: 19125137; PubMed Central PMCID: PMCPMC2836495.

72.   Russek LN, Fulk GD. Pilot study assessing balance in women with fibromyalgia syndrome. Physiother Theory Pract. 2009;25(8):555-65. Epub 2009/11/21. doi: 10.3109/09593980802668050. PubMed PMID: 19925263.

73.   Sawada F, Nomura Y, Goto F, Murakami M, Jike M, Toi T, et al. Relationship of physical distress to dizziness in patients with fibromyalgia. Acta Otolaryngol. 2016;136(1):56-61. Epub 2015/10/10. doi: 10.3109/00016489.2015.1088662. PubMed PMID: 26449588.

74.   Zeigelboim BS, Moreira DN. Achados Vestibulares Em Pacientes Portadores De Fibromialgia. Arquivos Int Otorrinolaringol. 2011;15(3):283-9.

75.   Lopez-Sola M, Woo CW, Pujol J, Deus J, Harrison BJ, Monfort J, Wager TD. Towards a neurophysiological signature for fibromyalgia. Pain. 2017;158(1):34-47. Epub 2016/09/02. doi: 10.1097/j.pain.0000000000000707. PubMed PMID: 27583567; PubMed Central PMCID: PMCPMC5161739.

76.   Arnold LM, Bennett RM, Crofford LJ, Dean LE, Clauw DJ, Goldenberg DL, et al. AAPT Diagnostic Criteria for Fibromyalgia. J Pain. 2019;20(6):611-28. Epub 2018/11/20. doi: 10.1016/j.jpain.2018.10.008. PubMed PMID: 30453109.

77.   Wolfe F, Clauw DJ, Fitzcharles MA, Goldenberg DL, Hauser W, Katz RL, et al. 2016 Revisions to the 2010/2011 fibromyalgia diagnostic criteria. Semin Arthritis Rheum. 2016;46(3):319-29. Epub 2016/12/06. doi: 10.1016/j.semarthrit.2016.08.012. PubMed PMID: 27916278.

78.   Clauw DJ. Fibromyalgia: an overview. Am J Med. 2009;122(12 Suppl):S3-S13. Epub 2010/01/09. doi: 10.1016/j.amjmed.2009.09.006. PubMed PMID: 19962494.

79.   Ablin J, Fitzcharles MA, Buskila D, Shir Y, Sommer C, Hauser W. Treatment of fibromyalgia syndrome: recommendations of recent evidence-based interdisciplinary guidelines with special emphasis on complementary and alternative therapies. Evid Based Complement Alternat Med. 2013;2013:485272. Epub 2013/12/19. doi: 10.1155/2013/485272. PubMed PMID: 24348701; PubMed Central PMCID: PMCPMC3856149.

80.   Bazzichi L, Giannaccini G, Betti L, Mascia G, Fabbrini L, Italiani P, et al. Alteration of serotonin transporter density and activity in fibromyalgia. Arthritis Res Ther. 2006;8(4):R99. Epub 2006/06/23. doi: 10.1186/ar1982. PubMed PMID: 16790074; PubMed Central PMCID: PMCPMC1779383.

81.   Geel SE. The fibromyalgia syndrome: musculoskeletal pathophysiology. Semin Arthritis Rheum. 1994;23(5):347-53. Epub 1994/04/01. doi: 10.1016/0049-0172(94)90030-2. PubMed PMID: 8036524.

82.   Meeus M, Nijs J. Central sensitization: a biopsychosocial explanation for chronic widespread pain in patients with fibromyalgia and chronic fatigue syndrome. Clin Rheumatol. 2007;26(4):465-73. Epub 2006/11/23. doi: 10.1007/s10067-006-0433-9. PubMed PMID: 17115100; PubMed Central PMCID: PMCPMC1820749.

83.	Jahan F, Nanji K, Qidwai W, Qasim R. Fibromyalgia syndrome: an overview of pathophysiology, diagnosis and management. Oman Med J. 2012;27(3):192-5. Epub 2012/07/20. doi: 10.5001/omj.2012.44. PubMed PMID: 22811766; PubMed Central PMCID: PMCPMC3394355.

84.	Bellato E, Marini E, Castoldi F, Barbasetti N, Mattei L, Bonasia DE, Blonna D. Fibromyalgia syndrome: etiology, pathogenesis, diagnosis, and treatment. Pain Res Treat. 2012;2012:426130. Epub 2012/12/06. doi: 10.1155/2012/426130. PubMed PMID: 23213512; PubMed Central PMCID: PMCPMC3503476.

85.	Hurtig IM, Raak RI, Kendall SA, Gerdle B, Wahren LK. Quantitative sensory testing in fibromyalgia patients and in healthy subjects: identification of subgroups. Clin J Pain. 2001;17(4):316-22. Epub 2002/01/11. doi: 10.1097/00002508-200112000-00005. PubMed PMID: 11783811.

86.	Mease P. Fibromyalgia syndrome: review of clinical presentation, pathogenesis, outcome measures, and treatment. J Rheumatol Suppl. 2005;75:6-21. Epub 2005/08/04. PubMed PMID: 16078356.

87.	Sontag ED. Some new directions in control theory inspired by systems biology. Syst Biol (Stevenage). 2004;1(1):9-18. Epub 2006/10/21. doi: 10.1049/sb:20045006. PubMed PMID: 17052111.

88.	Ader R. On the development of psychoneuroimmunology. Eur J Pharmacol. 2000;405(1-3):167-76. Epub 2000/10/18. doi: 10.1016/s0014-2999(00)00550-1. PubMed PMID: 11033324.

89.	Franca K, Lotti TM. Psycho-Neuro-Endocrine-Immunology: A Psychobiological Concept. Adv Exp Med Biol. 2017;996:123-34. Epub 2017/11/11. doi: 10.1007/978-3-319-56017-5_11. PubMed PMID: 29124696.

90.	Queiroz LP. Worldwide epidemiology of fibromyalgia. Curr Pain Headache Rep. 2013;17(8):356. doi: 10.1007/s11916-013-0356-5. PubMed PMID: 23801009.

91.	Arout CA, Sofuoglu M, Bastian LA, Rosenheck RA. Gender Differences in the Prevalence of Fibromyalgia and in Concomitant Medical and Psychiatric Disorders: A National Veterans Health Administration Study. J Womens Health (Larchmt). 2018;27(8):1035-44. Epub 2018/04/03. doi: 10.1089/jwh.2017.6622. PubMed PMID: 29608126; PubMed Central PMCID: PMCPMC6425926.

92.	Martinez-Lavin M. Biology and therapy of fibromyalgia. Stress, the stress response system, and fibromyalgia. Arthritis Res Ther. 2007;9(4):216. doi: 10.1186/ar2146. PubMed PMID: 17626613; PubMed Central PMCID: PMCPMC2206360.

93.	Gonzalez-Vives S, Diaz-Marsa M, De la Vega I, Palomares N, Vazquez S, Lopez-Villatoro JM, et al. Hypothalamic-pituitary axis response to a 0.25-MG dexamethasone test in women with fibromyalgia. Stress. 2020;23(3):284-9. Epub 20191018. doi: 10.1080/10253890.2019.1678024. PubMed PMID: 31591938.

94.	Neeck G, Riedel W. Hormonal pertubations in fibromyalgia syndrome. Ann N Y Acad Sci. 1999;876:325-38; discussion 39. doi: 10.1111/j.1749-6632.1999.tb07657.x. PubMed PMID: 10415628.

95.	Alciati A, Cirillo M, Masala IF, Sarzi-Puttini P, Atzeni F. Differences in depression, anxiety and stress disorders between fibromyalgia associated with rheumatoid arthritis and primary fibromyalgia. Stress Health. 2021;37(2):255-62. Epub 20201006. doi: 10.1002/smi.2992. PubMed PMID: 32991777.

96.	Nardi AE, Karam EG, Carta MG. Fibromyalgia patients should always be screened for post-traumatic stress disorder. Expert Rev Neurother. 2020;20(9):891-3. Epub 20200723. doi: 10.1080/14737175.2020.1794824. PubMed PMID: 32662698.

97.	Silver RA. Neuronal arithmetic. Nat Rev Neurosci. 2010;11(7):474-89. Epub 2010/06/10. doi: 10.1038/nrn2864. PubMed PMID: 20531421; PubMed Central PMCID: PMCPMC4750293.

98.	Chabrol FP, Arenz A, Wiechert MT, Margrie TW, DiGregorio DA. Synaptic diversity enables temporal coding of coincident multisensory inputs in single neurons. Nat Neurosci. 2015;18(5):718-27. Epub 2015/03/31. doi: 10.1038/nn.3974. PubMed PMID: 25821914; PubMed Central PMCID: PMCPMC4413433.

99.   Currin CB, Trevelyan AJ, Akerman CJ, Raimondo JV. Chloride dynamics alter the input-output properties of neurons. PLoS Comput Biol. 2020;16(5):e1007932. Epub 2020/05/27. doi: 10.1371/journal.pcbi.1007932. PubMed PMID: 32453795; PubMed Central PMCID: PMCPMC7307785.

100.   Kornijcuk V, Lim H, Seok JY, Kim G, Kim SK, Kim I, et al. Leaky Integrate-and-Fire Neuron Circuit Based on Floating-Gate Integrator. Front Neurosci. 2016;10:212. Epub 2016/06/01. doi: 10.3389/fnins.2016.00212. PubMed PMID: 27242416; PubMed Central PMCID: PMCPMC4876293.

101.   Barardi A, Garcia-Ojalvo J, Mazzoni A. Transition between Functional Regimes in an Integrate-And-Fire Network Model of the Thalamus. PLoS One. 2016;11(9):e0161934. Epub 2016/09/07. doi: 10.1371/journal.pone.0161934. PubMed PMID: 27598260; PubMed Central PMCID: PMCPMC5012668.

102.   Olsen SR, Bhandawat V, Wilson RI. Divisive normalization in olfactory population codes. Neuron. 2010;66(2):287-99. Epub 2010/05/04. doi: 10.1016/j.neuron.2010.04.009. PubMed PMID: 20435004; PubMed Central PMCID: PMCPMC2866644.

103.   Kanagasabapathi TT, Massobrio P, Barone RA, Tedesco M, Martinoia S, Wadman WJ, Decre MM. Functional connectivity and dynamics of cortical-thalamic networks co-cultured in a dual compartment device. J Neural Eng. 2012;9(3):036010. Epub 2012/05/23. doi: 10.1088/1741-2560/9/3/036010. PubMed PMID: 22614532.

104.   Uusisaari M, Obata K, Knopfel T. Morphological and electrophysiological properties of GABAergic and non-GABAergic cells in the deep cerebellar nuclei. J Neurophysiol. 2007;97(1):901-11. Epub 2006/11/10. doi: 10.1152/jn.00974.2006. PubMed PMID: 17093116.

105.   Rothman JS, Cathala L, Steuber V, Silver RA. Synaptic depression enables neuronal gain control. Nature. 2009;457(7232):1015-8. Epub 2009/01/16. doi: 10.1038/nature07604. PubMed PMID: 19145233; PubMed Central PMCID: PMCPMC2689940.

106.   Li L, Sultan S, Heigele S, Schmidt-Salzmann C, Toni N, Bischofberger J. Silent synapses generate sparse and orthogonal action potential firing in adult-born hippocampal granule cells. Elife. 2017;6. Epub 2017/08/23. doi: 10.7554/eLife.23612. PubMed PMID: 28826488; PubMed Central PMCID: PMCPMC5580881.

107.   Demori I, Giordano G, Mucci V, Losacco S, Marinelli L, Massobrio P, et al. Thalamocortical bistable switch as a theoretical model of fibromyalgia pathogenesis inferred from a literature survey. J Comput Neurosci. 2022;50(4):471-84. doi: 10.1007/s10827-022-00826-8. PubMed PMID: 35816263.

108.   Mastorakos G, Pavlatou MG, Mizamtsidi M. The hypothalamic-pituitary-adrenal and the hypothalamic- pituitary-gonadal axes interplay. Pediatr Endocrinol Rev. 2006;3 Suppl 1:172-81. PubMed PMID: 16641855.

109.   Breivik EK, Bjornsson GA, Skovlund E. A comparison of pain rating scales by sampling from clinical trial data. Clin J Pain. 2000;16(1):22-8. Epub 2000/03/31. doi: 10.1097/00002508-200003000-00005. PubMed PMID: 10741815.

110.   Freynhagen R, Baron R, Gockel U, Tolle TR. painDETECT: a new screening questionnaire to identify neuropathic components in patients with back pain. Curr Med Res Opin. 2006;22(10):1911-20. Epub 2006/10/07. doi: 10.1185/030079906X132488. PubMed PMID: 17022849.

111.   Brackett MA, Rivers SE, Shiffman S, Lerner N, Salovey P. Relating emotional abilities to social functioning: a comparison of self-report and performance measures of emotional intelligence. J Pers Soc Psychol. 2006;91(4):780-95. Epub 2006/10/04. doi: 10.1037/0022-3514.91.4.780. PubMed PMID: 17014299.

112.   Zotti AM, Bertolotti G, Michielin P, Sanavio E, Vidotto G. Linee guida per lo screening di tratti di personalità , cognizioni e comportamenti avversi alla salute. Manuale d'uso per il CBA Forma Hospital. Pavia, Italy: Maugeri Foundation Books; 2000. 126 p.

113.   Nola G, Mostardini C, Salvi C, Ercolani AP, Ralli G. Validity of Italian adaptation of the Dizziness Handicap Inventory (DHI) and evaluation of the quality of life in patients with acute dizziness. Acta Otorhinolaryngol Ital. 2010;30(4):190. Epub 2011/01/22. PubMed PMID: 21253284; PubMed Central PMCID: PMCPMC3008147.

114.   Colnaghi S, Rezzani C, Gnesi M, Manfrin M, Quaglieri S, Nuti D, et al. Validation of the Italian Version of the Dizziness Handicap Inventory, the Situational Vertigo Questionnaire, and the Activity-Specific Balance Confidence Scale for Peripheral and Central Vestibular Symptoms. Front Neurol. 2017;8:528. Epub 2017/10/27. doi: 10.3389/fneur.2017.00528. PubMed PMID: 29066999; PubMed Central PMCID: PMCPMC5641311.

115.   Groh A, Krieger P, Mease RA, Henderson L. Acute and Chronic Pain Processing in the Thalamocortical System of Humans and Animal Models. Neuroscience. 2018;387:58-71. Epub 2017/10/06. doi: 10.1016/j.neuroscience.2017.09.042. PubMed PMID: 28978414.

116.   Lam YW, Sherman SM. Functional organization of the thalamic input to the thalamic reticular nucleus. J Neurosci. 2011;31(18):6791-9. Epub 2011/05/06. doi: 10.1523/JNEUROSCI.3073-10.2011. PubMed PMID: 21543609; PubMed Central PMCID: PMCPMC3565464.

117.   Takata N. Thalamic reticular nucleus in the thalamocortical loop. Neurosci Res. 2020;156:32-40. Epub 2019/12/10. doi: 10.1016/j.neures.2019.12.004. PubMed PMID: 31812650.

118.   Feldmeyer D. Excitatory neuronal connectivity in the barrel cortex. Front Neuroanat. 2012;6:24. Epub 2012/07/17. doi: 10.3389/fnana.2012.00024. PubMed PMID: 22798946; PubMed Central PMCID: PMCPMC3394394.

119.   Doig AJ. Positive Feedback Loops in Alzheimer's Disease: The Alzheimer's Feedback Hypothesis. J Alzheimers Dis. 2018;66(1):25-36. Epub 2018/10/05. doi: 10.3233/JAD-180583. PubMed PMID: 30282364; PubMed Central PMCID: PMCPMC6484277.

120.   Wang M. Neurosteroids and GABA-A Receptor Function. Front Endocrinol (Lausanne). 2011;2:44. Epub 20111004. doi: 10.3389/fendo.2011.00044. PubMed PMID: 22654809; PubMed Central PMCID: PMCPMC3356040.

121.   Singh L, Kaur A, Bhatti MS, Bhatti R. Possible Molecular Mediators Involved and Mechanistic Insight into Fibromyalgia and Associated Co-morbidities. Neurochem Res. 2019;44(7):1517-32. Epub 20190419. doi: 10.1007/s11064-019-02805-5. PubMed PMID: 31004261.

122.   Charmandari E, Tsigos C, Chrousos G. Endocrinology of the stress response. Annu Rev Physiol. 2005;67:259-84. doi: 10.1146/annurev.physiol.67.040403.120816. PubMed PMID: 15709959.

123.   Peper JS, Brouwer RM, van Leeuwen M, Schnack HG, Boomsma DI, Kahn RS, Hulshoff Pol HE. HPG-axis hormones during puberty: a study on the association with hypothalamic and pituitary volumes. Psychoneuroendocrinology. 2010;35(1):133-40. doi: 10.1016/j.psyneuen.2009.05.025. PubMed PMID: 19570613.

124.   Schertzinger M, Wesson-Sides K, Parkitny L, Younger J. Daily Fluctuations of Progesterone and Testosterone Are Associated With Fibromyalgia Pain Severity. J Pain. 2018;19(4):410-7. Epub 20171214. doi: 10.1016/j.jpain.2017.11.013. PubMed PMID: 29248511; PubMed Central PMCID: PMCPMC6046191.

125.   Zhang L, Chang YH, Feldman AN, Ma W, Lahjouji F, Barker JL, et al. The expression of GABA(A) receptor alpha2 subunit is upregulated by testosterone in rat cerebral cortex. Neurosci Lett. 1999;265(1):25-8. doi: 10.1016/s0304-3940(99)00193-7. PubMed PMID: 10327197.

126.   Flores-Ramos M, Alcauter S, Lopez-Titla M, Bernal-Santamaria N, Calva-Coraza E, Edden RAE. Testosterone is related to GABA+ levels in the posterior-cingulate in unmedicated depressed women during reproductive life. J Affect Disord. 2019;242:143-9. Epub 20180825. doi: 10.1016/j.jad.2018.08.033. PubMed PMID: 30195172; PubMed Central PMCID: PMCPMC6484862.

127.   Paul SM, Purdy RH. Neuroactive steroids. FASEB J. 1992;6(6):2311-22. PubMed PMID: 1347506.

128. Lambert JJ, Cooper MA, Simmons RD, Weir CJ, Belelli D. Neurosteroids: endogenous allosteric modulators of GABA(A) receptors. Psychoneuroendocrinology. 2009;34 Suppl 1:S48-58. doi: 10.1016/j.psyneuen.2009.08.009. PubMed PMID: 19758761.

129. Reddy DS. Neurosteroids: endogenous role in the human brain and therapeutic potentials. Prog Brain Res. 2010;186:113-37. Epub 2010/11/26. doi: 10.1016/B978-0-444-53630-3.00008-7. PubMed PMID: 21094889; PubMed Central PMCID: PMCPMC3139029.

130. Reddy DS, Jian K. The testosterone-derived neurosteroid androstanediol is a positive allosteric modulator of GABAA receptors. J Pharmacol Exp Ther. 2010;334(3):1031-41. Epub 20100615. doi: 10.1124/jpet.110.169854. PubMed PMID: 20551294; PubMed Central PMCID: PMCPMC2939675.

131. Schumacher M, Weill-Engerer S, Liere P, Robert F, Franklin RJ, Garcia-Segura LM, et al. Steroid hormones and neurosteroids in normal and pathological aging of the nervous system. Prog Neurobiol. 2003;71(1):3-29. doi: 10.1016/j.pneurobio.2003.09.004. PubMed PMID: 14611864.

132. MacKenzie G, Maguire J. Neurosteroids and GABAergic signaling in health and disease. Biomol Concepts. 2013;4(1):29-42. doi: 10.1515/bmc-2012-0033. PubMed PMID: 25436563; PubMed Central PMCID: PMCPMC5469411.

133. Belelli D, Hogenkamp D, Gee KW, Lambert JJ. Realising the therapeutic potential of neuroactive steroid modulators of the GABA(A) receptor. Neurobiol Stress. 2020;12:100207. Epub 20191223. doi: 10.1016/j.ynstr.2019.100207. PubMed PMID: 32435660; PubMed Central PMCID: PMCPMC7231973.

134. Hellgren C, Akerud H, Skalkidou A, Backstrom T, Sundstrom-Poromaa I. Low serum allopregnanolone is associated with symptoms of depression in late pregnancy. Neuropsychobiology. 2014;69(3):147-53. Epub 20140426. doi: 10.1159/000358838. PubMed PMID: 24776841.

135. Stromberg J, Haage D, Taube M, Backstrom T, Lundgren P. Neurosteroid modulation of allopregnanolone and GABA effect on the GABA-A receptor. Neuroscience. 2006;143(1):73-81. Epub 20060828. doi: 10.1016/j.neuroscience.2006.07.031. PubMed PMID: 16938407.

136. Mtchedlishvili Z, Bertram EH, Kapur J. Diminished allopregnanolone enhancement of GABA(A) receptor currents in a rat model of chronic temporal lobe epilepsy. J Physiol. 2001;537(Pt 2):453-65. doi: 10.1111/j.1469-7793.2001.00453.x. PubMed PMID: 11731578; PubMed Central PMCID: PMCPMC2278949.

137. Callachan H, Cottrell GA, Hather NY, Lambert JJ, Nooney JM, Peters JA. Modulation of the GABAA receptor by progesterone metabolites. Proc R Soc Lond B Biol Sci. 1987;231(1264):359-69. doi: 10.1098/rspb.1987.0049. PubMed PMID: 2888123.

138. Westergard T, Salari R, Martin JV, Brannigan G. Interactions of L-3,5,3'-Triiodothyronine [corrected], Allopregnanolone, and Ivermectin with the GABAA Receptor: Evidence for Overlapping Intersubunit Binding Modes. PLoS One. 2015;10(9):e0139072. Epub 20150930. doi: 10.1371/journal.pone.0139072. PubMed PMID: 26421724; PubMed Central PMCID: PMCPMC4589331.

139. Haage D, Johansson S. Neurosteroid modulation of synaptic and GABA-evoked currents in neurons from the rat medial preoptic nucleus. J Neurophysiol. 1999;82(1):143-51. doi: 10.1152/jn.1999.82.1.143. PubMed PMID: 10400943.

140. Nik AM, Pressly B, Singh V, Antrobus S, Hulsizer S, Rogawski MA, et al. Rapid Throughput Analysis of GABA(A) Receptor Subtype Modulators and Blockers Using DiSBAC(1)(3) Membrane Potential Red Dye. Mol Pharmacol. 2017;92(1):88-99. Epub 20170420. doi: 10.1124/mol.117.108563. PubMed PMID: 28428226; PubMed Central PMCID: PMCPMC5452057.

141. Liu QY, Chang YH, Schaffner AE, Smith SV, Barker JL. Allopregnanolone activates GABA(A) receptor/Cl(-) channels in a multiphasic manner in embryonic rat hippocampal neurons. J Neurophysiol. 2002;88(3):1147-58. doi: 10.1152/jn.00942.2001. PubMed PMID: 12205136.

142. Dennerstein L, Spencer-Gardner C, Gotts G, Brown JB, Smith MA, Burrows GD. Progesterone and the premenstrual syndrome: a double blind crossover trial. Br Med J (Clin Res Ed).

1985;290(6482):1617-21. doi: 10.1136/bmj.290.6482.1617. PubMed PMID: 3924191; PubMed Central PMCID: PMCPMC1415816.

143. Backstrom T, Zetterlund B, Blom S, Romano M. Effects of intravenous progesterone infusions on the epileptic discharge frequency in women with partial epilepsy. Acta Neurol Scand. 1984;69(4):240-8. doi: 10.1111/j.1600-0404.1984.tb07807.x. PubMed PMID: 6430018.

144. Herzog AG. Progesterone therapy in women with complex partial and secondary generalized seizures. Neurology. 1995;45(9):1660-2. doi: 10.1212/wnl.45.9.1660. PubMed PMID: 7675223.

145. Smith SS, Gong QH, Hsu FC, Markowitz RS, ffrench-Mullen JM, Li X. GABA(A) receptor alpha4 subunit suppression prevents withdrawal properties of an endogenous steroid. Nature. 1998;392(6679):926-30. doi: 10.1038/31948. PubMed PMID: 9582073.

146. Gangisetty O, Reddy DS. Neurosteroid withdrawal regulates GABA-A receptor alpha4-subunit expression and seizure susceptibility by activation of progesterone receptor-independent early growth response factor-3 pathway. Neuroscience. 2010;170(3):865-80. Epub 20100727. doi: 10.1016/j.neuroscience.2010.07.037. PubMed PMID: 20670676; PubMed Central PMCID: PMCPMC2939139.

147. Reddy DS, Kim HY, Rogawski MA. Neurosteroid withdrawal model of perimenstrual catamenial epilepsy. Epilepsia. 2001;42(3):328-36. doi: 10.1046/j.1528-1157.2001.10100.x. PubMed PMID: 11442149.

148. Sun JY, Zhao SJ, Wang HB, Hou YJ, Mi QJ, Yang MF, et al. Ifenprodil Improves Long-Term Neurologic Deficits Through Antagonizing Glutamate-Induced Excitotoxicity After Experimental Subarachnoid Hemorrhage. Transl Stroke Res. 2021;12(6):1067-80. Epub 20210312. doi: 10.1007/s12975-021-00906-4. PubMed PMID: 33713028.

149. Cullinan WE, Ziegler DR, Herman JP. Functional role of local GABAergic influences on the HPA axis. Brain Struct Funct. 2008;213(1-2):63-72. Epub 20080812. doi: 10.1007/s00429-008-0192-2. PubMed PMID: 18696110.

150. Crowley SK, Girdler SS. Neurosteroid, GABAergic and hypothalamic pituitary adrenal (HPA) axis regulation: what is the current state of knowledge in humans? Psychopharmacology (Berl). 2014;231(17):3619-34. Epub 20140423. doi: 10.1007/s00213-014-3572-8. PubMed PMID: 24756763; PubMed Central PMCID: PMCPMC4135030.

151. Barbaccia ML, Roscetti G, Trabucchi M, Mostallino MC, Concas A, Purdy RH, Biggio G. Time-dependent changes in rat brain neuroactive steroid concentrations and GABAA receptor function after acute stress. Neuroendocrinology. 1996;63(2):166-72. doi: 10.1159/000126953. PubMed PMID: 9053781.

152. Yuen EY, Liu W, Karatsoreos IN, Feng J, McEwen BS, Yan Z. Acute stress enhances glutamatergic transmission in prefrontal cortex and facilitates working memory. Proc Natl Acad Sci U S A. 2009;106(33):14075-9. Epub 20090729. doi: 10.1073/pnas.0906791106. PubMed PMID: 19666502; PubMed Central PMCID: PMCPMC2729022.

153. Popoli M, Yan Z, McEwen BS, Sanacora G. The stressed synapse: the impact of stress and glucocorticoids on glutamate transmission. Nat Rev Neurosci. 2011;13(1):22-37. Epub 2011/12/01. doi: 10.1038/nrn3138. PubMed PMID: 22127301; PubMed Central PMCID: PMCPMC3645314.

154. Altemus M, Redwine LS, Leong YM, Frye CA, Porges SW, Carter CS. Responses to laboratory psychosocial stress in postpartum women. Psychosom Med. 2001;63(5):814-21. doi: 10.1097/00006842-200109000-00015. PubMed PMID: 11573030.

155. Childs E, de Wit H. Hormonal, cardiovascular, and subjective responses to acute stress in smokers. Psychopharmacology (Berl). 2009;203(1):1-12. Epub 20081021. doi: 10.1007/s00213-008-1359-5. PubMed PMID: 18936915; PubMed Central PMCID: PMCPMC2727744.

156. Harden KP, Wrzus C, Luong G, Grotzinger A, Bajbouj M, Rauers A, et al. Diurnal coupling between testosterone and cortisol from adolescence to older adulthood. Psychoneuroendocrinology. 2016;73:79-90. Epub 20160722. doi: 10.1016/j.psyneuen.2016.07.216. PubMed PMID: 27474909; PubMed Central PMCID: PMCPMC5048541.

157.	Solano ME, Arck PC. Steroids, Pregnancy and Fetal Development. Front Immunol. 2019;10:3017. Epub 20200122. doi: 10.3389/fimmu.2019.03017. PubMed PMID: 32038609; PubMed Central PMCID: PMCPMC6987319.

158.	Stadler A, Weidlinger S, Stute P. Impact of endogenous and exogenous progesterone exposure on stress biomarkers: a systematic review. Climacteric. 2019;22(5):435-41. Epub 20190703. doi: 10.1080/13697137.2019.1622085. PubMed PMID: 31267780.

159.	Oyola MG, Handa RJ. Hypothalamic-pituitary-adrenal and hypothalamic-pituitary-gonadal axes: sex differences in regulation of stress responsivity. Stress. 2017;20(5):476-94. Epub 20170831. doi: 10.1080/10253890.2017.1369523. PubMed PMID: 28859530; PubMed Central PMCID: PMCPMC5815295.

160.	Viau V. Functional cross-talk between the hypothalamic-pituitary-gonadal and -adrenal axes. J Neuroendocrinol. 2002;14(6):506-13. doi: 10.1046/j.1365-2826.2002.00798.x. PubMed PMID: 12047726.

161.	Caufriez A, Leproult R, Copinschi G. Circadian profiles of progesterone, gonadotropins, cortisol and corticotropin in cycling and postmenopausal women. Chronobiol Int. 2018;35(1):72-9. Epub 20171107. doi: 10.1080/07420528.2017.1381971. PubMed PMID: 29111782.

162.	Rahman SA, Grant LK, Gooley JJ, Rajaratnam SMW, Czeisler CA, Lockley SW. Endogenous Circadian Regulation of Female Reproductive Hormones. J Clin Endocrinol Metab. 2019;104(12):6049-59. doi: 10.1210/jc.2019-00803. PubMed PMID: 31415086; PubMed Central PMCID: PMCPMC6821202.

163.	Turner AI, Hemsworth PH, Canny BJ, Tilbrook AJ. Sustained but not repeated acute elevation of cortisol impaired the luteinizing hormone surge, estrus, and ovulation in gilts. Biol Reprod. 1999;61(3):614-20. doi: 10.1095/biolreprod61.3.614. PubMed PMID: 10456836.

164.	Chatterton RT, Jr., Kazer RR, Rebar RW. Depletion of luteal phase serum progesterone during constant infusion of cortisol phosphate in the cynomolgus monkey. Fertil Steril. 1991;56(3):547-54. PubMed PMID: 1894035.

165.	Junkermann H, Mangold H, Vecsei P, Runnebaum B. Circadian rhythm of serum progesterone levels in human pregnancy and its relation to the rhythm of cortisol. Acta Endocrinol (Copenh). 1982;101(1):98-104. doi: 10.1530/acta.0.1010098. PubMed PMID: 7124294.

166.	Runnebaum B, Rieben W, Bierwirth-von M, Zander J. Circadian variations in plasma progesterone in the luteal phase of the menstrual cycle and during pregnancy. Acta Endocrinol (Copenh). 1972;69(4):731-8. doi: 10.1530/acta.0.0690731. PubMed PMID: 5067077.

167.	Elsner CW, Buster JE, Preston DL, Killam AP. Interrelationships of circulating maternal steroid concentrations in third trimester pregnancies. III. Effect of intravenous cortisol infusion on maternal concentrations of estriol, 16 alpha-hydroxyprogesterone, 17 alpha-hydroxyprogesterone, progesterone, 20 alpha-dihydroprogesterone, delta 5-pregnenolone, delta5-pregnenolone sulfate, dehydroepiandrosterone sulfate, and cortisol. J Clin Endocrinol Metab. 1979;49(1):30-3. doi: 10.1210/jcem-49-1-30. PubMed PMID: 156194.

168.	Saketos M, Sharma N, Santoro NF. Suppression of the hypothalamic-pituitary-ovarian axis in normal women by glucocorticoids. Biol Reprod. 1993;49(6):1270-6. doi: 10.1095/biolreprod49.6.1270. PubMed PMID: 8286608.

169.	Segebladh B, Bannbers E, Moby L, Nyberg S, Bixo M, Backstrom T, Sundstrom Poromaa I. Allopregnanolone serum concentrations and diurnal cortisol secretion in women with premenstrual dysphoric disorder. Arch Womens Ment Health. 2013;16(2):131-7. Epub 20130118. doi: 10.1007/s00737-013-0327-1. PubMed PMID: 23329007.

170.	Karalis K, Goodwin G, Majzoub JA. Cortisol blockade of progesterone: a possible molecular mechanism involved in the initiation of human labor. Nat Med. 1996;2(5):556-60. doi: 10.1038/nm0596-556. PubMed PMID: 8616715.

171.	Thibier M, Rolland O. The effect of dexamethasone (DXM) on circulating testosterone (T) and luteinizing hormone (LH) in young postpubertal bulls. Theriogenology. 1976;5(2):53-60. doi: 10.1016/0093-691x(76)90168-0. PubMed PMID: 950066.

172.   Juniewicz PE, Johnson BH, Bolt DJ. Effect of adrenal steroids on testosterone and luteinizing hormone secretion in the ram. J Androl. 1987;8(3):190-6. doi: 10.1002/j.1939-4640.1987.tb02430.x. PubMed PMID: 3038815.

173.   Brownlee KK, Moore AW, Hackney AC. Relationship between circulating cortisol and testosterone: influence of physical exercise. J Sports Sci Med. 2005;4(1):76-83.

174.   Rubinow DR, Roca CA, Schmidt PJ, Danaceau MA, Putnam K, Cizza G, et al. Testosterone suppression of CRH-stimulated cortisol in men. Neuropsychopharmacology. 2005;30(10):1906-12. doi: 10.1038/sj.npp.1300742. PubMed PMID: 15841103; PubMed Central PMCID: PMCPMC1470424.

175.   Ullah R, Shen Y, Zhou YD, Huang K, Fu JF, Wahab F, Shahab M. Expression and actions of GnIH and its orthologs in vertebrates: Current status and advanced knowledge. Neuropeptides. 2016;59:9-20. Epub 20160524. doi: 10.1016/j.npep.2016.05.004. PubMed PMID: 27255391.

176.   Dubey AK, Plant TM. A suppression of gonadotropin secretion by cortisol in castrated male rhesus monkeys (Macaca mulatta) mediated by the interruption of hypothalamic gonadotropin-releasing hormone release. Biol Reprod. 1985;33(2):423-31. doi: 10.1095/biolreprod33.2.423. PubMed PMID: 3929850.

177.   Ullah R, Naz R, Batool A, Wazir M, Rahman TU, Nabi G, et al. RF9 Rescues Cortisol-Induced Repression of Testosterone Levels in Adult Male Macaques. Front Physiol. 2021;12:630796. Epub 20210225. doi: 10.3389/fphys.2021.630796. PubMed PMID: 33716777; PubMed Central PMCID: PMCPMC7946976.

178.   Rivier C, Rivier J, Vale W. Stress-induced inhibition of reproductive functions: role of endogenous corticotropin-releasing factor. Science. 1986;231(4738):607-9. doi: 10.1126/science.3003907. PubMed PMID: 3003907.

179.   Patchev VK, Hassan AH, Holsboer DF, Almeida OF. The neurosteroid tetrahydroprogesterone attenuates the endocrine response to stress and exerts glucocorticoid-like effects on vasopressin gene transcription in the rat hypothalamus. Neuropsychopharmacology. 1996;15(6):533-40. doi: 10.1016/S0893-133X(96)00096-6. PubMed PMID: 8946427.

180.   Almeida FB, Pinna G, Barros HMT. The Role of HPA Axis and Allopregnanolone on the Neurobiology of Major Depressive Disorders and PTSD. Int J Mol Sci. 2021;22(11). Epub 20210523. doi: 10.3390/ijms22115495. PubMed PMID: 34071053; PubMed Central PMCID: PMCPMC8197074.

181.   Brunton PJ, McKay AJ, Ochedalski T, Piastowska A, Rebas E, Lachowicz A, Russell JA. Central opioid inhibition of neuroendocrine stress responses in pregnancy in the rat is induced by the neurosteroid allopregnanolone. J Neurosci. 2009;29(20):6449-60. doi: 10.1523/JNEUROSCI.0708-09.2009. PubMed PMID: 19458216; PubMed Central PMCID: PMCPMC6665894.

182.   Prior JC. Women's reproductive system as balanced estradiol and progesterone actions—A revolutionary, paradigm-shifting concept in women's health. Drug Discovery Today: Disease Models. 2020;32:31–40. doi: 10.1016/j.ddmod.2020.11.005.

183.   Wang L, Moenter SM. Differential Roles of Hypothalamic AVPV and Arcuate Kisspeptin Neurons in Estradiol Feedback Regulation of Female Reproduction. Neuroendocrinology. 2020;110(3-4):172-84. Epub 20190830. doi: 10.1159/000503006. PubMed PMID: 31466075; PubMed Central PMCID: PMCPMC7047625.

184.   Goodman RL, Lehman MN. Kisspeptin neurons from mice to men: similarities and differences. Endocrinology. 2012;153(11):5105-18. Epub 20120918. doi: 10.1210/en.2012-1550. PubMed PMID: 22989628; PubMed Central PMCID: PMCPMC3473207.

185.   Lehman MN, Hileman SM, Goodman RL. Neuroanatomy of the kisspeptin signaling system in mammals: comparative and developmental aspects. Adv Exp Med Biol. 2013;784:27-62. doi: 10.1007/978-1-4614-6199-9_3. PubMed PMID: 23550001; PubMed Central PMCID: PMCPMC4059209.

186.   Stevenson H, Bartram S, Charalambides MM, Murthy S, Petitt T, Pradeep A, et al. Kisspeptin-neuron control of LH pulsatility and ovulation. Front Endocrinol (Lausanne). 2022;13:951938. Epub

20221121. doi: 10.3389/fendo.2022.951938. PubMed PMID: 36479214; PubMed Central PMCID: PMCPMC9721495.

187. Miller BH, Gore AC. N-Methyl-D-aspartate receptor subunit expression in GnRH neurons changes during reproductive senescence in the female rat. Endocrinology. 2002;143(9):3568-74. doi: 10.1210/en.2002-220346. PubMed PMID: 12193572.

188. Cravo RM, Margatho LO, Osborne-Lawrence S, Donato J, Jr., Atkin S, Bookout AL, et al. Characterization of Kiss1 neurons using transgenic mouse models. Neuroscience. 2011;173:37-56. Epub 20101118. doi: 10.1016/j.neuroscience.2010.11.022. PubMed PMID: 21093546; PubMed Central PMCID: PMCPMC3026459.

189. Han SK, Abraham IM, Herbison AE. Effect of GABA on GnRH neurons switches from depolarization to hyperpolarization at puberty in the female mouse. Endocrinology. 2002;143(4):1459-66. doi: 10.1210/endo.143.4.8724. PubMed PMID: 11897704.

190. Watanabe M, Fukuda A, Nabekura J. The role of GABA in the regulation of GnRH neurons. Front Neurosci. 2014;8:387. Epub 20141128. doi: 10.3389/fnins.2014.00387. PubMed PMID: 25506316; PubMed Central PMCID: PMCPMC4246667.

191. Piet R, de Croft S, Liu X, Herbison AE. Electrical properties of kisspeptin neurons and their regulation of GnRH neurons. Front Neuroendocrinol. 2015;36:15-27. Epub 20140605. doi: 10.1016/j.yfrne.2014.05.006. PubMed PMID: 24907402.

192. Alreja M. Electrophysiology of kisspeptin neurons. Adv Exp Med Biol. 2013;784:349-62. doi: 10.1007/978-1-4614-6199-9_16. PubMed PMID: 23550014.

193. Maffucci JA, Gore AC. Chapter 2: hypothalamic neural systems controlling the female reproductive life cycle gonadotropin-releasing hormone, glutamate, and GABA. Int Rev Cell Mol Biol. 2009;274:69-127. doi: 10.1016/S1937-6448(08)02002-9. PubMed PMID: 19349036; PubMed Central PMCID: PMCPMC2821833.

194. Ivanova D, O'Byrne KT. Optogenetics studies of kisspeptin neurons. Peptides. 2023;162:170961. Epub 20230131. doi: 10.1016/j.peptides.2023.170961. PubMed PMID: 36731655.

195. Putteeraj M, Soga T, Ubuka T, Parhar IS. A "Timed" Kiss Is Essential for Reproduction: Lessons from Mammalian Studies. Front Endocrinol (Lausanne). 2016;7:121. Epub 20160831. doi: 10.3389/fendo.2016.00121. PubMed PMID: 27630616; PubMed Central PMCID: PMCPMC5005330.

196. Donoso AO, Banzan AM. Blockade of the LH surge and ovulation by GABA-T inhibitory drugs that increase brain GABA levels in rats. Psychoneuroendocrinology. 1986;11(4):429-35. doi: 10.1016/0306-4530(86)90004-1. PubMed PMID: 3562742.

197. Herman JP, Mueller NK, Figueiredo H. Role of GABA and glutamate circuitry in hypothalamo-pituitary-adrenocortical stress integration. Ann N Y Acad Sci. 2004;1018:35-45. doi: 10.1196/annals.1296.004. PubMed PMID: 15240350.

198. Rasiah NP, Loewen SP, Bains JS. Windows into stress: a glimpse at emerging roles for CRH(PVN) neurons. Physiol Rev. 2023;103(2):1667-91. Epub 20221117. doi: 10.1152/physrev.00056.2021. PubMed PMID: 36395349.

199. Levy BH, Tasker JG. Synaptic regulation of the hypothalamic-pituitary-adrenal axis and its modulation by glucocorticoids and stress. Front Cell Neurosci. 2012;6:24. Epub 20120511. doi: 10.3389/fncel.2012.00024. PubMed PMID: 22593735; PubMed Central PMCID: PMCPMC3349941.

200. Maguire J. The relationship between GABA and stress: 'it's complicated'. J Physiol. 2018;596(10):1781-2. Epub 20180416. doi: 10.1113/JP275937. PubMed PMID: 29524241; PubMed Central PMCID: PMCPMC5978385.

201. Aguilera G, Liu Y. The molecular physiology of CRH neurons. Front Neuroendocrinol. 2012;33(1):67-84. Epub 20110818. doi: 10.1016/j.yfrne.2011.08.002. PubMed PMID: 21871477; PubMed Central PMCID: PMCPMC4341841.

202. Inoue W, Baimoukhametova DV, Fuzesi T, Wamsteeker Cusulin JI, Koblinger K, Whelan PJ, et al. Noradrenaline is a stress-associated metaplastic signal at GABA synapses. Nat Neurosci.

2013;16(5):605-12. Epub 20130407. doi: 10.1038/nn.3373. PubMed PMID: 23563580; PubMed Central PMCID: PMCPMC3984240.

203.   Fanelli F, Cantu M, Temchenko A, Mezzullo M, Lindner JM, Peitzsch M, et al. Report from the HarmoSter study: impact of calibration on comparability of LC-MS/MS measurement of circulating cortisol, 17OH-progesterone and aldosterone. Clin Chem Lab Med. 2022;60(5):726-39. Epub 20220216. doi: 10.1515/cclm-2021-1028. PubMed PMID: 35172417.

204.   Ventrella D, Elmi A, Bertocchi M, Aniballi C, Parmeggiani A, Govoni N, Bacci ML. Progesterone and Cortisol Levels in Blood and Hair of Wild Pregnant Red Deer (Cervus Elaphus) Hinds. Animals (Basel). 2020;10(1). Epub 20200116. doi: 10.3390/ani10010143. PubMed PMID: 31963117; PubMed Central PMCID: PMCPMC7022734.

205.   Groschl M, Rauh M, Dorr HG. Circadian rhythm of salivary cortisol, 17alpha-hydroxyprogesterone, and progesterone in healthy children. Clin Chem. 2003;49(10):1688-91. doi: 10.1373/49.10.1688. PubMed PMID: 14500602.

206.   Henriksen R, Groothuis TG, Rettenbacher S. Elevated plasma corticosterone decreases yolk testosterone and progesterone in chickens: linking maternal stress and hormone-mediated maternal effects. PLoS One. 2011;6(8):e23824. Epub 20110823. doi: 10.1371/journal.pone.0023824. PubMed PMID: 21886826; PubMed Central PMCID: PMCPMC3160319.

207.   Nyongesa AW, Patel NB, Onyango DW, Odongo HO, Wango EO. Khat (Catha edulis) lowers plasma luteinizing hormone (LH) and testosterone secretion, but increases cortisol levels in male rabbits. J Ethnopharmacol. 2008;116(2):245-50. Epub 20071122. doi: 10.1016/j.jep.2007.11.022. PubMed PMID: 18180121.

208.   Awalu JC, Onyenekwe CC, Ukibe NR, Ahaneku JE, Ejemete SE, Udeh T, Ukibe EG. Serum Cortisol, Progesterone and Total Antioxidant Status of Students Pre-and Post-Examination. Indian Journal of Public Health Research & Development. 2020;11(12):197–206. doi: 10.37506/ijphrd.v11i12.13238.

209.   Anderson T, Lane AR, Hackney AC. Cortisol and testosterone dynamics following exhaustive endurance exercise. Eur J Appl Physiol. 2016;116(8):1503-9. Epub 20160604. doi: 10.1007/s00421-016-3406-y. PubMed PMID: 27262888.

210.   Etches RJ. Plasma concentrations of progesterone and corticosterone during the ovulation cycle of the hen (Gallus domesticus). Poult Sci. 1979;58(1):211-6. doi: 10.3382/ps.0580211. PubMed PMID: 471886.

211.   Pluchino N, Ninni F, Stomati M, Freschi L, Casarosa E, Valentino V, et al. One-year therapy with 10mg/day DHEA alone or in combination with HRT in postmenopausal women: effects on hormonal milieu. Maturitas. 2008;59(4):293-303. Epub 20080403. doi: 10.1016/j.maturitas.2008.02.004. PubMed PMID: 18394829.

212.   Endrenyi L, Fajszi C, Kwong FHF. Evaluation of Hill Slopes and Hill Coefficients when the Saturation Binding or Velocity is not Known. Eur J Biochem. 1975; 51:317-28.

213.   Weiss JN. The Hill equation revisited: uses and misuses. FASEB J. 1997;11(11):835-41. PubMed PMID: 9285481.

214.   Somvanshi PR, Venkatesh KV. Hill Equation. In: Dubitzky W, Wolkenhauer O, Cho K, Yokota H, editors. Encyclopedia of Systems Biology. New York, NY, USA: Springer; 2013. p. 892--5.

215.   Ehring GR, Kerschbaum HH, Eder C, Neben AL, Fanger CM, Khoury RM, et al. A nongenomic mechanism for progesterone-mediated immunosuppression: inhibition of K+ channels, Ca2+ signaling, and gene expression in T lymphocytes. J Exp Med. 1998;188(9):1593-602. doi: 10.1084/jem.188.9.1593. PubMed PMID: 9802971; PubMed Central PMCID: PMCPMC2212508.

216.   Somvanshi PR, Mellon SH, Yehuda R, Flory JD, Makotkine I, Bierer L, et al. Role of enhanced glucocorticoid receptor sensitivity in inflammation in PTSD: insights from computational model for circadian-neuroendocrine-immune interactions. Am J Physiol Endocrinol Metab. 2020;319(1):E48-E66. Epub 20200421. doi: 10.1152/ajpendo.00398.2019. PubMed PMID: 32315214.

217.   Demori I, Molinari E, Rapallo F, Mucci V, Marinelli L, Losacco S, Burlando B. Online Questionnaire with Fibromyalgia Patients Reveals Correlations among Type of Pain, Psychological Alterations, and Effectiveness of Non-Pharmacological Therapies. Healthcare (Basel). 2022;10(10). Epub 20221009. doi: 10.3390/healthcare10101975. PubMed PMID: 36292422; PubMed Central PMCID: PMCPMC9602604.

218.   Bailly F, Cantagrel A, Bertin P, Perrot S, Thomas T, Lansaman T, et al. Part of pain labelled neuropathic in rheumatic disease might be rather nociplastic. RMD Open. 2020;6(2). Epub 2020/09/07. doi: 10.1136/rmdopen-2020-001326. PubMed PMID: 32892169; PubMed Central PMCID: PMCPMC7508212.

219.   Mucci V, Demori I, Browne CJ, Deblieck C, Burlando B. Fibromyalgia in Pregnancy: Neuro-Endocrine Fluctuations Provide Insight into Pathophysiology and Neuromodulation Treatment. Biomedicines. 2023;11(2). Epub 20230218. doi: 10.3390/biomedicines11020615. PubMed PMID: 36831148; PubMed Central PMCID: PMCPMC9953487.

220.   Koné M, Kambiré N, Ahoua Y. Impact of Fibromyalgia on Female Infertility. Open Journal of Epidemiology. 2021;11(4):457-72 doi: 10.4236/ojepi.2021.114037.

221.   Schloemer N, Lenz M, Tegenthoff M, Dinse HR, Hoffken O. Parallel modulation of intracortical excitability of somatosensory and visual cortex by the gonadal hormones estradiol and progesterone. Sci Rep. 2020;10(1):22237. Epub 20201217. doi: 10.1038/s41598-020-79389-6. PubMed PMID: 33335211; PubMed Central PMCID: PMCPMC7747729.

222.   Keenan DM, Roelfsema F, Carroll BJ, Iranmanesh A, Veldhuis JD. Sex defines the age dependence of endogenous ACTH-cortisol dose responsiveness. Am J Physiol Regul Integr Comp Physiol. 2009;297(2):R515-23. Epub 20090617. doi: 10.1152/ajpregu.00200.2009. PubMed PMID: 19535673; PubMed Central PMCID: PMCPMC2724232.

223.   Wilkinson CW, Peskind ER, Raskind MA. Decreased hypothalamic-pituitary-adrenal axis sensitivity to cortisol feedback inhibition in human aging. Neuroendocrinology. 1997;65(1):79-90. doi: 10.1159/000127167. PubMed PMID: 9032777.

224.   Ratner MH, Kumaresan V, Farb DH. Neurosteroid Actions in Memory and Neurologic/Neuropsychiatric Disorders. Front Endocrinol (Lausanne). 2019;10:169. Epub 20190409. doi: 10.3389/fendo.2019.00169. PubMed PMID: 31024441; PubMed Central PMCID: PMCPMC6465949.

225.   Tuveri A, Paoletti AM, Orru M, Melis GB, Marotto MF, Zedda P, et al. Reduced serum level of THDOC, an anticonvulsant steroid, in women with perimenstrual catamenial epilepsy. Epilepsia. 2008;49(7):1221-9. doi: 10.1111/j.1528-1167.2008.01555.x. PubMed PMID: 18325018.

226.   Reddy DS. The role of neurosteroids in the pathophysiology and treatment of catamenial epilepsy. Epilepsy Res. 2009;85(1):1-30. Epub 20090429. doi: 10.1016/j.eplepsyres.2009.02.017. PubMed PMID: 19406620; PubMed Central PMCID: PMCPMC2696558.

227.   Hantsoo L, Epperson CN. Allopregnanolone in premenstrual dysphoric disorder (PMDD): Evidence for dysregulated sensitivity to GABA-A receptor modulating neuroactive steroids across the menstrual cycle. Neurobiol Stress. 2020;12:100213. Epub 20200204. doi: 10.1016/j.ynstr.2020.100213. PubMed PMID: 32435664; PubMed Central PMCID: PMCPMC7231988.

228.   Reddy DS, Rogawski MA. Enhanced anticonvulsant activity of neuroactive steroids in a rat model of catamenial epilepsy. Epilepsia. 2001;42(3):337-44. doi: 10.1046/j.1528-1157.2001.10200.x. PubMed PMID: 11442150.

229.   Zorumski CF, Paul SM, Covey DF, Mennerick S. Neurosteroids as novel antidepressants and anxiolytics: GABA-A receptors and beyond. Neurobiol Stress. 2019;11:100196. Epub 20190927. doi: 10.1016/j.ynstr.2019.100196. PubMed PMID: 31649968; PubMed Central PMCID: PMCPMC6804800.

230.   Etkin A. A Reckoning and Research Agenda for Neuroimaging in Psychiatry. Am J Psychiatry. 2019;176(7):507-11. doi: 10.1176/appi.ajp.2019.19050521. PubMed PMID: 31256624.

231.   Meltzer-Brody S, Colquhoun H, Riesenberg R, Epperson CN, Deligiannidis KM, Rubinow DR, et al. Brexanolone injection in post-partum depression: two multicentre, double-blind, randomised, placebo-controlled, phase 3 trials. Lancet. 2018;392(10152):1058-70. Epub 20180831. doi: 10.1016/S0140-6736(18)31551-4. PubMed PMID: 30177236.

232.   Gunduz-Bruce H, Silber C, Kaul I, Rothschild AJ, Riesenberg R, Sankoh AJ, et al. Trial of SAGE-217 in Patients with Major Depressive Disorder. N Engl J Med. 2019;381(10):903-11. doi: 10.1056/NEJMoa1815981. PubMed PMID: 31483961.

233.   Carvalho T. New depression drug zuranolone one step closer to FDA ruling. Nat Med. 2023;29(5):1032-3. doi: 10.1038/d41591-023-00032-8. PubMed PMID: 37041352.

234.   Mullard A. FDA approves first oral drug for postpartum depression, but rejects it for major depressive disorder. Nat Rev Drug Discov. 2023. Epub 20230811. doi: 10.1038/d41573-023-00134-5. PubMed PMID: 37568055.

235.   Macfarlane GJ, Kronisch C, Dean LE, Atzeni F, Hauser W, Fluss E, et al. EULAR revised recommendations for the management of fibromyalgia. Ann Rheum Dis. 2017;76(2):318-28. Epub 2016/07/06. doi: 10.1136/annrheumdis-2016-209724. PubMed PMID: 27377815.

236.   Bair MJ, Robinson RL, Katon W, Kroenke K. Depression and pain comorbidity: a literature review. Arch Intern Med. 2003;163(20):2433-45. Epub 2003/11/12. doi: 10.1001/archinte.163.20.2433. PubMed PMID: 14609780.

237.   Raja SN, Carr DB, Cohen M, Finnerup NB, Flor H, Gibson S, et al. The revised International Association for the Study of Pain definition of pain: concepts, challenges, and compromises. Pain. 2020;161(9):1976-82. Epub 2020/07/23. doi: 10.1097/j.pain.0000000000001939. PubMed PMID: 32694387; PubMed Central PMCID: PMCPMC7680716.

238.   Coaccioli S, Varrassi G, Sabatini C, Marinangeli F, Giuliani M, Puxeddu A. Fibromyalgia: nosography and therapeutic perspectives. Pain Pract. 2008;8(3):190-201. Epub 2008/04/01. doi: 10.1111/j.1533-2500.2008.00188.x. PubMed PMID: 18373513.

239.   Guillery RW, Sherman SM. Thalamic relay functions and their role in corticocortical communication: generalizations from the visual system. Neuron. 2002;33(2):163-75. Epub 2002/01/24. doi: 10.1016/s0896-6273(01)00582-7. PubMed PMID: 11804565.

240.   Chinn S, Caldwell W, Gritsenko K. Fibromyalgia Pathogenesis and Treatment Options Update. Curr Pain Headache Rep. 2016;20(4):25. Epub 2016/02/29. doi: 10.1007/s11916-016-0556-x. PubMed PMID: 26922414.

241.   Maffei ME. Fibromyalgia: Recent Advances in Diagnosis, Classification, Pharmacotherapy and Alternative Remedies. Int J Mol Sci. 2020;21(21). Epub 2020/10/30. doi: 10.3390/ijms21217877. PubMed PMID: 33114203; PubMed Central PMCID: PMCPMC7660651.

242.   Galvez-Sanchez CM, Duschek S, Reyes Del Paso GA. Psychological impact of fibromyalgia: current perspectives. Psychol Res Behav Manag. 2019;12:117-27. Epub 2019/03/13. doi: 10.2147/PRBM.S178240. PubMed PMID: 30858740; PubMed Central PMCID: PMCPMC6386210.

243.   Braz Ade S, de Paula AP, Diniz Mde F, de Almeida RN. Non-pharmacological therapy and complementary and alternative medicine in fibromyalgia. Rev Bras Reumatol. 2011;51(3):269-82. Epub 2011/06/01. PubMed PMID: 21625815.

244.   Tzadok R, Ablin JN. Current and Emerging Pharmacotherapy for Fibromyalgia. Pain Res Manag. 2020;2020:6541798. Epub 2020/02/28. doi: 10.1155/2020/6541798. PubMed PMID: 32104521; PubMed Central PMCID: PMCPMC7036118.

245.   Busch AJ, Webber SC, Brachaniec M, Bidonde J, Bello-Haas VD, Danyliw AD, et al. Exercise therapy for fibromyalgia. Curr Pain Headache Rep. 2011;15(5):358-67. doi: 10.1007/s11916-011-0214-2. PubMed PMID: 21725900; PubMed Central PMCID: PMCPMC3165132.

246.   Araujo FM, DeSantana JM. Physical therapy modalities for treating fibromyalgia. F1000Res. 2019;8. Epub 2020/02/13. doi: 10.12688/f1000research.17176.1. PubMed PMID: 32047594; PubMed Central PMCID: PMCPMC6979469.

247.   Wright SL. Limited Utility for Benzodiazepines in Chronic Pain Management: A Narrative Review. Adv Ther. 2020;37(6):2604-19. Epub 20200506. doi: 10.1007/s12325-020-01354-6. PubMed PMID: 32378069; PubMed Central PMCID: PMCPMC7467435.

248.   Meyer L, Taleb O, Patte-Mensah C, Mensah-Nyagan AG. Neurosteroids and neuropathic pain management: Basic evidence and therapeutic perspectives. Front Neuroendocrinol. 2019;55:100795. Epub 20190925. doi: 10.1016/j.yfrne.2019.100795. PubMed PMID: 31562849.

249.   Calvin WH. Neural Darwinism. The Theory of Neuronal Group Selection. Gerald M. Edelman. Basic Books, New York, 1987. xxii, 371 pp., illus. $29.95. Science. 1988;240(4860):1802. Epub 1988/06/24. doi: 10.1126/science.240.4860.1802. PubMed PMID: 17842436.

250.   Tononi G, Sporns O, Edelman GM. A measure for brain complexity: relating functional segregation and integration in the nervous system. Proc Natl Acad Sci U S A. 1994;91(11):5033-7. Epub 1994/05/24. doi: 10.1073/pnas.91.11.5033. PubMed PMID: 8197179; PubMed Central PMCID: PMCPMC43925.

251.   Sporns O. Structure and function of complex brain networks. Dialogues Clin Neurosci. 2013;15(3):247-62. Epub 2013/11/01. doi: 10.31887/DCNS.2013.15.3/osporns. PubMed PMID: 24174898; PubMed Central PMCID: PMCPMC3811098.

252.   Palop JJ, Chin J, Mucke L. A network dysfunction perspective on neurodegenerative diseases. Nature. 2006;443(7113):768-73. Epub 2006/10/20. doi: 10.1038/nature05289. PubMed PMID: 17051202.

253.   McMackin R, Bede P, Pender N, Hardiman O, Nasseroleslami B. Neurophysiological markers of network dysfunction in neurodegenerative diseases. Neuroimage Clin. 2019;22:101706. Epub 2019/02/10. doi: 10.1016/j.nicl.2019.101706. PubMed PMID: 30738372; PubMed Central PMCID: PMCPMC6370863.

254.   Shein-Idelson M, Ben-Jacob E, Hanein Y. Engineered neuronal circuits: a new platform for studying the role of modular topology. Front Neuroeng. 2011;4:10. Epub 2011/10/13. doi: 10.3389/fneng.2011.00010. PubMed PMID: 21991254; PubMed Central PMCID: PMCPMC3180629.

255.   Callegari F, Brofiga M, Poggio F, Massobrio P. Stimulus-Evoked Activity Modulation of In Vitro Engineered Cortical and Hippocampal Networks. Micromachines (Basel). 2022;13(8). Epub 2022/08/27. doi: 10.3390/mi13081212. PubMed PMID: 36014137; PubMed Central PMCID: PMCPMC9413227.

256.   Brofiga M, Losacco S, Poggio F, Zerbo RA, Milanese M, Massobrio P, Burlando B. Multiple neuron clusters on Micro-Electrode Arrays as an in vitro model of brain network. Sci Rep. 2023;13(1):15604. Epub 2023/09/21. doi: 10.1038/s41598-023-42168-0. PubMed PMID: 37730890; PubMed Central PMCID: PMCPMC10511538.

257.   McGrath JC, Lilley E. Implementing guidelines on reporting research using animals (ARRIVE etc.): new requirements for publication in BJP. Br J Pharmacol. 2015;172(13):3189-93. Epub 2015/05/13. doi: 10.1111/bph.12955. PubMed PMID: 25964986; PubMed Central PMCID: PMCPMC4500358.

258.   Pfrieger FW, Barres BA. Synaptic efficacy enhanced by glial cells in vitro. Science. 1997;277(5332):1684-7. Epub 1997/09/12. doi: 10.1126/science.277.5332.1684. PubMed PMID: 9287225.

259.   Maccione A, Gandolfo M, Massobrio P, Novellino A, Martinoia S, Chiappalone M. A novel algorithm for precise identification of spikes in extracellularly recorded neuronal signals. J Neurosci Methods. 2009;177(1):241-9. Epub 2008/10/30. doi: 10.1016/j.jneumeth.2008.09.026. PubMed PMID: 18957306.

260.   Wagenaar DA, Pine J, Potter SM. An extremely rich repertoire of bursting patterns during the development of cortical cultures. BMC Neurosci. 2006;7:11. Epub 2006/02/09. doi: 10.1186/1471-2202-7-11. PubMed PMID: 16464257; PubMed Central PMCID: PMCPMC1420316.

261.   Chiappalone M, Novellino A, Vajda I, Vato A, Martinoia S, Pelt Jv. Burst detection algorithms for the analysis of spatio-temporal patterns in cortical networks of neurons. Neurocomputing. 2005;65-66:653-62.

262.   Pasquale V, Martinoia S, Chiappalone M. A self-adapting approach for the detection of bursts and network bursts in neuronal cultures. J Comput Neurosci. 2010;29(1-2):213-29. Epub 2009/08/12. doi: 10.1007/s10827-009-0175-1. PubMed PMID: 19669401.

263.   Wagner JG. Kinetics of pharmacologic response. I. Proposed relationships between response and drug concentration in the intact animal and man. J Theor Biol. 1968;20(2):173-201. Epub 1968/08/01. doi: 10.1016/0022-5193(68)90188-4. PubMed PMID: 5727238.

264.   Shannon CE. The mathematical theory of communication. 1963. MD Comput. 1997;14(4):306-17. Epub 1997/07/01. PubMed PMID: 9230594.

265.   Marom S, Shahaf G. Development, learning and memory in large random networks of cortical neurons: lessons beyond anatomy. Q Rev Biophys. 2002;35(1):63-87. Epub 2002/05/10. doi: 10.1017/s0033583501003742. PubMed PMID: 11997981.

266.   Zbinden C. Leader neurons in leaky integrate and fire neural network simulations. J Comput Neurosci. 2011;31(2):285-304. Epub 2011/01/15. doi: 10.1007/s10827-010-0308-6. PubMed PMID: 21234795.

267.   Eckmann J-P, Jacobi S, Marom S, Moses E, Zbinden C. Leader neurons in population bursts of 2D living neural networks. New Journal of Physics. 2008;10.

268.   He C, Chen F, Li B, Hu Z. Neurophysiology of HCN channels: from cellular functions to multiple regulations. Prog Neurobiol. 2014;112:1-23. Epub 2013/11/05. doi: 10.1016/j.pneurobio.2013.10.001. PubMed PMID: 24184323.

269.   Marionneau C, Couette B, Liu J, Li H, Mangoni ME, Nargeot J, et al. Specific pattern of ionic channel gene expression associated with pacemaker activity in the mouse heart. J Physiol. 2005;562(Pt 1):223-34. Epub 2004/10/23. doi: 10.1113/jphysiol.2004.074047. PubMed PMID: 15498808; PubMed Central PMCID: PMCPMC1665484.

270.   Novella Romanelli M, Sartiani L, Masi A, Mannaioni G, Manetti D, Mugelli A, Cerbai E. HCN Channels Modulators: The Need for Selectivity. Curr Top Med Chem. 2016;16(16):1764-91. Epub 2016/03/16. doi: 10.2174/1568026616999160315130832. PubMed PMID: 26975509; PubMed Central PMCID: PMCPMC5374843.

271.   Mckay S, Bengtson CP, Bading H, Wyllie DJA, Hardingham GE. Recovery of NMDA receptor currents from MK-801 blockade is accelerated by Mg2+ and memantine under conditions of agonist exposure. Neuropharmacology. 2013;74:119-25.

272.   Huettner JE, Bean BP. Block of N-methyl-D-aspartate-activated current by the anticonvulsant MK-801: selective binding to open channels. Proc Natl Acad Sci U S A. 1988;85(4):1307-11. Epub 1988/02/01. doi: 10.1073/pnas.85.4.1307. PubMed PMID: 2448800; PubMed Central PMCID: PMCPMC279756.

273.   Frega M, van Gestel SH, Linda K, van der Raadt J, Keller J, Van Rhijn JR, et al. Rapid Neuronal Differentiation of Induced Pluripotent Stem Cells for Measuring Network Activity on Micro-electrode Arrays. J Vis Exp. 2017;(119). Epub 2017/01/25. doi: 10.3791/54900. PubMed PMID: 28117798; PubMed Central PMCID: PMCPMC5407693.

274.   Okujeni S, Egert U. Inhomogeneities in Network Structure and Excitability Govern Initiation and Propagation of Spontaneous Burst Activity. Front Neurosci. 2019;13:543. Epub 2019/06/20. doi: 10.3389/fnins.2019.00543. PubMed PMID: 31213971; PubMed Central PMCID: PMCPMC6554329.

275.   Chiappalone M, Massobrio P, Martinoia S. Network plasticity in cortical assemblies. Eur J Neurosci. 2008;28(1):221-37. Epub 2008/07/30. doi: 10.1111/j.1460-9568.2008.06259.x. PubMed PMID: 18662344.

276.   Papatheodoropoulos C, Kouvaros S. High-frequency stimulation-induced synaptic potentiation in dorsal and ventral CA1 hippocampal synapses: the involvement of NMDA receptors, mGluR5, and (L-type) voltage-gated calcium channels. Learn Mem. 2016;23(9):460-4. Epub

2016/08/18. doi: 10.1101/lm.042531.116. PubMed PMID: 27531836; PubMed Central PMCID: PMCPMC4986856.

277.   Yamamoto H, Moriya S, Ide K, Hayakawa T, Akima H, Sato S, et al. Impact of modular organization on dynamical richness in cortical networks. Sci Adv. 2018;4(11):eaau4914. Epub 2018/11/18. doi: 10.1126/sciadv.aau4914. PubMed PMID: 30443598; PubMed Central PMCID: PMCPMC6235526.

278.   Muldoon SF, Bridgeford EW, Bassett DS. Small-World Propensity and Weighted Brain Networks. Sci Rep. 2016;6:22057. Epub 2016/02/26. doi: 10.1038/srep22057. PubMed PMID: 26912196; PubMed Central PMCID: PMCPMC4766852.

279.   Amarillo Y, Tissone AI, Mato G, Nadal MS. Inward rectifier potassium current I(Kir) promotes intrinsic pacemaker activity of thalamocortical neurons. J Neurophysiol. 2018;119(6):2358-72. Epub 2018/03/22. doi: 10.1152/jn.00867.2017. PubMed PMID: 29561202.

280.   Smith JC, Butera RJ, Koshiya N, Del Negro C, Wilson CG, Johnson SM. Respiratory rhythm generation in neonatal and adult mammals: the hybrid pacemaker-network model. Respir Physiol. 2000;122(2-3):131-47. Epub 2000/09/01. doi: 10.1016/s0034-5687(00)00155-9. PubMed PMID: 10967340.

281.   Matschke LA, Rinne S, Snutch TP, Oertel WH, Dolga AM, Decher N. Calcium-activated SK potassium channels are key modulators of the pacemaker frequency in locus coeruleus neurons. Mol Cell Neurosci. 2018;88:330-41. Epub 2018/03/11. doi: 10.1016/j.mcn.2018.03.002. PubMed PMID: 29524627.

282.   Le Bon-Jego M, Yuste R. Persistently active, pacemaker-like neurons in neocortex. Front Neurosci. 2007;1(1):123-9. Epub 2008/11/05. doi: 10.3389/neuro.01.1.1.009.2007. PubMed PMID: 18982123; PubMed Central PMCID: PMCPMC2518052.

283.   Kocsis B, Martinez-Bellver S, Fiath R, Domonkos A, Sviatko K, Schlingloff D, et al. Huygens synchronization of medial septal pacemaker neurons generates hippocampal theta oscillation. Cell Rep. 2022;40(5):111149. Epub 2022/08/05. doi: 10.1016/j.celrep.2022.111149. PubMed PMID: 35926456.

284.   Surmeier DJ, Mercer JN, Chan CS. Autonomous pacemakers in the basal ganglia: who needs excitatory synapses anyway? Curr Opin Neurobiol. 2005;15(3):312-8. Epub 2005/05/27. doi: 10.1016/j.conb.2005.05.007. PubMed PMID: 15916893.

285.   Thoby-Brisson M, Telgkamp P, Ramirez JM. The role of the hyperpolarization-activated current in modulating rhythmic activity in the isolated respiratory network of mice. J Neurosci. 2000;20(8):2994-3005. Epub 2001/02/07. doi: 10.1523/JNEUROSCI.20-08-02994.2000. PubMed PMID: 10751452; PubMed Central PMCID: PMCPMC6772196.

286.   Varga V, Hangya B, Kranitz K, Ludanyi A, Zemankovics R, Katona I, et al. The presence of pacemaker HCN channels identifies theta rhythmic GABAergic neurons in the medial septum. J Physiol. 2008;586(16):3893-915. Epub 2008/06/21. doi: 10.1113/jphysiol.2008.155242. PubMed PMID: 18565991; PubMed Central PMCID: PMCPMC2538919.

287.   Zucker RS, Regehr WG. Short-term synaptic plasticity. Annu Rev Physiol. 2002;64:355-405. Epub 2002/02/05. doi: 10.1146/annurev.physiol.64.092501.114547. PubMed PMID: 11826273.

288.   Abramets II, Yu. Kuznetsov V, Samoi IMI. Effects of low-frequency tetanic stimulation of the synaptic inputs on different forms of long-term potentiation in the rat hippocampus. Neurophysiology. 1999;31(5):310-5.

289.   Gritsun TA, Le Feber J, Stegenga J, Rutten WL. Network bursts in cortical cultures are best simulated using pacemaker neurons and adaptive synapses. Biol Cybern. 2010;102(4):293-310. Epub 2010/02/17. doi: 10.1007/s00422-010-0366-x. PubMed PMID: 20157725.

290.   Gee MM, Lenhoff AM, Schwaber JS, Ogunnaike BA, Vadigepalli R. Closed-loop modeling of central and intrinsic cardiac nervous system circuits underlying cardiovascular control. AIChE J. 2023;69(4). Epub 2023/05/30. doi: 10.1002/aic.18033. PubMed PMID: 37250861; PubMed Central PMCID: PMCPMC10211393.

291.	Fisher ST. A New Method of Amplifying with High Efficiency a Carrier Wave Modulated in Amplitude by a Voice Wave. Proceedings of the IRE. 1946;34:3-13.